JOURNAL OF HYDRO - METEOROLOGY

ISSN 2525 - 2208

VIETNAM METEOROLOGICAL AND HYDROLOGICAL ADMINISTRATION

No 21
12-2024

Publishing licence
No: 166/GP-BTTTT - Ministry of Information and Communication dated 17/04/2018

Editorial office
No 8 Phao Dai Lang, Dong Da, Ha Noi
Tel: 024.39364963
Email: tapchikttv@gmail.com

Engraving and printing
Ha Thanh Thang Long Printing And Trading Joint Stock Company
Tel: 0243.2022639

JOURNAL OF HYDRO-METEOROLOGY
Volume 21 - 12/2024

TABLE OF CONTENT

JOURNAL OF
HYDRO-METEOROLOGY

Research Article

Temporal change of Son Island in Bassac River, Can Tho city, Vietnam by remote sensing

Tran Minh Doan[1], and Dinh Van Duy[2]*

[1] Master student, Faculty of Water Resource Engineering, College of Engineering, Can Tho University; doanm4222017@gstudent.ctu.edu.vn
[2] Faculty of Water Resource Engineering, College of Engineering, Can Tho University; dvduy@ctu.edu.vn

*Corresponding author: dvduy@ctu.edu.vn; Tel.: +84–906975999

Received: 27 July 2024; Accepted: 23 August 2024; Published: 25 December 2024

Abstract: This study utilizes remote sensing to assess the temporal variation of Son Island on the Bassac River, Can Tho City, Vietnam, from 1987 to 2020. The findings indicate that the evolution of Son Island can be divided into two distinct periods. From 1987 to 2013, the island experienced significant migration from upstream to downstream, covering a distance of approximately 250 meters. In contrast, the period from 2013 to 2020 showed stability, with no significant changes in the island's area or center of gravity. Despite noticeable fluctuations in the island's area throughout the observed period, no clear trend was identified, suggesting overall stability. These fluctuations are likely due to errors in image analysis caused by the coarse resolution of Landsat images, tidal effects, and vegetation changes along the island's banks. The migration of Son Island is attributed to erosion at the island's head and deposition at its tail.

Keywords: Son Island; Bassac River; Google earth; Satellite image; Remote sensing; Migration.

1. Introduction

A river island is a land area elevated above the river water level at river branching sections. These islands divide the river section flowing through them into river branches and play a significant role in connecting and influencing the hydraulic, hydrological, morphological, and environmental interactions between the tributaries [1]. River islands have a significant impact on the morphological changes, environment, waterway traffic, and the lives of people on both sides of the river [2, 3, 4–7]. Therefore, research on river islands has been widely conducted around the world [8–12]. In Vietnam, studies on river engineering mainly focus on riverbank erosion. Although river islands play a crucial role in the river ecosystem and environment, research on river islands in Vietnam is still very limited. Particularly in the Vietnamese Mekong Delta (VMD), notable research on river islands includes the River Channel Improvement [13], analysis of factors affecting the change in the area of Long Khanh island, Hong Ngu district, Dong Thap province [14]. Most previous studies only analyzed riverbank erosion, and islands were only mentioned as part of studies on riverbank erosion in the two main river systems, Mekong River and Bassac River, such as applying the Google Earth Engine (GEE) cloud computing platform in monitoring shoreline changes in the VMD region [15]; applying remote sensing and GIS technology to monitor shoreline changes and assess the erosion situation on the Mekong river systems from 1989 to 2017 [16]; and the study on the causes of increased riverbank erosion in the VMD [17].

As mentioned above, there is a gap in the research on river engineering and management in the VMD, particularly concerning the study of river islands along the Mekong River system. Therefore, this study conducts an analysis of the migration of Son Island, located in Can Tho City, to provide a better understanding of the temporal changes of river islands in the VMD.

Son Island is located in the middle of the Bassac River (across from Co Bac Ferry), in Bui Huu Nghia ward, Binh Thuy district, Can Tho city (Figure 1). The island has a surface area (cultivated area) of 67 hectares [18]. Since 2015, Son Island has become a famous tourist destination in Can Tho City, known for its natural beauty, environment, customs, rituals, and the spirit of mutual support within the community [18, 19].

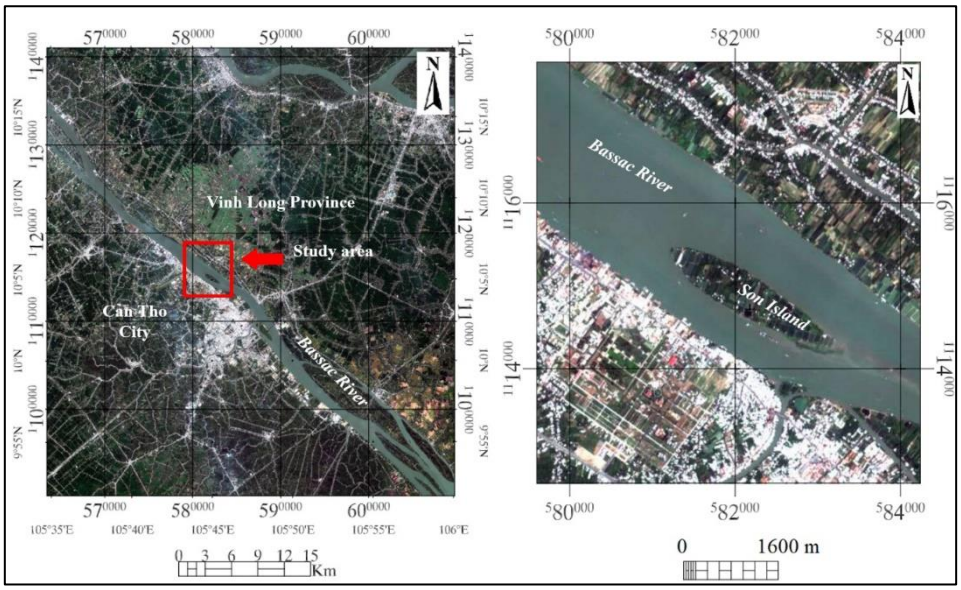

Figure 1. Study area.

2. Materials and Methods

2.1. Satellite image analysis

Landsat images from 1987 to 2020 were used for analysis. Details of the Landsat images are presented in Table 1. In which, there are two types of Landsat images were collected for the analysis with a consistant resolution of 30 m/pixel. The cloud cover varies from 0% to 50%. There are two images collected for each year in the dry and wet seasons. No tidal correction was performed in the image analysis.

Table 1. Information on the Landsat images.

Captured date	Sources	Sensor	Resolution (m)	Cloud cover (%)	Coordinate system
29/12/1987	Landsat 5	TM	30	10.00	UTM
30/01/1988	Landsat 5	TM	30	1.00	UTM
31/12/1988	Landsat 5	TM	30	38.00	UTM
06/04/1989	Landsat 5	TM	30	2.00	UTM
18/12/1989	Landsat 5	TM	30	2.00	UTM
03/01/1990	Landsat 5	TM	30	3.00	UTM
14/05/1991	Landsat 5	TM	30	9.00	UTM
25/01/1992	Landsat 5	TM	30	3.00	UTM
11/01/1993	Landsat 5	TM	30	23.00	UTM
01/04/1993	Landsat 5	TM	30	10.00	UTM
29/12/1993	Landsat 5	TM	30	19.00	UTM
13/10/1994	Landsat 5	TM	30	27.00	UTM
02/02/1995	Landsat 5	TM	30	5.00	UTM

Captured date	Sources	Sensor	Resolution (m)	Cloud cover (%)	Coordinate system
06/03/1995	Landsat 5	TM	30	19.00	UTM
21/02/1996	Landsat 5	TM	30	1.00	UTM
09/04/1996	Landsat 5	TM	30	6.00	UTM
06/01/1997	Landsat 5	TM	30	1.00	UTM
01/07/1997	Landsat 5	TM	30	22.00	UTM
09/01/1998	Landsat 5	TM	30	0.00	UTM
21/06/1999	Landsat 5	TM	30	10.00	UTM
07/07/1999	Landsat 5	TM	30	4.00	UTM
19/03/2000	Landsat 5	TM	30	38.00	UTM
14/11/2000	Landsat 5	TM	30	10.00	UTM
18/02/2001	Landsat 5	TM	30	7.00	UTM
09/05/2001	Landsat 5	TM	30	9.00	UTM
23/11/2003	Landsat 5	TM	30	18.00	UTM
18/06/2004	Landsat 5	TM	30	48.00	UTM
27/12/2004	Landsat 5	TM	30	46.00	UTM
24/08/2005	Landsat 5	TM	30	1.00	UTM
04/03/2006	Landsat 5	TM	30	3.00	UTM
17/12/2006	Landsat 5	TM	30	11.00	UTM
02/01/2007	Landsat 5	TM	30	50.00	UTM
25/03/2008	Landsat 5	TM	30	8.00	UTM
09/12/2009	Landsat 5	TM	30	1.00	UTM
18/05/2010	Landsat 5	TM	30	11.00	UTM
27/06/2013	Landsat 8	OLI_TIRS	30	20.90	UTM
21/01/2014	Landsat 8	OLI_TIRS	30	23.35	UTM
18/09/2014	Landsat 8	OLI_TIRS	30	0.27	UTM
24/01/2015	Landsat 8	OLI_TIRS	30	1.55	UTM
26/12/2015	Landsat 8	OLI_TIRS	30	14.86	UTM
29/01/2017	Landsat 8	OLI_TIRS	30	22.63	UTM
31/10/2018	Landsat 8	OLI_TIRS	30	6.42	UTM
05/12/2019	Landsat 8	OLI_TIRS	30	9.84	UTM
06/01/2020	Landsat 8	OLI_TIRS	30	2.18	UTM
23/02/2020	Landsat 8	OLI_TIRS	30	0.30	UTM

For Landsat imagery, the Normalized Difference Water Index (NDWI) has served as a vital tool for distinguishing water bodies from land. Hence, this study will utilize the NDWI to extract the shoreline between the land area of Son Island and the surrounding water. The application of NDWI follows a specified formula [20]:

$$\mathrm{NDWI} = \frac{\mathrm{GREEN} - \mathrm{NIR}}{\mathrm{GREEN} + \mathrm{NIR}} \quad (1)$$

where GREEN refers to the green light channel and NIR refers to the near-infrared channel. For Landsat 5 satellite images, the GREEN channel corresponds to Band 2 and the NIR channel corresponds to Band 4 [21]. Hence:

$$\mathrm{NDWI} = \frac{\mathrm{Band\,2} - \mathrm{Band\,4}}{\mathrm{Band\,2} + \mathrm{Band\,4}} \quad (2)$$

For Landsat 8, the GREEN component corresponds to channel 3, while the NIR component aligns with channel 5 [22]. Therefore, equation (1) becomes:

$$\mathrm{NDWI} = \frac{\mathrm{Band\,3} - \mathrm{Band\,5}}{\mathrm{Band\,3} + \mathrm{Band\,5}} \quad (3)$$

After applying the NDWI index to the Landsat images, the resulting NDWI images will be classified to convert the shoreline into polygons. These polygons will be imported into AutoCAD to calculate the geometric characteristics of Son Island in plan view, such as area and center of gravity coordinates. Figure 2a shows the NDWI image of Son Island and the classification process, while Figures 2b-2d details the classification process.

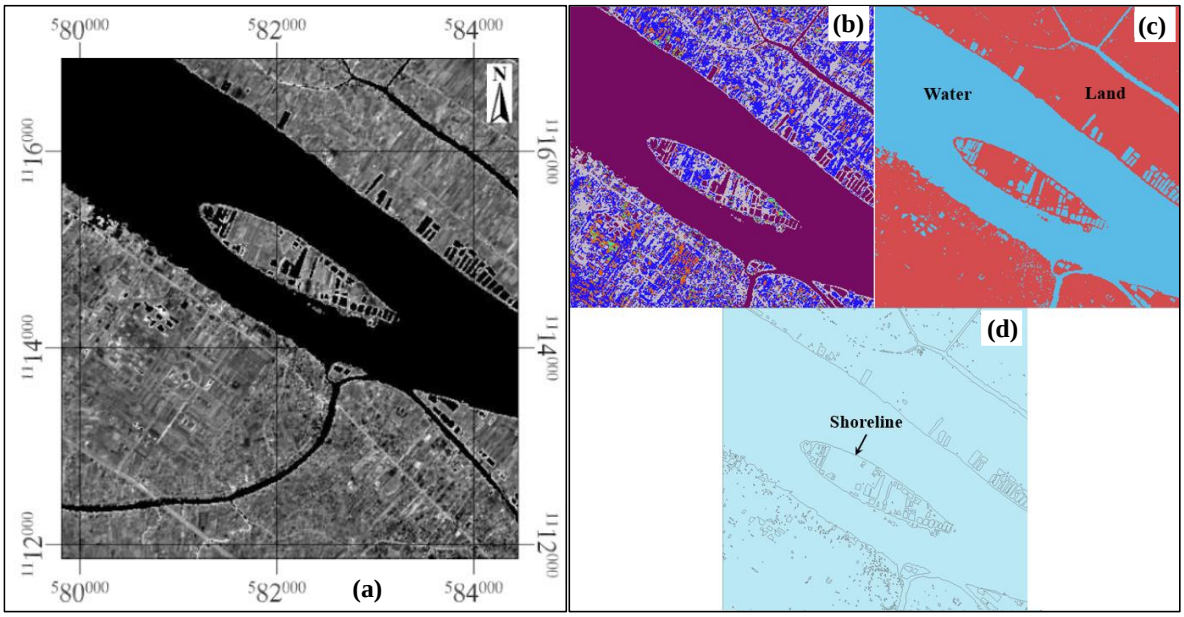

Figure 2. (a) NDWI image of Son Island, (b-d) Classification and shoreline extraction.

2.2. Geometric characteristics of Son Island

In parallel with monitoring the shoreline changes of Son Island, the geometric characteristics of Son Island, such as the center of gravity coordinates and surface area, are also used to analyze the changes of Son Island. The geometric characteristics of Son Island are illustrated in Figure 3.

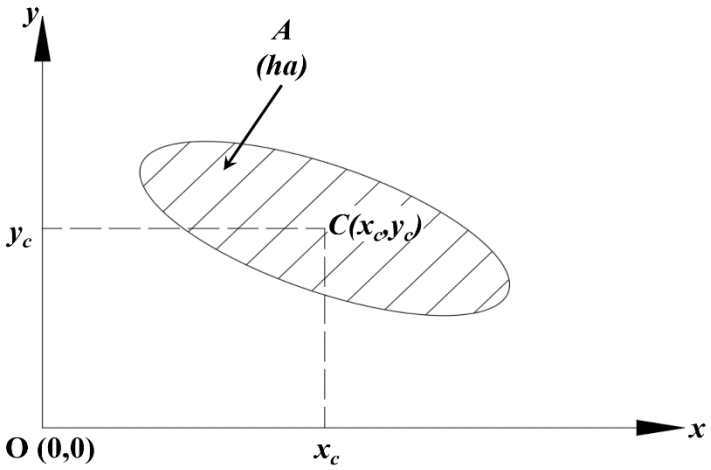

Figure 3. Geometric characteristics of Son Island.

3. Results

3.1. Shoreline changes

Shoreline changes of Son Island from 1987 to 2020 are presented in Figure 4. For readability, only four selected shorelines from 1987, 1995, 2010, and 2020 are shown. As illustrated in the figure, the island migrated approximately 250 meters from 1987 to 2010 due to erosion at the island's head and deposition at its tail. Since 2010, the shoreline of Son Island appears to have stabilized. The development of tourism on Son Island since 2010 may have contributed to this stabilization, as local people have worked to stabilize the riverbank to facilitate tourism.

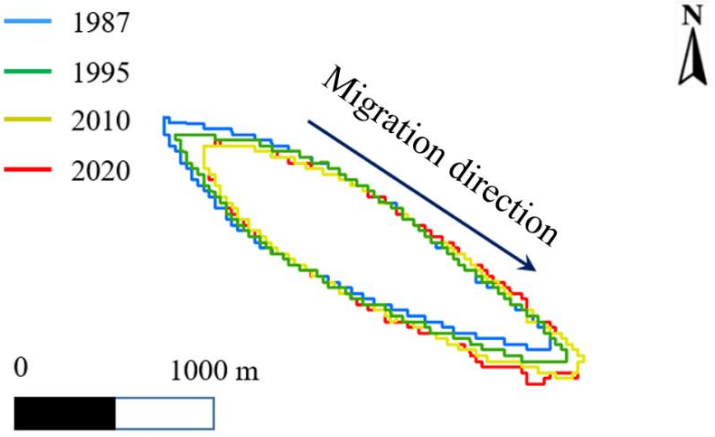

Figure 4. Shoreline changes of Son Island.

3.2. Geometric characteristics of Son Island

The temporal variation of Son Island's area is presented in Figure 5. Although there is significant fluctuation in the area throughout the observed period, there is no clear trend in the variation of the island's area, as indicated by a very small regressor (0.0003). This negligible regressor indicates that the island's area remained stable during the observed period from 1987 to 2020. The significant scatter in the island's area may be a result of errors due to the coarse resolution of the Landsat image, tidal effects, and the appearance/disappearance of vegetation along the riverbanks.

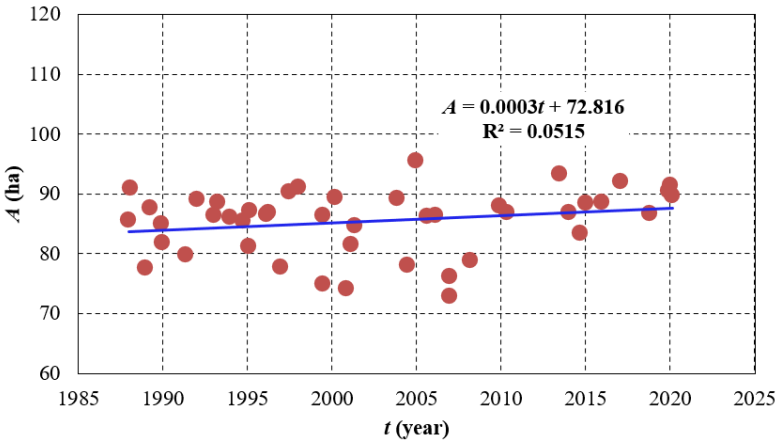

Figure 5. Temporal variation of the Son Island's area.

The figures display the temporal variation of the center of gravity coordinates (x_c and y_c) of Son Island from 1987 to 2020. Figure 6a shows the variation in the x-coordinate (x_c) over time, with blue squares representing the data points and red lines indicating the trend. The first trend line, covering 1987 to approximately 2013, shows a strong positive trend with the equation x_c = 0.024t + 581193 and a high R^2 value of 0.93. From 2013 onwards, the trend line x_c = −0.0003t + 582169 exhibits a near-zero slope and a very low R^2 value of 0.0006, indicating no significant trend. Figure 6b illustrates the variation in the y-coordinate (y_c) over the same period. The first trend line, from 1987 to around 2013, shows a strong negative trend with the equation y_c = −0.0146t + 1E + 06 and an R^2 value of 0.91. Post-2005, the trend line y_c=0.0003t + 1E + 06 has a near-zero slope and an R^2 value of 0.0015, indicating no significant change. These figures suggest that the center of gravity of Son Island shifted significantly in both *x* and *y* directions from 1987 to 2013 but has remained relatively stable since 2013. These results agree well with the shoreline changes mentioned in the previous section.

Table 2. Temporal variation of the center of gravity coordinates (x_c and y_c) of Son Island.

Periods	**1987-2013**		**2013-2020**	
Variables	Regression equation	R^2	Regression equation	R^2
x_c	x_c = 0.024t+581193	0.93	x_c = −0.0003t+582169	0.0006
y_c	y_c = −0.0146t+1E+06	0.91	y_c = 0.0003t+1E+06	0.0015

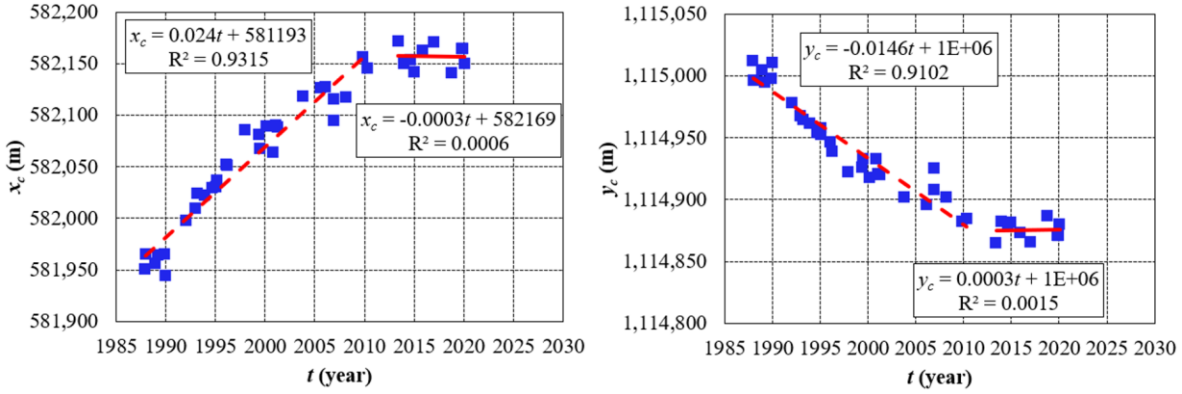

Figure 6. Temporal variation of the Son Island's center of gravity.

4. Conclusions

Remote sensing has been applied to rapidly assess the temporal variation of Son Island on the Bassac River, Can Tho City, Vietnam, from 1987 to 2020. The main findings of this study can be summarized as follows:

- The evolution of Son Island from 1987 to 2020 can be divided into two periods: the first period from 1987 to 2013, during which the island significantly shifted from upstream to downstream by approximately 250 meters; and the second period from 2013 to 2020, which showed the stability of the island with no changes in its area or center of gravity.
- Although there was significant fluctuation in the island's area from 1987 to 2020, there is no obvious trend in the evolution of the island's area, indicating that the island's area remained stable during the observed period. The fluctuation in the island's area can be attributed to errors in image analysis due to the coarse resolution of the Landsat images, tidal effects, and vegetation along the island's banks.
- The migration of Son Island from upstream to downstream is the result of erosion at the island's head and deposition at the island's tail.

Author contribution statement: Developing research ideas: D.V.D.; Process data: processing, manuscript writing: D.V.D., T.M.D.; GIS: D.V.D., T.M.D.; Reviewed and completed the manuscript: D.V.D.

Competing interest statement: The authors declare no conflict of interest.

References

1. Shi, H.; Gao, C.; Dong, C.; Xia, C.; Xu, G. Variation of river islands around a large city along the Yangtze River from satellite remote sensing images. *Sensors* **2017**, *17(10)*, 2213.
2. Liu, X.; Huang, H.; Deng, C. A theoretical investigation of the hydrodynamic conditions for equilibrium island morphology in anabranching rivers. *Adv. Water Sci.* **2014**, *25(4)*, 477–483.
3. Sun, J.; Ding, L.; Li, J.; Qian, H.; Huang, M.; Xu, N. Monitoring Temporal Change of River Islands in the Yangtze River by Remotely Sensed Data. *Water* **2018**, *10(10)*, 1484.
4. Knighton, A.D.; Nanson, G.C. Anastomosis and the continuum of channel pattern. *Earth Surf. Processes Landforms* **1993**, *18(7)*, 613–625.
5. Hooke, J.; Yorke, L. Channel bar dynamics on multi-decadal timescales in an active meandering river. *Earth Surf. Processes Landforms* **2011**, *36(14)*, 1910–1928.
6. Picco, L.; Mao, L.; Rainato, R.; Lenzi, M.A. Medium-term fluvial island evolution in a disturbed gravel-bed river (Piave River, Northeastern Italian Alps). *Geogr. Ann. Ser. A Phys. Geogr.* **2014**, *96(1)*, 83–97.
7. Wu, J.; Fan, M.; Zhang, H.; Shaukat, M.; Best, J.L.; Li, N.; Gao, C. Decadal evolution of fluvial islands and its controlling factors along the lower Yangtze River. *Front. Environ. Sci*. **2024**, *12*, 1388854.
8. Gilvear, D.; Willby, N. Channel dynamics and geomorphic variability as controls on gravel bar vegetation; River Tummel, Scotland. *River Res. Appl.* **2006**, *22(4)*, 457–474.
9. Joeckel, R.; Henebry, G. Channel and island change in the lower Platte River, Eastern Nebraska, USA: 1855–2005. *Geomorphology* **2008**, *102(3-4)*, 407–418.
10. Mani, P.; Kumar, R.; Chatterjee, C. Erosion study of a part of Majuli River-Island using remote sensing data. *J. Indian Soc. Remote Sens*. **2003**, *31*, 12–18.
11. Sadek, N. Island development impacts on the Nile River morphology. *Ain Shams Eng. J.* **2013**, ***4(1)***, 25–41.

12. Wyrick, J.; Klingeman, P. Proposed fluvial island classification scheme and its use for river restoration. *River Res. Appl.* **2011**, *27(7)*, 814–825.
13. Hau, L.P.; Hoang, T.B.; Hung, N.N. River and cannal regulation. Construction Publishing House, Hanoi, 2020, pp. 305.
14. Tu, L.H.; Duy, D.V.; Tri, L.H.; An, N.T.; Minh, H.V.T.; Hong, H.T.C.; Ty, T.V. Analyzing the factors affecting the surface area change of Long Khanh island in Hong Ngu district, Dong Thap province. *VN J. Hydrometeol.* **2021**, *732*, 1–12.
15. Long, V.H.; Giang, N.V.; Hoanh, T.P.; Hoa, P.V. Applying google earth engine in river bank erosion monitoring – A case study in lower Mekong river. *J. Sci.* **2019**, *16(6)*, 38–49.
16. Diep, N.T.H.; Thanh, L.K.; Vinh, L.T.Q.; Minh, V.Q.; Truong, P.N. Progress of landslide situation along Tien and Hau rivers, Mekong Delta. *Can Tho Uni. Sci. J* **2019**, *55*, 125–133.
17. Hoai, H.C.; Bay, N.T.; Khoi, D.N.; Nga, T.N.Q. Analyzing the causes producing the rapidity of river Bank erosion in mekong delta. *VN J. Hydrometeol.* **2019**, *703*, 42–50.
18. Van, T.T.T.; An, N.D.; Nga, T.H.T. Women and rural tourism in the integration context–case study in Con Son, Can Tho. *VNUHCM J. Social Sci. Humanit.* **2020**, *4(4)*, 638–646.
19. Dũ, V.T.; Phương, L.V. Community-based tourism activities in Con Son Island (Mekong Delta- Vietnam) with the issue of preserving cultural and natural values before changes. *Migr. Lett.* **2024**, *21(4)*, 1371–1380.
20. McFeeters, S.K. The use of the normalized difference water index (NDWI) in the delineation of open water features. *Int. J. Remote Sens.* **1996**, *17(7)*, 1425–1432.
21. Ji, L.; Zhang, L.; Wylie, B. Analysis of dynamic thresholds for the normalized difference water index. *Photogramm. Eng. Remote Sens.* **2009**, *75(11)*, 1307–1317.
22. Loveland, T.R.; Irons, J.R. Landsat 8: The plans, the reality, and the legacy. *Remote Sens. Environ.* **2016**, *185*, 1–6.

JOURNAL OF
HYDRO-METEOROLOGY

Research Article

Indicator-based assessment of environmental sustainability of a metalware handicraft village in Hanoi, Vietnam

Nguyen Thi Thuy Hang[1,2], Pham Thu Hien[3], Tran Thi Huyen Nga[3], Nguyen Thi Khanh Huyen[2], Bui Thi Hoa[2], Nguyen Thi Tam Thu[4], Nguyen Thi Hoang Ha[2]*

[1] VNU School of Interdisciplinary Sciences and Arts, Vietnam National University, Hanoi, 100000, Vietnam; ntt.hang@vju.ac.vn
[2] Vietnam Japan University, Vietnam National University, Hanoi, Luu Huu Phuoc, Hanoi, Vietnam; nth.ha@vju.ac.vn; huyenn0707@gmail.com; buihoa.molisa@gmail.com
[3] University of Science, Vietnam National University, Hanoi, 334 Nguyen Trai, Hanoi, Vietnam; phamthuhien_t63@hus.edu.vn; tranthihuyennga@hus.edu.vn
[4] Institute of New Technology, Academy of Military Science and Technology, Hanoi 10072, Vietnam; thu.n3t.cnm@gmail.com

*Corresponding author: nth.ha@vju.ac.vn; hoangha.nt@vnu.edu.vn; Tel.: +84–968046008

Received: 17 August 2024; Accepted: 19 September 2024; Published: 25 December 2024

Abstract: This research was conducted to assess the environmental sustainability of a metalware handicraft village in Hanoi, Vietnam using 17 indicators of 4 components (Environmental systems - S1, reducing environmental stresses - S2, reducing human vulnerability - S3, and social institutional capacity - S4). All indicators were quantified on a scale of 0-1, reflecting a range from low to high sustainability. A combination of soil and water analysis, and a social survey of 67 local households were conducted. The results show that the number of water samples exceeding the allowable limits for wastewater (QCVN 40:2011/BTNMT, Column B), domestic water (QCVN 01-1:2018/BYT), groundwater (QCVN 09:2023/BTNMT), and surface water (QCVN 08:2023/BTNMT, Column B) was 13/14 (NH_4^+), 9/14 (COD), 8/14 (BOD_5), 4/14 (PO_4^{3-}), 5/14 (Fe), and 6/14 (Mn). The concentrations of heavy metals in soil were within acceptable limits for agricultural soil (QCVN 03:2023/BTNMT). The social survey results present high percentages of households dissatisfaction with the quality of air (43%) and water (74.5%), which were also perceived to negatively impact on human health by 67% and 81% of respondents, respectively. The environmental sustainability of the study area is 0.38 (low sustainability) with the following order: S3 (0.25) < S2 (0.26) < S4 (0.44) < S1 (0.57). Solutions on management, policy, and technology are proposed for ensuring environmental sustainability of the metalware handicraft village.

Keywords: Environmental Sustainability; Handicraft village; Indicator; Metalware; Vietnam.

1. Introduction

Handicraft villages play an important role in socio-economic development, livelihood creation, traditionally cultural value maintenance, and tourism promotion in rural areas. Hanoi is home to 1,350 craft villages, of which 305 have been recognized as traditional villages with their own unique identity, producing sophisticated products that reflect the nation's cultural heritage [1]. The products from these craft villages are diverse, have beautiful designs and high quality, and hold competitive advantages in both domestic and

international markets. These products span various sectors, including textiles, ceramics, weaving, embroidery, wooden furniture, mechanics, agriculture, and food processing. However, outdated technology, scattered production, and improper pollutant treatments have posed serious impacts on the environment, ecosystems, and human health [2]. Ensuring environmental sustainability is of great importance which can significantly contribute to food security, human security, and sustainable development [3].

Sustainability refers to the maintenance of core ecosystems and supporting long-term ecological balance while developing the global economy [4]. Several tools and methodologies were developed to evaluate their sustainability performance such as indicators and indices, life cycle sustainability assessment, monetary approach, and integrated assessment [5, 6]. Environmental sustainability was introduced as meeting the resources and services needs of current and future generations without compromising the health of the ecosystems that provide them [7]. Numerous studies have evaluated environmental sustainability in diverse fields, including the digitalization of production [8], the circular economy [9], energy [10, 11], construction [12], and agricultural systems [13]. In which, indicator-based assessment - the most common method for sustainability assessment - is considered as a measure of overall progress toward environmental sustainability, serving as an important tool for evaluating system sustainability, and providing essential information for stakeholders [14]. Some indexes have been widely used for environmental sustainability assessment such as Environmental Sustainability Index (ESI) [15], Environmental Performance Index (EPI) [16]. Driver-Pressure-State-Impact-Response (DPSIR) framework provides an especially effective approach for designing assessments, identifying indicators, communicating results, and supporting environmental monitoring [17–19]. In Vietnam, indicators for environmental sustainability were also mentioned in Decision No. 2157/QĐ-TTg in 2013 [20], Decision No. 2782/QĐ-BTNMT in 2019 [21], and Vietnam Agenda 21 [22]. These indicators were designed for large-scale applications (e.g., regions, countries, provinces, cities, and districts). For smaller scales, especially in craft villages, the sustainability of specific trades and craft villages has also been studied, such as in Minh Hong traditional vermicelli production village [23], Phu Lang pottery village [24], and Dong Ky carpentry village [25]. However, in these studies, environmental sustainability was only mentioned as a sub-criterion within the environmental component, alongside economic, social, cultural, and administrative aspects. In addition, issue-based frameworks were used in which driver and response information for enhancing sustainability may be limited in comparison to the DPSIR framework [26].

This study aimed to assess environmental sustainability of a metalware handicraft village in Hanoi, Vietnam using indicator-based approach. The findings from this research are expected to provide valuable solutions to ensure environmental sustainability in the study area.

2. Materials and methods

2.1. Study area

The metalware handicraft village in this research has started since the 15th century with a total area of 4.65 km^2, of which the percentage of agricultural, specialized-use, residential, and unused land is 63.4%, 19.2%, 16%, and 1.4%, respectively [27]. Up to now, the number of employees in the study area is over 3,000 people and is divided into 2 producing areas, including concentrated production industrial clusters and scattered production households in the village with 428 production facilities and 310 metalworking businesses [27]. The entire production process was firstly handmade with some crude machines and supporting devices. However, at present, high-tech machinery is used to create a wide variety of products with high productivity.

2.2. Methodology

2.2.1. Indicator-based assessment of environmental sustainability

Indicators for environmental sustainability assessment of the metalware handicraft village were proposed mainly based on the Environmental Sustainability Index (ESI) [15] and the Environmental Performance Index (EPI) [16], referring the indicators evaluating the sustainability of specific trades and craft villages [23-25] (Table 1). Selection, adjustment, and addition of indicators were performed following the Bellagio principles for sustainability assessment [26]. A set of 17 indicators belonging to 4 components were introduced including Environmental systems (S1), Reducing environmental stresses (S2), Reducing human vulnerability (S3), and Social institutional capacity (S4) (Table 1).

2.2.2. Sampling and analysis

Field surveys were conducted from May to August in 2024 in the metalware handicraft village for assessing the current status of production activities, society, and environment. Surface soil samples were collected at 0-20 cm depth at 14 points of the gardens and agricultural fields in the study area. Soil samples were then dried in the drying oven at 40°C, sieved through a 2-mm mesh and ground using a HERZOG grinder for further analysis.

A total of 14 water samples were collected including wastewater, surface water, domestic water, and groundwater. The pH value of the water was measured onsite by using the multi-parameter meter HACH HQ30D. The analyses of wastewater, surface water, domestic water, and groundwater were conducted in accordance with guidelines TCVN 5999:1995 [28], TCVN 5994:1995 [29], TCVN 6663-5:2009 [30], and TCVN 6663-11:2011 [31], respectively, and reserved following guidelines TCVN 6663-3:2016 [32]. Concentrations of heavy metals in soil and water were performed by the Plasma Emission Spectrometer (ICP-OES, iCAP PRO X). Nutritional parameters including NH_4^+, PO_4^{3-}, and NO_3^- were measured by the spectrophotometric by UV-VIS Hach Dr6000 (λ = 640 nm), UV-VIS Dynamica Halo RB-10 (λ = 880 nm), and (λ = 415 nm), respectively. Distillation and titration methods SMEWW 5220 C:2017 and SMEWW 5210 D:2017 were used to determine COD and BOD_5 in water, respectively.

Soil and water samples were pre-treated and then analyzed at the Key Laboratory of Geo-environment and Climate Change Response and the Laboratory of Environmental Analysis, University of Science, Vietnam National University, Hanoi and the Institute of New Technology, Academy of Military Science and Technology.

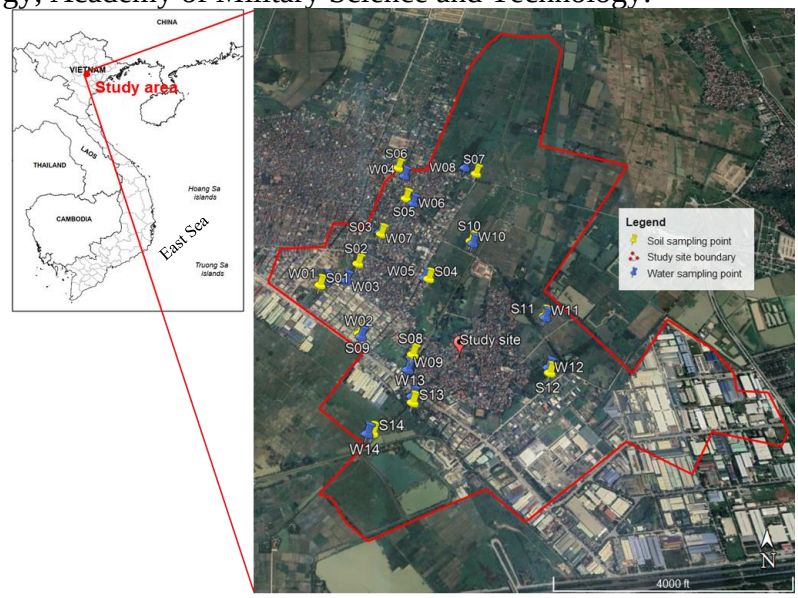

Figure 1. Soil and sampling points in the study area (https://www.google.com/maps/).

2.2.3. Social survey

A semi-structured interview was conducted based on the questionnaire developed from the proposed indicators in Table 1. A total of 67 households in the study area were randomly interviewed to ensure the spatial distribution, production and non-production households, and diversity of livelihoods with the confidence level 90% and margin of error 10% [33].

Table 1. Indicators for environmental sustainability assessment of the metalware handicraft village.

Component	Indicator	Code	Reference	Description	Calculation equation
Environmental systems (S1)	Air quality	S1-1	[15, 16]	The level of people's satisfaction with air quality	1
	Soil quality	S1-2	[15]	Soil quality	3
				The level of people's satisfaction with soil quality	1
	Water quality	S1-3	[15, 16]	Water quality	3
				Water quality index (WQI)	1
				The level of people's satisfaction with water quality	1
	Land resources	S1-4	[15]	The degree of impact of human activities on land resources	2
	Water quantity	S1-5	[15]	The degree of impact of human activities on water resources	2
Reducing environmental stresses (S2)	Reducing air pollution	S2-1	[15, 16]	Increased level of air pollution	2
	Reducing soil stress	S2-2		Increased level of soil pollution	2
	Reducing water stress	S2-3	[15, 16]	Increased level of wastewater	2
				The level of chemical fertilizer use in agriculture	2
				The level of pesticide use in agriculture	2
	Reducing waste discharge pressure	S2-4	[15]	The level of solid waste generation	2
				The level of hazardous waste generation	2
				The level of fossil fuel use for human activities	2
Reducing human vulnerability (S3)	Air quality's impact on health	S3-1	[15, 16]	Assessment of local people about the impact of air quality on health	2
	Soil quality's impact on health	S3-2	[15, 16]	Assessment of local people about the impact of soil quality on health	2
	Water quality's impact on health	S3-3	[15, 16]	Assessment of local people about the impact of water quality on health	2
Social institutional capacity (S4)	Environmental management efficiency	S4-1	[15]	Assessment of local people about environmental management efficiency of local authorities	1
	Wealth	S4-2		Proportion of poor and near-poor households	
	Awareness	S4-3		Awareness about environment protection responsibility	1
	Knowledge	S4-4		The degree of participation in training courses on environmental protection	1
	Environmental protection efforts	S4-5	[15]	The level of environmental protection efforts of local authorities	1

2.2.4. Data analysis

The water quality index (WQI) was calculated following the Decision No.1460/QD-TCMT on Technical Guideline for Calculation and Publication of Vietnam's Water Quality Index [34]. In this study, 3 parameter groups were used for WQI calculation including pH, nutrients (COD, BOD_5, NH_4^+, PO_4^{3-}, and NO_3^-), and heavy metals (As, Cd, Pb, Cr, Cu, and Zn). The data corresponding to the indicators of social survey were coded, normalized by the Min-Max method (on a scale of 0-1) using Eq. (1) and Eq. (2) [23] for positive and negative correlation with environmental sustainability, respectively, and Eq. (3) for analytical indicators.

$$X_{ij} = \frac{X_{ij} - MinX_{ij}}{MaxX_{ij} - MinX_{ij}} \quad (1)$$

$$X_{ij} = \frac{MaxX_{ij} - X_{ij}}{MaxX_{ij} - MinX_{ij}} \quad (2)$$

where x_{ij} represents the normalized value of indicator i of the household j; X_{ij} refers to the value of the indicator i for household j; Max and Min indicate the maximum and minimum scaled values of indicator i, respectively.

$$A = \frac{\text{Number of samples} - \text{Number of polluted samples}}{\text{Number of samples}} \quad (3)$$

Component sustainability and environmental sustainability were calculated by average values of corresponding indicators and components. The scale for environmental sustainability assessment of the metalware handicraft village (on a scale of 0-1) is proposed as follows: unsustainability (0.00-0.20), low sustainability (0.21-0.40), medium sustainability (0.41-0.60), relatively high sustainability (0.61-0.80), and high sustainability (0.81-1.00) [23]. The Analytic Hierarchy Process (AHP) method was used to calculate and analyze the weights, make the pairwise comparison for setting priorities of indicators and categories [35]. The input data for AHP was collected from the structure questionnaire of 9 experts including experts in the field of environment and sustainability (3), local authorities (3), and households in the study area (3).

3. Results and discussions

3.1. Assessment of environmental sustainability of the metalware handicraft village

3.1.1. Environmental systems (S1)

Air quality (S1-1): The interview results show that 43% of households were dissatisfied with the air quality in the study area (Figure 2a). Several reasons were mentioned, including the geographical proximity between the study area and a carpentry village where the production process emits a lot of smoke and dust. In addition, the impact of the local industrial park and a nearby tobacco factory on the air quality in the area was also highlighted.

Soil quality (S1-2): The analytical results of soil in the metalware handicraft village are shown in Table 2. Compared to QCVN 03:2023/BTNMT for agriculture soil [36], soil quality in the study area was within acceptable limits.

Table 2. Concentrations of heavy metals in soils in the metalware handicraft village (mg/kg).

Sampling point	As	Cd	Cr	Cu	Mn	Ni	Pb	Zn
S1	3.59	ND	21.2	13.8	480	10.8	15.4	67.6
S2	0.46	ND	125	22.4	276	20.7	26.5	120
S3	3.95	ND	15.4	11.2	237	10.5	19.4	62.7
S4	4.21	ND	21.2	17.5	192	18.5	30.2	73.5
S5	4.89	ND	18.8	12.4	388	17.4	23.5	88.6
S6	10.4	ND	17.7	29.6	530	21.3	17.7	104
S7	6.76	ND	26.2	14.6	490	24.8	22.8	59.0
S8	4.51	ND	18.4	17.4	226	15.6	24.7	89.3
S9	7.35	ND	18.4	8.0	536	12.0	18.2	47.3
S10	5.01	ND	20.9	20.7	98.2	18.2	20.1	71.4
S11	7.24	ND	24.5	22.8	355	27.4	20.7	59.3
S12	3.13	ND	17.7	19.5	171	15.1	24.0	84.5
S13	3.99	ND	20.1	16.8	322	15.8	20.2	62.9
S14	7.33	ND	20.6	13.7	421	15.5	19.9	119
Average	*5.20*	*ND*	*27.6*	*17.2*	*337*	*17.4*	*21.7*	*79.2*
QCVN 03:2023/BTNMT [36]	25	4	150	150	–	100	200	300

Note: ND: Not detectable

The research area is a low-lying area with 63.4% of its land dedicated to agriculture, primarily for rice and seasonal vegetables, is decreasing in farmland area due to industrial development. According to the interview result, the levels of satisfaction with soil quality

among households were as follows: very satisfied (2%), satisfied (28%), neutral (54%), dissatisfied (12%), and very dissatisfied (4%) (Figure 2b).

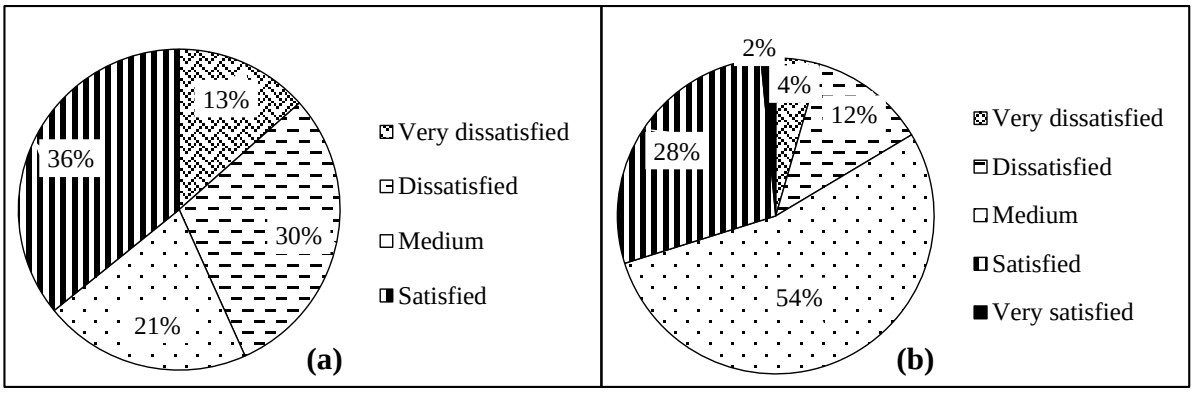

Figure 2. (a) The level of people's satisfaction with air quality; (b) The level of people's satisfaction with soil quality.

Water quality (S1-3): Water quality of the metalware handicraft village including wastewater, domestic water, groundwater, and surface water is shown in Table 3. The analytical results show that COD values in wastewater and surface water ranged within 53-171 mg/L and 26-95 mg/L, respectively. The COD values in surface water were 1.7-6.3 times higher than the QCVN 08:2023/BTNMT (Column B). High BOD_5 values (10-77 mg/L) were also found in all 8 sampling points. High concentrations of NH_4^+ were recorded in 13/14 water sampling points. This result can be explained by NH_4^+ sources such as using chemical NH_4Cl in the plating process (particularly highest in the W1 sample with 33 mg NH_4^+/L), domestic, and agricultural activities. Groundwater and domestic water (tap water) which are pre-treated and supplied by a water supply are also contaminated with NH_4^+, possibly due to the fact that groundwater with high NH_4^+ concentrations is the input water source for the local water supply plant. Some surface water samples collected in the river and lake near paddy field and vegetable gardens (W8, W9, W12, and W14) show that the concentrations of both PO_4^{3-} and NH_4^+ exceeded regulation limitations, implying the possibility of residues of chemical fertilizers. Regarding heavy metals, the concentrations of Fe and Mn found in domestic water (W3), groundwater (W6) and surface water (W9-W14) exceeded the allowable values [38–40]. The concentrations of heavy metals agreed with the village's current status of restricting and removing the plating in the production process, decreasing the discharge of the heavy metal polluted wastewater after plating into the environment.

The water quality index (WQI) was calculated for surface water based on the analytical results of 3 parameter groups: pH, heavy metals, and organic and nutritional parameters [34]. The WQI of the metalware handicraft village is presented in Table 4, ranging within 31-61, indicating the water quality status as moderate (W7, W10, and W11), and poor (W8, W9, W12, W13, and W14). In which, WQI in W8, W9, and W12 were lower than other points because surface water at these points received wastewater from both domestic, production,

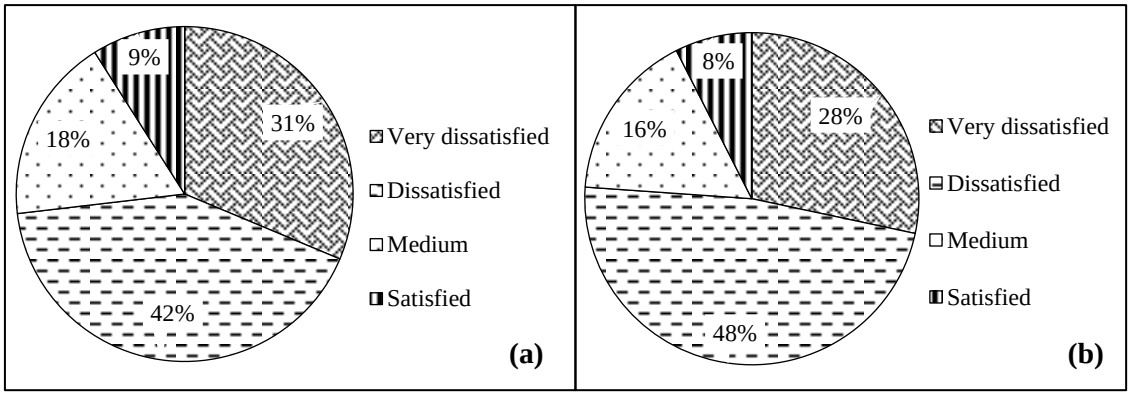

Figure 3. (a) The level of people's satisfaction with drinking water quality; (b) The level of people's satisfaction domestic water quality.

and agricultural activities. According to the report of local authorities in 2023, 83% of households in the metalware handicraft village used tap water supplied by a local water supply plant, while the remaining households still primarily relied on groundwater for their daily needs [27]. However, both groundwater and surface water in the commune have been possibly affected by metalware production activities, livestock farming, and agriculture. As a result, only 9% of residents were satisfied with the drinking water quality (Figure 3a), and 8% were satisfied with the water quality for domestic use (Figure 3b). Most households have installed water filtration systems at home to ensure the water quality before use.

Table 3. Water quality in the metalware handicraft village (mg/L).

	Sampling point	pH	PO_4^{3-}	NO_3^-	COD	BOD_5	NH_4^+	As	Cd	Pb	Zn	Cu	Ni	Fe	Mn	Cr
Wastewater	W1	6.7	0.54	0.18	**171**	10	**32.8**	0.002	0	0.005	0.98	0.004	0.012	2.288	0.125	0.11
	W2	6.7	0.32	0.21	53	14	5.55	0.006	0.001	0.003	0.15	0.005	0.006	0.806	0.388	0.03
	Average	6.7	0.43	0.19	112	12	**19.2**	0.004	0.001	0.004	0.57	0.004	0.009	1.547	0.256	0.07
	QCVN 40:2011[1]	5.5–9.0	6	40	150	50	10.0	0.1	0.1	0.5	3	2	0.5	5	1	1.1
Domestic water	W3	6.5	0.05	1.01	–	–	**1.24**	0.006	0	**0.011**	0.08	0.004	0.004	**0.568**	0.082	0.001
	W4	6.8	0.02	1.21	–	–	**1.04**	0.005	0.002	0.004	0.049	0.005	0.009	0.084	0.017	0.001
	Average	6.6	0.04	1.11	–	–	**1.14**	0.01	0.001	0.01	0.06	0.004	0.007	0.326	0.05	0.001
	QCVN 01-1:2018[2]	6.0–8.5	–	2	–	–	0.30	0.01	0.003	0.01	2	1	0.07	0.3	0.1	0.05
Groundwater	W5	8.3	0.07	2.20	–	–	**4.25**	0.005	0	0.006	0.126	0.002	0.005	0.606	0.055	0.002
	W6	5.7	0.46	2.36	–	–	**5.51**	0.004	**0.01**	0.002	0.047	ND	0.002	**14.2**	0.376	0.008
	Average	7.0	0.27	2.28	–	–	**4.88**	0.005	0.005	0.004	0.087	0.002	0.003	7.42	0.216	0.005
	QCVN 09:2023[3]	5.5–8.5	-	15	–	–	1.00	0.05	0.005	0.01	3	1	0.02	5	0.5	0.05
Surface water	W7	7.9	0.09	0.28	**60**	**24**	**4.19**	0.005	0	0.001	0.023	0.002	0.003	0.576	0.067	0.001
	W8	7.1	**1.97**	0.54	**95**	**77**	**10.01**	0.002	0.001	0.003	0.109	0.004	0.004	0.126	0.053	0.001
	W9	6.8	**0.47**	0.39	**55**	**29**	**6.88**	0.016	0	0.005	0.034	0.003	0.006	0.945	**0.604**	0.001
	W10	6.9	0.14	0.54	**26**	**17**	**3.80**	0.008	0	0.005	0.033	0.003	0.013	**6.157**	**0.562**	0.004
	W11	5.9	0.12	0.70	**28**	**10**	**4.75**	0.006	0	0.003	0.026	0.002	0.005	**3.342**	**0.338**	0.002
	W12	6.0	**0.88**	0.26	**48**	**35**	**8.26**	0.002	0.003	0.004	0.193	0.001	0.011	0.48	**0.379**	0.002
	W13	6.6	0.15	0.68	**67**	**48**	**5.89**	0.004	0	0.002	0.03	0.002	0.002	0.386	**0.138**	0.001
	W14	6.6	**0.92**	0.57	**35**	**14**	**4.87**	0.004	0	0.004	0.022	0.002	0.005	**0.957**	**0.333**	0.002
	Average	6.7	**0.59**	0.49	**52**	**32**	**6.08**	0.006	0.001	0.003	0.059	0.002	0.006	**1.621**	**0.309**	0.002
	QCVN 08:2023[4]	6.0–8.5	≤0.3	≤1.5	≤15	≤6	0.30	0.01	0.01	0.02	0.5	0.1	0.1	0.5	0.1	0.05

Note: Bold values represent concentrations exceeding the allowable standards; QCVN 40:2011[1]: QCVN 40:2011/BTNMT (Column B) [37]; QCVN 01-1:2018[2]: QCVN 01-1:2018/BYT [38]; QCVN 09:2023[3]: QCVN 09:2023/BTNMT [39]; QCVN 08:2023[4]: QCVN 08:2023/BTNMT (Column B) [40].

Table 4. Water quality index (WQI) in the metalware handicraft village.

Sampling point	WQI	Water quality status	Sampling point	WQI	Water quality status
W7	53	Moderate	W11	56	Moderate
W8	31	Poor	W12	36	Poor
W9	36	Poor	W13	46	Poor
W10	61	Moderate	W14	46	Poor

Land resources (S1-4): In the past, most plating wastewater was directly discharged into the environment, with only a small portion collected and treated at the industrial cluster's treatment plant. This wastewater contaminated the soil, impacting agricultural production and reducing crop yields. Over the past decade, increased awareness of the toxicity and pollution from metal plating has led most households in the study area to discontinue this process, resulting in gradual improvements in soil quality. The result of the social survey shows that the impact of the craft village's production on soil quality was rated as very

influential (16.4%), moderately influential (20.9%), slightly influential (50.7%), and not at all influential (16.4%). In addition, according to social surveys, the impact of farming on soils was assessed as very high by 1.5%, high by 41.8%, moderate and low by 23.9% each, and no impact by 9%.

Water quantity (S1-5): Similar to their impact on soil resources, both metalworking and agricultural activities directly affected local water resources. Residents have gradually reduced pollution by using organic chemicals and fertilizers or implementing nature-based agricultural solutions. However, 41.8% of residents thought that metalworking had a significant impact on water resources, while 17.9% believed agriculture had a major effect.

3.1.2. Reducing environmental stresses (S2)

The results of the social survey demonstrate that environmental quality gradually decreased in both air, soil, and water (S2-1, S2-2, and S2-3) because of population growth and expansion of production area. However, 100% surveyed households used chemical fertilizers and pesticides with different frequencies of use, from little to completely. Metalware handicraft village generates solid waste from both domestic activities and production processes. Waste is collected regularly, four times a week, and transported to the landfill, which covers an area of 800m². This system ensures that 100% of residential waste is collected promptly. With the increasing population and expansion of production areas, the social survey shows that solid waste from domestic sources increased by 83.6%, and from production by 53.7% (S2-4). However, some residents reported a decrease in domestic waste (14.9%), and production waste (25.4%), attributing this to improved waste management practices such as sorting, collection, recycling, and reuse at the source. Hazardous waste from production in the study area includes tools, chemical-contaminated rags from plating, welding, and painting processes. However, this waste is not separated, collected, and treated regularly. According to interviews with residents, hazardous waste decreased slightly by 53.7%, significantly by

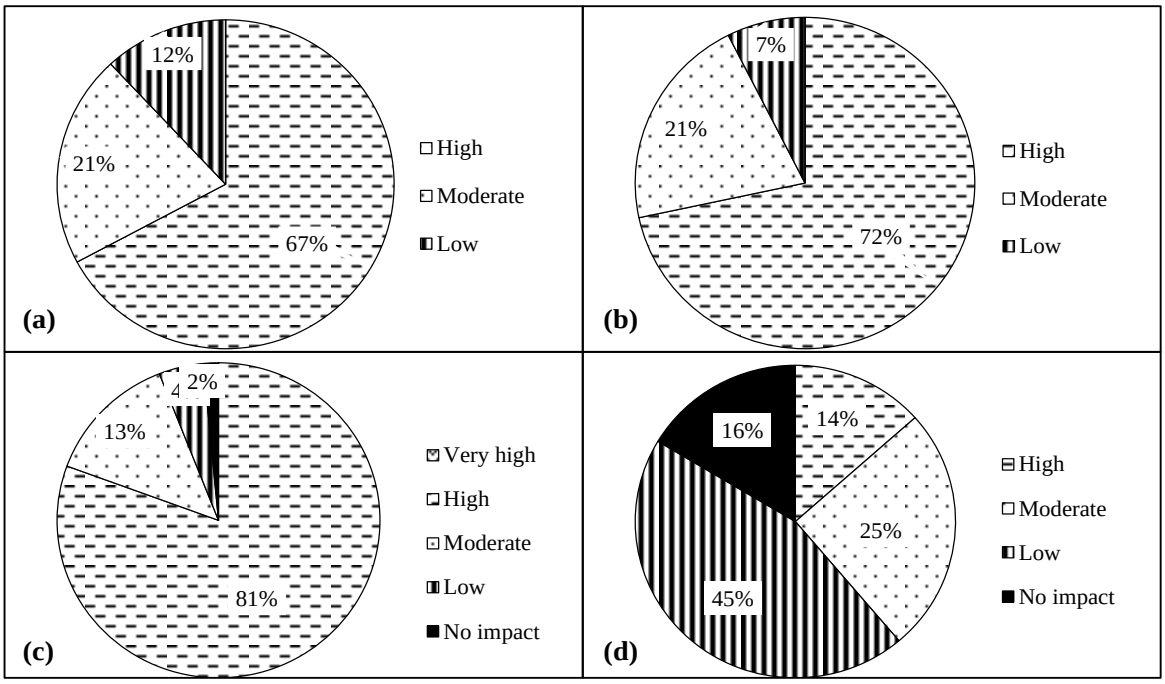

Figure 4. (a) Assessment of local people about the impact of air quality on health; (b) Assessment of local people about the impact of noise on health; (c) Assessment of local people about the impact of water quality on health; (d) Assessment of local people about the impact of soil quality on health.

11.9%, and increased slightly by 28.4% (S2-4). Moreover, along with the advancements in science and technology, production equipment and machinery become more modernized.

High-capacity and electrically-powered devices are replaced by those running on fossil fuels, contributing to a reduction in the local consumption of non-renewable energy.

3.1.3. Reducing human vulnerability (S3)

The result of the social survey shows that the environmental quality affected directly to human health, especially air, noise (S3-1), and water (S3-3) with 67%, 72%, and 81% (Figures 4a-c), respectively, whereas the impact of soil on human health (S3-2) was evaluated as high (14%), moderate (25%), low (45%), and has no impact (16%) (Figure 4d). Noise pollution is a concerning issue in the study area, disrupting the daily lives of non-craft households, and leading to deep environmental conflicts between production and non-production households.

3.1.4. Social institutional capacity (S4)

Environmental management efficiency (S4-1): The social survey results show that persistent conflicts and complaints about the environment and clean water remain unresolved. Community meetings and dialogues are lacking, requiring better coordination among local authorities. According to residents, 6% rated management as very poor, 23.9% as poor, 49.3% as average, and 20.9% as good.

Wealth (S4-2): According to a report of Commune People's Committee, the study site had no household classified as poor, with 134 near-poor households, accounting for 3.78%, a decrease of 1.02% from 2022 [27]. Compared to the national multidimensional poverty rate of 5.71% in 2023, which included 2.93% poor and 2.78% near-poor households [41], the rate in the village is 1.93% lower than the national average.

Awareness (S4-3): The metalware handicraft village lacks an effective centralized wastewater treatment system. Most household wastewater is only pre-treated through basic methods such as septic tanks before being discharged into the environment. The metalware industrial cluster in the study area had a 500 m^2 wastewater treatment plant, operated from 2006 with a capacity of 200 m^3/day. However, the operation of the treatment plant has stopped since 2020. In contrast, all domestic waste is collected and transformed to treat regularly, 4 times per week to ensure the clean environment of residents. For agricultural residues, particularly rice straw, 56.7% of surveyed households have utilized it for organic fertilizer, creating a natural and sustainable source for the next crop, improving soil quality, increasing crop yields, and reducing costs.

Knowledge (S4-4): Interview results show that people have not actively participated in the training courses on environmental protection. Approximately 67.2% of households did not attend any training courses, while 33.8% attended 1-2 times per year.

Environmental protection efforts (S4-5): According to residents, local authorities have gradually paid more attention to environmental protection and have addressed emerging environmental issues. However, there are still delays and obstacles in enforcing environmental regulations, especially concerning craft village production sites. The survey results demonstrate that 26.9% of residents rated the local government's concern for environmental protection as good, 41.8% as average, 20.9% as poor, and 10.4% as very poor.

3.1.5. Environmental sustainability assessment of the metalware handicraft village

AHP results show that the weight of components S1, S2, S3, and S4 was 0.27, 0.26, 0.25, and 0.22, respectively. In detail, indicators of S1-3, S2-3, S3-3, and S4-1 had the highest weight in the components S1, S2, S3, and S4, respectively, indicating the priority for indicators regarding water source and environmental management efficiency of local authorities.

The results of quantitative environmental sustainability assessment of the metalware handicraft village demonstrate that 1/17 indicators are at high sustainability (0.81-1.00) (S4-2), 1/17 indicators are at relatively high sustainability (0.61-0.80) (S1-2), 7/17 indicators are at medium sustainability (0.41-0.60) (S1-1, S1-4, S1-5, S2-4, S3-2, S4-1, and S4-3), 3/17

indicators are at low sustainability (0.21-0.40) (S1-3, S2-3, and S4-5), and 5/17 indicators are classified as at unsustainable (0-0.20) (S2-1, S2-2, S3-1, S3-3, and S4-4) (Table 5). The sustainability of S1, S2, S3, and S4 categories is 0.57, 0.26, 0.25, and 0.44, respectively (Figure 5). The total environmental sustainability of the metalware handicraft village is 0.38, indicating the low sustainability.

Table 5. Environmental sustainability assessment of the metalware handicraft village.

Categories	Indicator	Weighted assessment (Scale 0–1)	Categories	Indicator	Weighted assessment (Scale 0–1)
Environmental systems (S1)	S1-1	0.47	Reducing human vulnerability (S3)	S3-1	0.13
	S1-2	0.80		S3-2	0.54
	S1-3	0.30		S3-3	0.09
	S1-4	0.59	Social institutional capacity (S4)	S4-1	0.54
	S1-5	0.48		S4-2	1.00
Reducing environmental stresses (S2)	S2-1	0.19		S4-3	0.48
	S2-2	0.06		S4-4	0.10
	S2-3	0.32		S4-5	0.36
	S2-4	0.43	**Overall assessment**		**0.38**

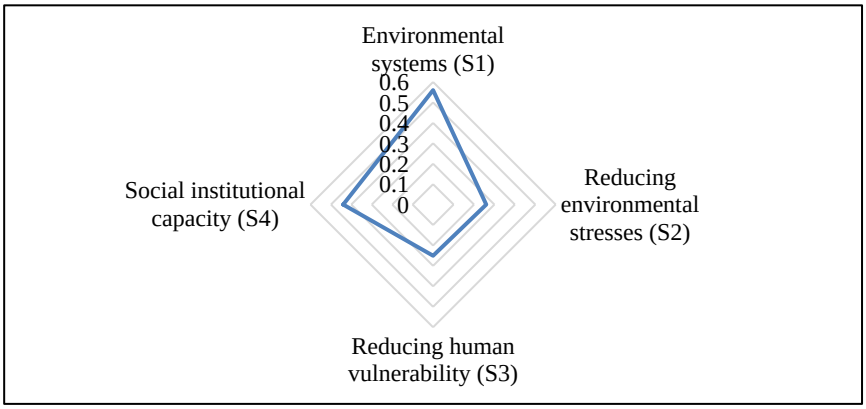

Figure 5. The environmental sustainability of the metalware handicraft village.

3.2. Solutions for enhancing the environmental sustainability of the metalware handicraft village

The study results point out that the environmental sustainability of the metalware handicraft village has faced the high stresses from air, and water pollution, the increasing health risk and the challenges in environmental management and protection of local authorities and residents. Therefore, the following solutions are needed to ensure environmental sustainability in the study area.

3.2.1. Policy

Hanoi has issued various policies not only to develop rural crafts and craft villages [42–45] but also to protect the environment in these areas [46–49]. However, the implementation of these policies in the study area faces many challenges, primarily due to a lack of financial support from local authorities and insufficient community participation. The technical infrastructure in the craft village such as water supply and drainage systems, waste and wastewater treatment remain incomplete, significantly affecting water quality (S1-3) and increasing environmental pressure (S2-2, S2-3, and S2-4). Therefore, investment is needed to improve clean water infrastructure to ensure the quality of domestic water, to construct effective wastewater drainage systems, and to establish waste treatment facilities, along with other

specific infrastructure plans for the village. In addition, monitoring activities for environmental compliance should be strengthened, with strict actions taken against non-compliant production facilities.

3.2.2. Technology

According to analysis results, water quality in the metalware craft village was polluted with PO_4^{3-}, NH_4^+, COD, BOD_5, and heavy metals (i.e., Cd, Pb, Fe, and Mn). Water quality (S1-3) is assessed as low sustainability, the other criteria regarding tresses on air (S2-1) and soil (S2-2) and the impacts of air and water quality on human health (S3-1 and S3-3) are at unsustainability level (Table 5). Therefore, to ensure environmental sustainability in the study area, appropriate technological solutions are proposed as follows: (1) Innovating production equipment from manual to automated systems, using environmentally friendly technology and cleaner production methods to increase productivity, to maximize resource efficiency, to minimize waste generation, and to reduce environmental pollution; (2) Upgrading outdated waste and wastewater treatment systems; (3) Applying more cost-effective and environmental friendly for remediation of contaminated water.

3.2.2. Others

Interview results and environmental sustainability assessment of the metalware craft village indicate that 67% of surveyed households were affected by air quality issues, particularly noise from production, with the indicator S3-1 being evaluated as unsustainable (0.13). Therefore, regulations on production hours are needed to ensure workers' rest, to minimize impacts on neighboring households, and to reduce environmental conflicts. Additionally, air quality is also affected by nearby production activities (carpentry village and industrial park). Therefore, air quality issues require coordinated attention and action from various levels of government and local authorities.

The low percentage of households participating in environmental protection training and unsustainability level of the related indicator (S4-4 = 0.1) imply the necessity to enhance communication, to share information, and to organize environmental protection training sessions effectively to encourage active participation from residents.

Other administrative solutions are recommended such as (1) Control and treat pollution at the source; (2) Develop long-term, medium-term, and short-term environmental protection plans, ensure alignment of goals and available resources; and (3) Strengthen effective collaboration among stakeholders in environmental protection and sustainability maintenance.

4. Conclusions

A set of 17 indicators belonging to 4 components (environmental systems, reducing environmental stresses, reducing human vulnerability, and social institutional capacity) is proposed and applied for quantitatively environmental sustainability assessment of a metalware handicraft village in Hanoi, Vietnam. The results demonstrate that the environmental sustainability of the study area is 0.38, indicating low sustainability. It is crucial to implement measures to promote sustainability in both the metalware village and other craft villages. This result may provide scientific data and solutions for ensuring sustainability not only in the study area but also in other craft villages in Vietnam. This is an initial study that provides a preliminary assessment of environmental sustainability. Further research is needed to quantify air quality parameters, pollution levels, health impacts, and to propose additional indicators for a more comprehensive evaluation of environmental sustainability in the study area.

Author contribution statement: Conceptualization, N.T.T.H., N.T.H.H., T.T.H.N.; Investigation, N.T.T.H.; Sampling, N.T.T.H., P.T.H.; Methodology, N.T.T.H., N.T.H.H., B.T.H.,

T.T.H.N., N.T.T.T.; Data analysis, N.T.T.H., N.T.H.H., T.T.H.N., P.T.H., N.T.K.H.; Writing draft manuscript, N.T.T.H.; Editing manuscript, N.T.H.H., T.T.H.N., B.T.H.; All authors have read and agreed to the published version of the manuscript.

Acknowledgements: The authors would like to extend our sincere thanks to the officers, craft village association and households in the study areas for their valuable support. We are grateful to the Key Laboratory of Geo-environment and Climate Change Response and Laboratory of Environmental Analysis, University of Science, Vietnam National University, Hanoi, and the Institute of New Technology, Academy of Military Science and Technology for their support in the analysis processes.

Competing interest statement: The authors declare no conflict of interest.

References

1. Lan, N.T.M. Hanoi develops traditional craft villages, contributing to the development of cultural industry. *Communist Rev*. **2023**.
2. Nguyen, T.L.; Nguyen, T.B.H., Nguyen, T.H.; Le, V.L.H. Environmental protection policies at craft villages in Hanoi in the context of sustainable development. *E3S Web Conf.* **2021**, *258*, 05014.
3. Lonergan, S. Human security, environmental security and sustainable development. Environment and Security: Discourses and Practices, London: Palgrave Macmillan UK, 2000, 66–83.
4. World Commission on environment and development. Our Common Future Oxford, UK: Oxford University Press, 1987.
5. Ness, B.; Urbel-Piirsalu, E.; Anderberg, S.; Olsson, L. Categorising tools for sustainability assessment. *Ecol. Econ.* **2007**, *60*(3), 498–508.
6. Gasparatos, A.; Scolobig, A. Choosing the most appropriate sustainability assessment tool. *Ecol. Econ.* **2012**, *80*, 1–7.
7. Morelli, P. Environmental sustainability: A definition for environmental professionals. *J. Environ. Sustainability*. **2011**, *1*(1), 1–9.
8. Chen, X.; Despeisse, M.; Johansson, B. Environmental sustainability of digitalization in manufacturing: A review. *Sustainability* **2020**, *12(24)*, 10298. https://doi.org/10.3390/su122410298.
9. Haupt, M.; Hellweg, S. Measuring the environmental sustainability of a circular economy. *Environ. Sustainability Indic*. **2019**, *1*, 100005.
10. Singh, R.; Srivastava, M.; Shukla, A. Environmental sustainability of bioethanol production from rice straw in India: a review. *Renewable Sustainable Energy Rev*. **2016**, *54*, 202-216. https://doi.org/10.1016/j.rser.2015.10.005
11. Jeswani, H.K.; Chilvers, A.; Azapagic, A. Environmental sustainability of biofuels: A review. *Proc. R. Soc. A.* **2020**, *476(2243)*, 20200351. https://doi.org/10.1098/rspa.2020.0351.
12. Opoku, D.G.J.; Ayarkwa, J.; Agyekum, K. Barriers to environmental sustainability of construction projects. *Smart Sustainable Built Environ.* **2019**, *8(4)*, 292–306.
13. Franco, S. Assessing the environmental sustainability of local agricultural systems: How and Why?. *Curr. Res. Environ. Sustainability* **2021**, *3*, 100028.
14. Waas, T.; Hugé, J.; Block, T.; Wright, T.; Benitez-Capistros, F.; Verbruggen, A. Sustainability assessment and indicators: Tools in a decision-making strategy for sustainable development. *Sustainability* **2014**, *6(9)*, 5512–5534.
15. Esty, D.C.; Levy, M.A.; Srebotnjak, T.; de Sherbinin, A. 2005 Environmental Sustainability Index: Benchmarking national environmental stewardship. New Haven. CT: Yale Center for Environmental Law and Policy, 2005.
16. Wolf, M.J.; Emerson, J.W.; Esty, D.C.; de Sherbinin, A.; Wendling, Z.A.; et al. Environmental Performance Index. New Haven. CT: Yale Center for Environmental

Law & Policy, 2022.
17. Centre for Development Finance. Environmental sustainability index for Indian States 2009. XIFRM Research. Institute for Finance Management and Research, 2009.
18. Dong, Y.; Hauschild, M.Z. Indicators for environmental sustainability. *Procedia Cirp*. **2017**, *61*, 697–702. https://doi.org/10.1016/j.procir.2016.11.173.
19. Rivière, C.; Béthinger, A.; Bergez, J.E. The effects of cover crops on multiple environmental sustainability indicators - A review. *Agronomy* **2022**, *12(9)*, 2011. https://doi.org/10.3390/agronomy12092011.
20. Prime Ministry. Decision No. 2157/QĐ-TTg dated November 11, 2013 on promoting a set of indicators for monitoring and evaluating local sustainable development in the period of 2013–2020. 2013.
21. Ministry of Natural Resources and Environment. Decision No. 2782/QĐ-BTNMT dated October 31, 2019 on issuing a set of indicators to assess the environmental protection results of provinces and municipal cities. 2019.
22. Prime Ministry. Decision No. 153/2004/QĐ-TTg dated August 17, 2004 on he Strategic Orientation for Sustainable Development in Vietnam, Vietnam's Agenda 21. 2004.
23. Ha, N.T. H.; Lan, N.D.; Hang, N.T.A. Sustainability of traditional vermicelli production in Minh Hong village, Ba Vi district, Hanoi, Vietnam. *IOP Conf. Ser.: Earth Environ. Sci*. **2019**, *266*, 012015.
24. Nam, T.T. Research on evaluating the sustainability of Phu Lang traditional pottery village, Bac Ninh province in the context of international integration. Master's thesis in Sustainable Science, School of Sciences interdisciplinary and Art, Hanoi National University, 2017.
25. Thien, T.D. Solutions for sustainable development of traditional craft villages - Dong Ky fine art woodworking in the context of urbanization in Tu Son town, Bac Ninh province. Master's thesis in Sustainable Science, School of Sciences interdisciplinary and Art, Hanoi National University, 2023.
26. Wu, J.; Wu, T. Sustainability indicators and indices: an overview. *Handb. Sustainability Manage*. **2012**, 65–86.
27. Commune People's Committee. Report on the results of socio-economic development, security and defense in 2023 and implementing plans for 2024. 2023.
28. Ministry of Science, Technology and Environment of Vietnam. Water quality - Sampling - Guidance on sampling of wastewater (TCVN 5999:1995). 1995.
29. Ministry of Science, Technology and Environment of Vietnam. Water quality - Sampling - Guidance on sampling from natural lakes and man- made lakes (TCVN 5994:1995). 1995.
30. Ministry of Science and Technology of Vietnam. Water quality - Sampling - Part 5: Guidance on sampling of drinking water from treatment works and piped distribution systems (TCVN 6663–5:2009). 2009.
31. Ministry of Science and Technology of Vietnam. Water quality - Sampling - Part 11: Guidance on sampling of groundwaters (TCVN 6663-11:2011). 2011.
32. Ministry of Science and Technology of Vietnam. Water quality - Sampling - Part 3: Preservation and handling of water samples (TCVN 6663-3:2016). 2016.
33. Franklin, I.P. Survey Methods and Practices. Stat. Canada. 2003. ISBN 978-1-100-16410-6.
34. Vietnam Environment Administration. Decision 1460/QD-TCMT on the Issuing of the Technical Guide to Calculation and Disclosure Vietnam Water Quality Index (VN_WQI). 2019.
35. Saaty, T.L. Decision making with the analytic hierarchy process. *Int. J. Services Sci*. **2008**, *1(1)*, 83–98.

36. Ministry of Natural Resources and Environment of Vietnam. QCVN 03:2023/BTNMT: National Technical Regulation on Soil Quality. 2023.
37. Ministry of Natural Resources and Environment of Vietnam. QCVN 40:2011/BTNMT: National Technical Regulation on Industrial Wastewater.
38. Ministry of Health of Vietnam. QCVN 01-1:2018/BYT: National Technical Regulation on Domestic Water Quality. 2018.
39. Ministry of Natural Resources and Environment of Vietnam. QCVN 09:2023/BTNMT: National Technical Regulation on Groundwater Quality. 2023.
40. Ministry of Natural Resources and Environment of Vietnam. QCVN 08:2023/BTNMT: National Technical Regulation on Surface Water Quality. 2023.
41. Ministry of Labor, Invalids and Social Affairs of Vietnam. Decision 134/QD-BLĐTBXH dated January 31, 2024 on announcement of the results of the review of poor households and near poverty households in 2023 according to multidimensional poverty standards for the period of 2022-2025. 2024.
42. Prime Minister. Decree No. 52/2018/ND-CP dated April 12, 2018 on rural industry development. 2018.
43. Prime Minister. Decision No. 801/QD-Ttg dated July 7, 2022 Approving the Program to preserve and develop Vietnamese craft villages in the period 2021 - 2030. 2022.
44. Hanoi People's Committee. Plan No. 67/KH-UBND dated March 3, 2023 on Preserving and developing craft villages and rural industries in Hanoi City in the period of 2023-2025. 2023.
45. Hanoi People's Committee. Plan No. 111/KH-UBND dated April 8, 2023 on Rural Industry Development of Hanoi City in 2024. 2024.
46. Hanoi People's Committee. Decision No. 23/2019/QD-UBND dated October 24, 2019 on Regulations on environmental protection of craft villages in Hanoi. 2019.
47. Hanoi People's Committee. Plan No. 107/KH-UBND dated May 28, 2020 on Support for environmental impact assessment of craft villages in 2020. 2020.
48. Hanoi People's Committee. Plan No. 307/KH-UBND dated December 27, 2021 on strengthening management, inspection, supervision, and prevention of environmental pollution in villages occupations, industrial zones and clusters in the period 2021 - 2025. 2021.
49. Hanoi People's Committee. Decision No. 2546/QD-UBND dated April 28, 2023 on promulgating the List, roadmap and plan for environmental pollution treatment for craft villages in the City Hanoi city to 2025, orientation to 2030. 2023.

JOURNAL OF
HYDRO-METEOROLOGY

Research Article

Integrating UAVs and AI for shrimp pond mapping: A case study in Can Giuoc district, Long An province, Vietnam

Tran Ngoc Huyen Trang[1,2,3]*, Le Van Trung[1,2], Vo Le Phu[1,2]

[1] Faculty of Environment and Natural Resources, Ho Chi Minh City University of Technology (HCMUT); tnhtrang.sdh222@hcmut.edu.vn; volephu@hcmut.edu.vn; lvtrungbk@gmail.com
[2] Vietnam National University Ho Chi Minh City (VNU-HCM); tnhtrang.sdh222@hcmut.edu.vn; volephu@hcmut.edu.vn; lvtrungbk@gmail.com
[3] Department of Geodesy, Cartography and GIS, Ho Chi Minh City University of Natural Resources and Environment; tnhtrang@hcmunre.edu.vn

*Corresponding author: tnhtrang.sdh222@hcmut.edu.vn; Tel.: +84–98615481

Received: 15 August 2024; Accepted: 26 September 2024; Published: 25 December 2024

Abstract: Worldwide, the utilization of Unmanned Aerial Vehicles (UAVs) has been deployed in a wide range of resources management practices. The UAVs serve as valuable and visible tools for managing water resources, forests, agriculture, and land use change. Undoubtedly, the application of UAVs surpasses traditional methods in terms of efficiency, offering significant time and cost savings. Meanwhile, Artificial intelligence (AI) has emerged as a critical technology in the realm of information technology, particularly when it comes to image segmentation. The purpose of this study is to integrate UAVs and AI for mapping shrimp farms in Long An province, Mekong Delta. By leveraging AI, we empower systems to learn intricate image features and subsequently identify and segment objects within those images. In the context of modern agricultural management practices, we leverage UAV imagery as input data for AI systems to identify shrimp ponds, the image recognition platform is Deep Learning (DL) based on U – Net structure. Using the shrimp pond boundary on the 1:1000 scale topographic map as reference data, the results of this method showed a recall of 83.3%, corresponding to a miss rate of 16.7%. The precision of the method was 85.7%, corresponding to a misidentified shrimp pond extraction rate of 14.3%. The results suggest that the combination of UAVs and AI to mapping shrimp farms can facilitate efficient monitoring and management practices for local authorities. Thus, this integration is a promising application to assist and enable agricultural planning and regional economic development activities.

Keywords: UAV; AI; DL; Shrimp pond map.

1. Introduction

Since 1970, the global practices of shrimp farming cultivation have undergone the rapid growth of both area and intensive cultivation. Particularly, Southeast Asia is the most burgeoning region, which remains a dominance of the world's shrimp production [1]. Asian countries collectively contribute approximately 55% to the world's total shrimp exports. Notably, Vietnam stands out as one of the top three shrimp exporters globally, alongside India and Ecuador [2]. Among the top Asian shrimp exporters, India, Vietnam, Indonesia, Thailand, Bangladesh, and China contributed to nearly 92% of the regional shrimp exports [3]. As a part of the Mekong Delta's broader policy, Long An province specifically promoted the transformation of low productive rice-cultivation land into aquaculture areas. The shift of this strategic aims to enhance land utilization efficiency and boost income for the livelihoods

of local households [4]. Simultaneously, this conversion initiative seeks to restructure agricultural production in specific regions and localities, leveraging the unique advantages of specific land areas and natural conditions. The ultimate goal is to foster favorable conditions for sustainable agricultural development [5–6]. Thus, Long An province has chosen shrimp cultivation as one of aquaculture's mainstay to benefit from high-tech production methods during the 2021-2025 period. To enhance production efficiency, Can Giuoc district and the broader province have actively promoted the transition from traditional shrimp practices to high-tech farming approaches. These advanced methods include multi-stage nursery ponds, bottom siphons, bottom oxygen, automatic feeding machines, frequency converters, Biofloc water treatment technology, and microbiological techniques [7].

As high-tech methods revolutionize shrimp farming, modern solutions are also employed to collect, construct, and manage aquaculture map data specifically related to shrimp. This data serves as the foundation for analyzing local climate, soil conditions, and farmers' practices and techniques in shrimp farming. Simultaneously, it plays a crucial role in land management, aligning with state policies [8].

An aircraft that operates without a human pilot onboard is commonly known as An Unmanned Aerial Vehicle (UAV). This kind of facility has evolved significantly over time and now serves a multitude of purposes, from military reconnaissance to civilian applications like aerial photography and environmental monitoring [9]. UAVs are revolutionizing global agriculture by enabling precision management of critical inputs, including the use and type of fertilizers, agrochemicals, and natural resources (soil and water). The impact of UAV applications is far-reaching such as efficiently survey implementation in large areas in a short time, offering real-time solutions through advanced data analytics tools [10]. In fact, UAVs serve as a valuable platform for efficiently managing resources and monitoring the environment, especially in the face of complex challenges posed by rapid changes in anthropogenic activities and climate change effects.

Researchers harnessed multispectral imagery captured by a UAV to monitor the cultivation of *Kappaphycus alvarezii* (commonly known as *Kappaphycus*), a type of seaweed. By estimating fresh weights of seaweed and carrageenan across different days in three cultivation cycles, they derived daily growth rates. The innovative approach of UAVs - a kind of remote sensing facility - performs an amplitude application for precision aquaculture, specifically benefiting *Kappaphycus* cultivation [11]. Due to prominent features, UAVs play a crucial role in aquaculture farm management and monitoring, particularly for offshore cages (floating fish-cage cultivation). Accordingly, UAVs assist to collect data on various parameters such as the quality and pollutants of water, temperature of water bodies, the velocity of water flow, and the behavior of fish. Equipped with sensors and advanced technologies, UAVs can even detect the cages themselves and monitor for illegal fishing activities. This integration of UAVs contributes to a precision aquaculture framework [12–14]. Previous studies have explored the use of UAVs to establish marine ecosystem zoning and create aquaculture status maps. These maps synchronize data, offer valuable information for management, and aid decision-making processes [15–16].

Recent far-reaching developments of artificial neural network, AI has brought a magnitude of its application for various areas. AI refers to the capability of machines to operate independently, without manual guidance. These AI-based systems are typically programmed for automation, and they incorporate human intelligence to make decisions, especially in critical situations [9–10]. The algorithms of image recognition constitute statistical, syntax, and pattern matching data. In recent years, advancements in neural network and support vector machine technologies have propelled image recognition to new heights [11]. Deep learning (DL), a subset of AI, operates through artificial neural networks. It excels at analyzing and processing data, simulating aspects of the human brain [12]. DL architecture encompasses both supervised and unsupervised models. In the supervised realm, different types of DL

were deployed, including recurrent neural networks (RNNs), long short-term memory (LSTM), gated recurrent unit (GRU), convolutional neural networks (CNNs), and generative adversarial networks (GANs). On the unsupervised side, we encounter deep belief networks (DBNs), Deep Transfer Networks (DTNs), Tensor Deep Stack Networks (TDSN), and auto-encoders (AEs). These models play crucial roles in tasks ranging from image recognition to feature extraction [13]. The U-Net is known as a popular architecture of neural network made its debut in 2015 within the medical field. It's a DL framework specifically crafted to maximize efficiency when working with limited data while still achieving impressive speed and accuracy [14]. Accordingly, the U-Net architecture was applied for image segmentation, that features a distinctive design comprising two main components of path: the contracting path and the expansive one. In the contracting path, encoder layers extract contextual information and down sample the input's spatial resolution. In order to decode layers, the expansive path was employed to reconstruct the encoded data, leveraging skip connections that incorporate information from the contracting path. Ultimately, U-Net generates accurate segmentation maps [15]. The U-Net architecture derives its name from its distinctive "U" shape (Figure 1).

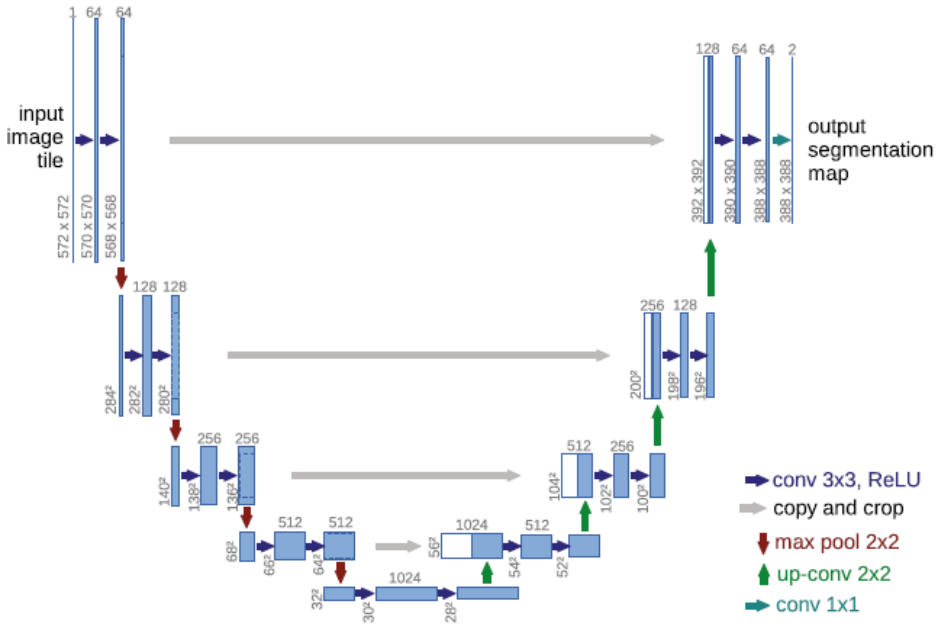

Figure 1. U-net architecture [16].

The study objective is to deploy the integration of UAV and AI for constructing shrimp pond maps with a case of Can Giuoc district, Long An province. In this study, we leverage the U-Net architecture to meticulously segment and distinguish shrimp ponds. The input data comprises processed UAV images, then transformed into detailed image maps.

2. Materials and Methods

2.1. Study area

The study area constitutes two communes (Phuoc Lai and Phuoc Vinh Tay) of Can Giuoc District, Long An province. Can Giuoc District, situated in the south-eastern part of Long An Province, which holds a significant geographical importance since it serves as a gateway to both Ho Chi Minh City and south-western provinces of the Mekong Delta area. The study area lies at approximately 10°36'15" North latitude and 106°41'44" East longitude. Its terrain resembles a river delta near the mouth, characterized by flat expansion intersected by a network of rivers and canals. Notably, 48.34% of the natural area consists of saline and alum soil, making it well-suited for high-yield aquaculture.

Situated along the banks of the Can Giuoc River, the District has emerged as a prominent hub of the provincial brackish water shrimp production. Approximately 90% of shrimp production consists of white-leg shrimp (scientifically known as *Litopenaeus vannamei*). The study area spans approximately 135 hectares and is strategically positioned within a government-invested zone dedicated to advancing shrimp farming by adopting high-tech agricultural practices.

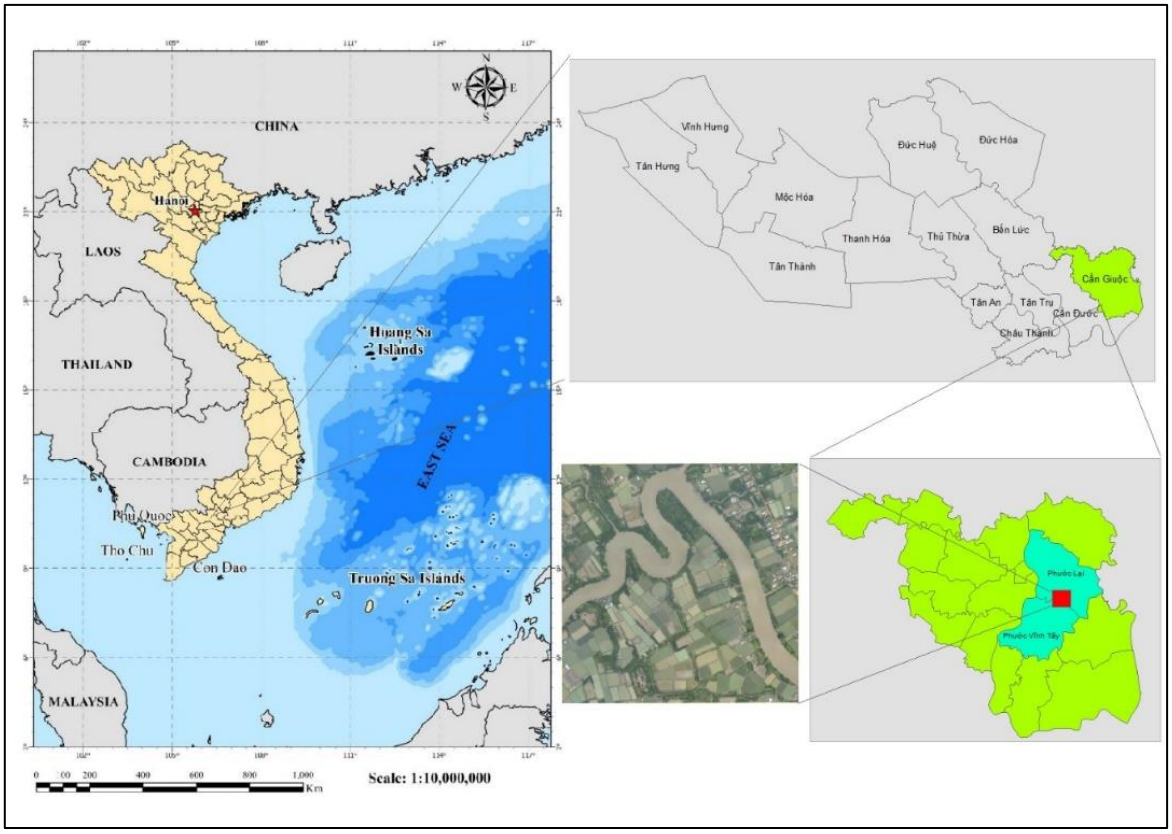

Figure 2. The study area is located between two communes (Phuoc Lai and Phuoc Vinh Tay).

2.2. Data and methods

The data collection process relies on the Trimble UX5 device, a specialized tool with a long history in mapping applications. The UX5 system comprises five key components: the aircraft fuselage, camera, ground control, launcher, and device detector. Notably, the fuselage weighs 2.5 kg, boasts a 100 cm wingspan, and features a wing area of 34 dm² enhancing UAV stability during photo capture (Figure 3a). As for imaging, the Sony A5100 camera plays a crucial role, offering a resolution of 24.3 megapixels (Figure 3b).

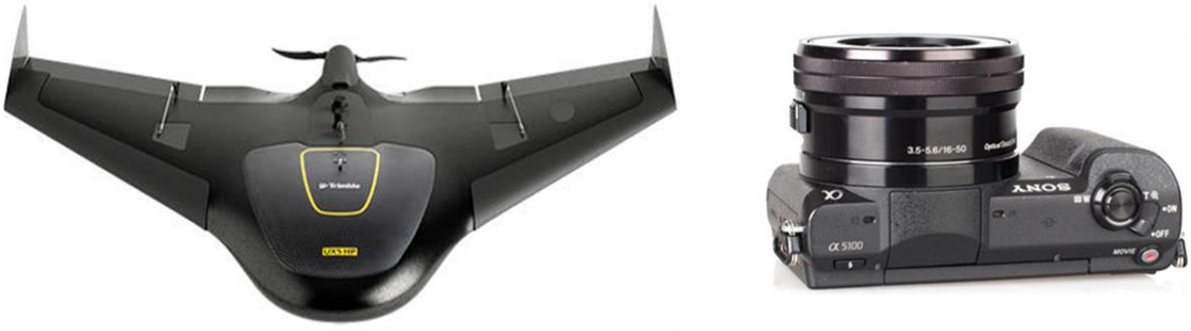

a) UAV UX5 b) Camera Sony A5100

Figure 3. UAV and camera attached to UAV.

The field investigation was carried out on March 30, 2023, in which flights of the UAV took place at 300 m of altitude. For coverage, both overlap tracks of along and across sides were set to 80%. Additionally, the vertical angle during the flight was 90 degrees (Figure 4).

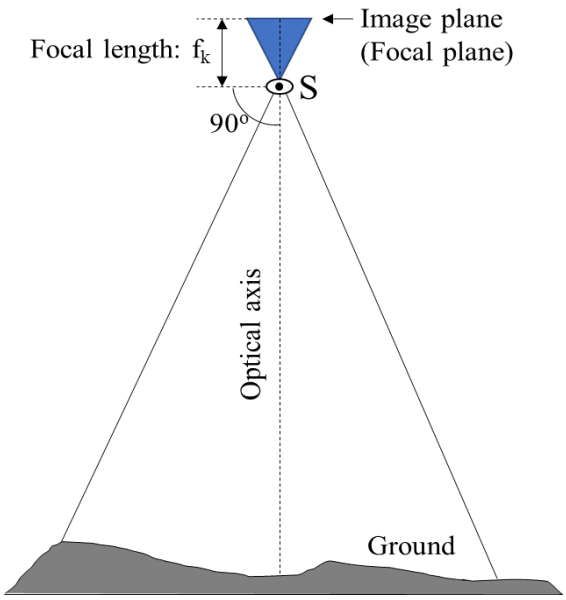

Figure 4. Camera angle is 90 degrees for all photos taken.

The Trimble UX5 utilizes advanced technology of Post Processed Kinematic - Global Navigation Satellite System (PPK GNSS) to precisely determine the location of captured images, resulting in time savings during field operations. Before feeding these images into the image processing software, their locations are adjusted and recalculated for high accuracy. Agisoft Metashape software plays a crucial role in processing the collected data. It takes the raw input and transforms it into the orthomosaic, following the steps as depicted in Figure 5.

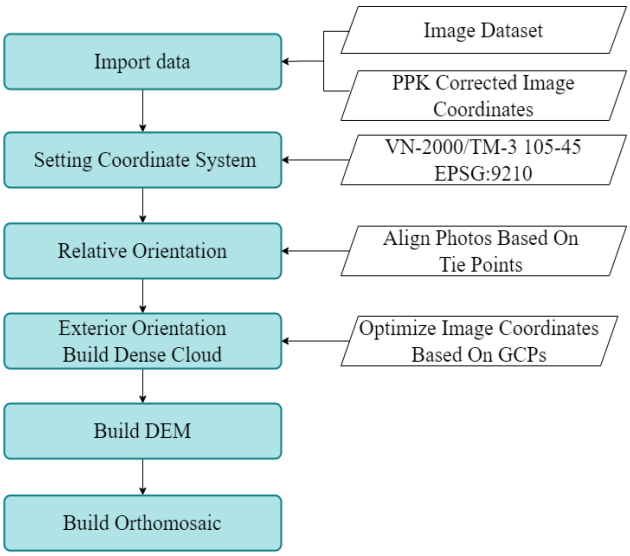

Figure 5. Procedure of image processing.

In this study, the DL model was developed and coded within the Google Colab platform, utilizing Python as the programming language. Google Colab offers access to Graphics Processing Units (GPUs), significantly enhancing model training especially when dealing with large datasets by harnessing the power of the computing cloud.

The process of using a DL model to extract shrimp ponds typically involves three phases. First, there's data preparation, where relevant imagery or data about the ponds is gathered. Next comes model training, during which the DL model learns from this collected data. Finally, model implementation is deployed to analyze new image sets and identify shrimp ponds.

During the data collection phase for shrimp pond mapping with DL, several key steps are involved. First, unprepared image data is gathered, including data captured by UAVs in the project area and other available sources. Next, preprocessing steps are performed to standardize image sizes and remove noise. The dataset is then enriched by incorporating algorithmic variables. Subsequently, the data image set is categorized into training and test data. The dataset is essential to training the DL model, while a data checker evaluates optimal values and parameters within the model (Figure 6).

In the module training phase, several key steps are involved. First, the processed dataset is assigned to the DL model using a U-Net architecture. Next, the output data is evaluated after the model is applied to the input dataset. The training dataset plays a crucial role in training the DL model. Additionally, during this step, optimization functions are tested to select the optimal parameters for enhancing the model's performance.

The model implementation phase involves several critical steps. First, the output data from the optimized DL model is digitized. Next, this digitized data is synchronized with the

web application's database, where it undergoes processing and storage either on an on-premises server or in the cloud. Finally, a web application is created to facilitate end users' access to and modeling of map data. In our study, we structure the output data in two formats: raster and shapefile with polygon geometry. These formats allow us to represent spatial information effectively. Additionally, we link the results to background data available on the web. This preliminary verification process ensures the correctness of the coordinate system alignment and the accurate classification of characteristic objects.

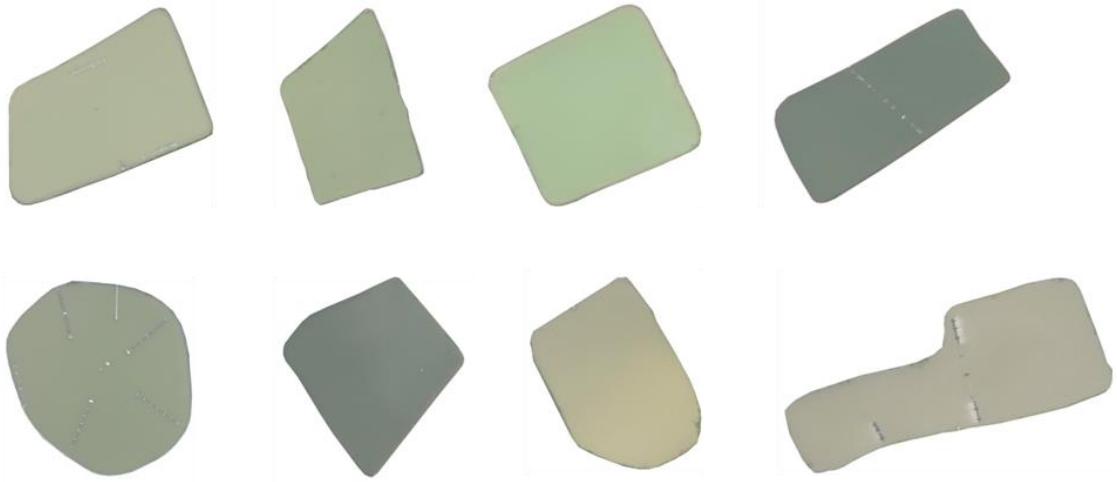

Figure 6. Different data samples of shrimp ponds.

The confusion matrix is like a trusty compass for data scientists and DL enthusiasts. It helps us navigate the performance of our models when dealing with segmentation tasks (like identifying objects within an image) or distinguishing between different classes (such as "cat" vs. "dog") (Figure 7).

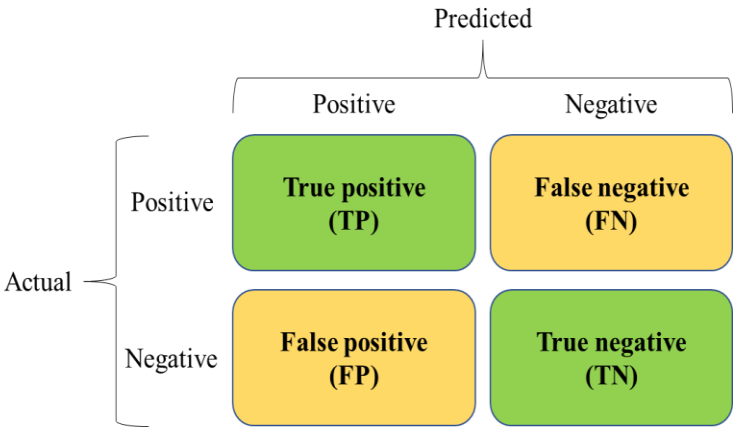

Figure 7. Confusion matrix.

The results of shrimp ponds recognition and classification from the DL model are evaluated through the parameters of precision and recall. Each evaluation parameter will have different meanings and serve different purposes. The formula for evaluating these parameters is shown as follows:

$$\text{Precision} = \frac{TP}{TP + FP} \quad (1)$$

$$\text{Recall} = \frac{TP}{TP + FN} \quad (2)$$

3. Results

3.1. Identification of shrimp ponds using AI (DL)

After the DL model processes the data, the resulting output is transformed into a shapefile format (specifically, a polygon format). This shapefile is then uploaded to OpenStreetMap an excellent resource that combines features of a free and open website, an online map, a search engine, and a geodata editor. After uploading, the Shapefile data can be downloaded and further processed using ArcGIS software on a personal computer.

The verification dataset comprises a 1:2000 scale topographic map generated from UAV images. Technicians manually digitized the data layers on this map, which was officially accepted in 2023. To assess the performance of the DL model, the hydrological layer containing shrimp ponds from the topographic map was overlaid with the DL-generated shrimp pond data. A confusion matrix was then constructed by using this combined dataset to evaluate the model's accuracy (Table 1).

Table 1. The confusion matrix with data evaluation values of DL model for shrimp pond.

Topography map	Predicted based on DL	
	Shrimp Pond	Other
Shrimp Pond	204 (TP)	41 (FN)
Other	34 (FP)	10 (TN)

Using formulas (1) and (2) we can calculate the following results: Precision = 85.7%; Recall = 83.3%.

The detection and extraction of shrimp ponds from the DL model achieved a precision of 85.7%, showing that out of 238 shrimp ponds extracted by DL, 204 were correct, and the remaining 34 were mistakenly identified. The reason for the mistake was the similarity in shape and color between shrimp ponds and rice fields that had not been sown or had newly grown rice plants that were still very small (Figure 8).

a) Shrimp pond b) Rice paddy field

Figure 8. Similarity in shape and color between shrimp pond and rice paddy field.

The recall of the DL model when identifying shrimp ponds is 83.3%, showing that out of 245 shrimp ponds on the topographic map, DL correctly identified 204 shrimp ponds, while the remaining 41 shrimp ponds were missed and could not be identified by the DL model. This shortcoming comes from the fact that the actual shrimp ponds at the time of taking the photos were abandoned, leading to water drying up and weeds covering the ponds (Figure 9).

a) Abandoned shrimp pond on UAV images b) Shrimp pond in totographic map

Figure 9. Similarity in shape and color between shrimp pond and rice field.

3.2. Shrimp pond map editor

In the study area, the shrimp ponds exhibit consistent shapes. Their total area amounts to 42.4 hectares, which corresponds to 31.4% of the entire area (135 hectares). On average, each shrimp pond covers 1843.8 m^2. Interestingly, there's one pond specifically designed in a circular shape for shrimp larval cultivation.

In the center of this area lies the Rach Van River, dividing it between the two communes (Phuoc Lai and Phuoc Vinh Tay). The meticulously edited map of shrimp ponds is rendered at a scale of 1:5000 (Figure 10). Amidst this landscape, scattered rice fields dot the terrain some still under cultivation, while others lie abandoned due to the challenges of low rice productivity.

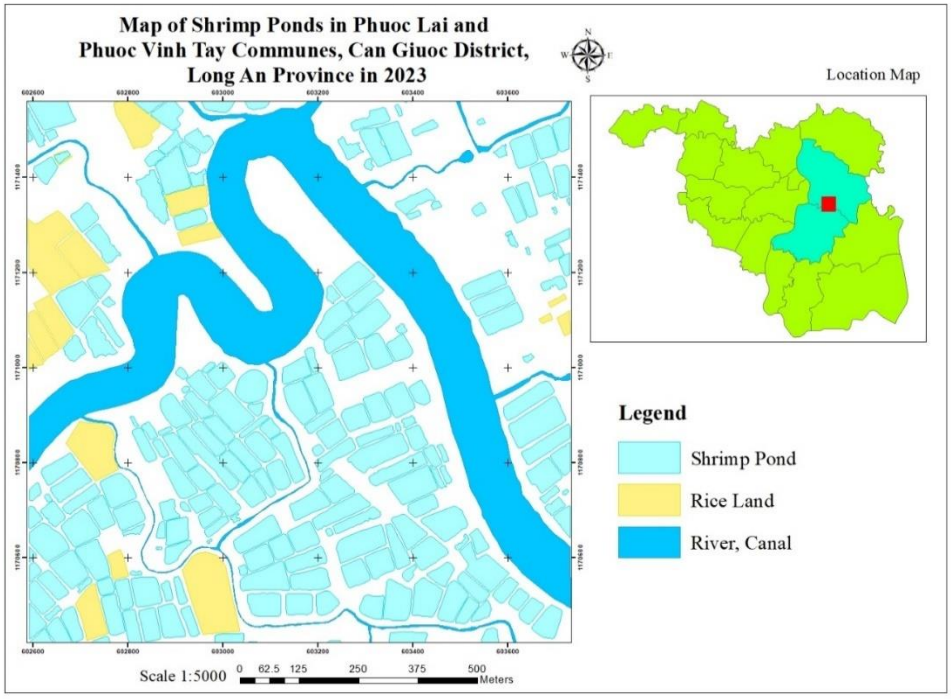

Figure 10. Map of Shrimp Ponds in two communes (Phuoc Lai and Phuoc Vinh Tay) in 2023.

4. Discussion

In our study, we employed DL technology based on the U-Net architecture to extract shrimp ponds. The achieved accuracy of 85.7% and recall of 83.3% is commendable, although it falls short when compared to previous studies focused on object extraction. Notably, Farajzadeh and colleagues successfully extracted building footprints with an impressive accuracy of 97% and a recall of 91% [25]. The key lies in the distinct features of buildings clear shapes and colors which facilitate their recognition. Additionally, Farajzadeh et al. leveraged a combination of orthomosaics and Digital Surface Models (DSMs), where buildings of varying heights were represented in different colors. This approach led to highly accurate and well-recalled building footprint extraction, minimizing misclassification and omission.

During our study, we encountered an important consideration when extracting shrimp pond boundaries: situations where the waterline and the actual shrimp pond boundary do not align perfectly. Dry ponds, in particular, exhibit this discrepancy, which can lead the DL model to mistakenly identify the waterline as the pond boundary (Figure 11). To address this, specific parameters must be fine-tuned for the DL model when identifying shrimp ponds in such cases.

Another challenge arises when extracting shrimp ponds using DL: the robust growth of trees within these ponds. Sometimes, trees can obscure parts of the pond boundaries,

complicating the extraction process (Figure 12). To address this issue, field investigations and surveys become essential for making accurate adjustments.

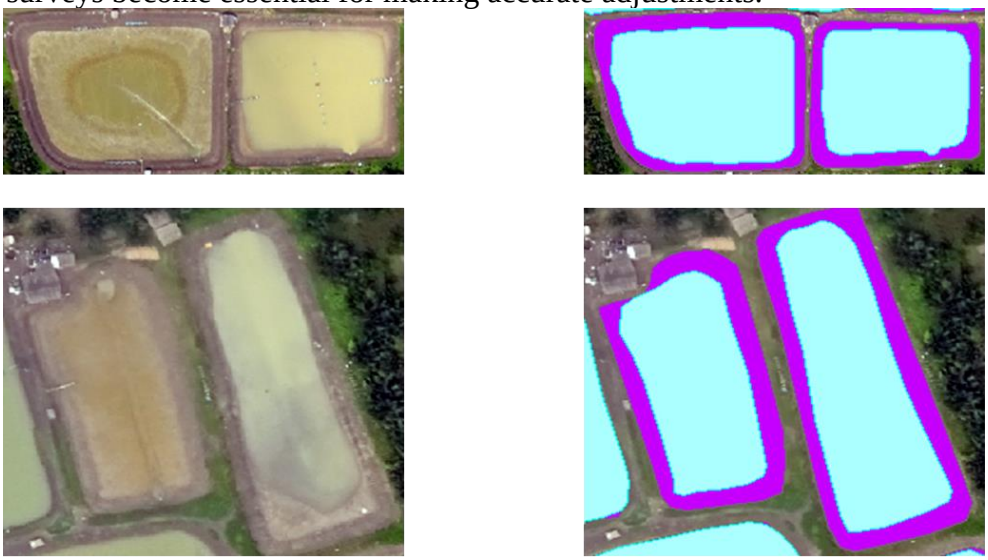

a) Shrimp Ponds in UAV images

b) Shrimp Ponds (Blue green pastel polygon is the pond created by DL, the dark violet polygon is the pond on the topographic map

Figure 11. The waterline and the shrimp pond boundary do not coincide.

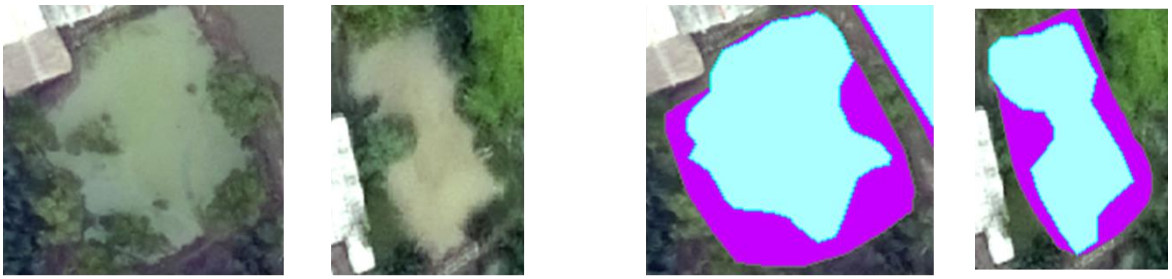

a) Shrimp Ponds in UAV images

b) Shrimp Ponds (Blue green pastel polygon is the pond created by DL, the dark violet polygon is the pond on the topographic map

Figure 12. Shrimp pond boundary covered by vegetation.

5. Conclusion

AI is gradually becoming familiar in various fields. When we use DL technology with image recognition, it significantly reduces the need for manual digitization, ultimately saving valuable time and effort.

In our research, achieving an accuracy of 85.7% and a recall of 83.3% for shrimp ponds extraction is a positive outcome. It underscores the successful synergy between remote sensing technology particularly utilizing UAV images and AI techniques. Notably, this approach isn't limited to shrimp ponds alone; it holds promise for creating other thematic maps as well.

However, there is no coincidence of waterline and shrimp pond boundary or shrimp pond boundary covered by vegetation. These are the problems that this study encountered, making it difficult for the DL model to accurately segment the image. Future studies on this hurdle should be made to improve precision.

To enhance work efficiency, we recommend combining the U-Net architecture with other neural network architectures within the DL model. Additionally, if feasible, leveraging multispectral data collected from UAVs as input material for the DL image recognition model

holds great promise. This approach can lead to more accurate and comprehensive results in identifying and mapping features like shrimp ponds.

Authors' contribution: Conceptualization: T.N.H.T., V.L.P.; Methodology: L.V.T., T.N.H.T.; Data collectiong and processing: T.N.H.T.; Writing - original draft: T.N.H.T., V.L.P., L.V.T.; Writing, reviewing and editing: T.N.H.T., V.L.P.

Declaration: The authors declare that there is no conflict of interest among them. This article is the findings of their own studies, not previously published elsewhere, and not copied from previous studies.

Acknowledgements: We would like to express our thankfulness to Ho Chi Minh City **University** of Technology (HCMUT), VNU-HCM for the support of time and facilities for this study.

References

1. Mônica, C.S.; Paloma, de M.; Pedro, E.S.L.; Antonio, D.P. Shrimp farming in coastal Brazil: Reasons for market failure and sustainability challenges. *Ocean Coastal Manage*. **2011**, *54(9)*, 658–667.
2. The Observatory of Economic Complexity (OEC). Shrimps and prawns, frozen. 2021.
3. Md. Akhtaruzzaman, K.; Md. Emran, H.; Md. Sayemul, I.; Md. Takibur, R.; Madan, M.D. Shrimp export competitiveness and its determinants: a novel dynamic ARDL simulations approach. *Aquacult. Econ. Manage*. **2022**, 1–28.
4. Pavan, K.B.; Murali, K.G.; Pranay, P.; Ismail, M.; Aya, S. Mapping shrimp pond dynamics: A spatiotemporal study using remote sensing data and machine learning. *Agri. Eng*. **2023**, *5*, 1432–1447.
5. Sharmin, A.; Md. Sadique, R.; Shopna, A.; Shirajum, M.; Tahrima, H.B. Factors driving the shifting of land from rice to aquaculture farming in Bangladesh. *J. Agribus. Rural Dev*. **2023**, *4(70)*, 369–377.
6. Ha, T.T.T.; Simon, R.B. Transformations of Vietnamese shrimp aquaculture policy: Empirical evidence from the Mekong Delta. *Environ. Plann. C Gov. Policy* **2010**, *28(6)*, 1101–1119.
7. Zulkarnain, R.; Adiyana, K.; Nugroho, H.; Nugraha, B.; Thesiana, L.; Supriyono, E. Selection of intensive shrimp farming technology for small farmers with analytical hierarchy process: a case for whiteleg shrimp (Litopenaeus vannamei). *IOP Conf. Ser.: Earth Environ. Sci*. **2020**, *404*, 1–8.
8. Min-Chie, C.; Wei-Mon, Y.; Showkat, A.B.; Nen-Fu, H. Development of smart aquaculture farm management system using IoT and AI-based surrogate models. *J. Agric. Food Res.* **2022**, *9*, 1–11.
9. Rohit, C.; Vandana, M. Unmanned aerial vehicles for Internet of Things (IoT): Concepts, techniques, and applications - Chapter: Unmanned aerial vehicle (UAV): A comprehensive survey. Wiley online library, 2021.
10. Amresh, C.; Singh, R.N.; Vikas, K.R.; Saurabh, K.D.; Kavita, K. Soil science: Fundamentals to recent advances – Chapter: Introduction to drone technology for natural resource management in agriculture. Springer, 2021.
11. Nurjannah, N.; Evangelos, A.; Rajuddin, S.; Hasni, A.; Elmi, N.Z.; Agus, A.; Simon, O.; Guillaume, B.; Teruhisa, K.; Laurent, B. Precision aquaculture drone mapping of the spatial distribution of Kappaphycus alvarezii Biomass and Carrageenan. *J. Remote Sens.* **2023**, *15(3674)*, 1–21.
12. Sheng-I, C.; Jih-Gau, J. UAV control based on pattern recognition in aquaculture application. *Aerospace* **2024**, *11(302)*, 1–33.

13. Naomi, A.U.; Shyi-Chyi, C. A Review of unmanned system technologies with its application to aquaculture farm monitoring and management. *Drones* **2022**, *6(12)*, 1–41.
14. Wei-Yi, L.; Jih-Gau, J. Application of image identification to UAV control for cage culture. *Sci. Prog*. **2022**, *105(4)*, 1–38.
15. Khang, N.H.T.; Duong, N.T.T.; Thi, T.T.Q.; Tien, N.M.; Chung, T.V.; Nguyen, C.V. Research on the application of UAV technology in establishing aquaculture status maps: Experiment at Hon Yen population, Phu Yen province. *Duy Tan University Sci. Technol. J*. **2022**, *4(53)*, 23–30.
16. Doi, N.T.; Xuan, N.H.; Tu, N.A.; Nghi, D.T. Application of unmanned aerial vehicles (UAV) for monitoring coastal ecosystems: a study at Hon Yen Group, Phu Yen Province. National scientific and technological conference "Research on application and development of national geospatial data infrastructure: The role of modern mapping technology". 2021, pp. 187–199.
17. Subarna, S. Analysis of artificial intelligence based image classification techniques. *J. Innovative Image Process* **2020**, *2(1)*, 44–54.
18. Ritica, T.; Manekar, V.L. Artificial intelligence-based image classification techniques for hydrologic applications. *Appl. Artif. Intell*. **2022**, *36(1)*, 1138–1156.
19. Xi, Z. Application of artificial intelligence recognition technology in digital image processing. *Wireless Commun. Mobile Comput*. **2022**, *3*, 1–10.
20. Aya, H.M.; Moatamed, R.; Ashraf, M.H. Image classification based deep learning: A review. *Aswan University J. Sci. Technol*. **2022**, *2(1)*, 11–35.
21. Babita, P.; Devendra, P.; Brijendra, P.M.; Wasiur, R. A comprehensive survey of deep learning in the field of medical imaging and medical natural language processing: Challenges and research directions. *J. King Saud Univ. Comput. Inf. Sci*. **2022**, *34(8)*, 5083–5099.
22. David, G.; Miljana, H.; Danesh, A.; April, K.; Umberto, B. A U-net convolutional neural network deep learning model application for identification of energy loss in infrared thermographic images. *Appl. Energy*. **2024**, *360*, 1–15.
23. Nahian, S.; Paheding, S.; Colin, E.; Vijay, D. U-Net and its variants for medical image segmentation: Theory and applications. *IEEE Access*. **2021**, *9*, 82031–82057.
24. Olaf, R.; Philipp, F.; Thomas, B. U-Net: Convolutional networks for biomedical image segmentation. Proceeding of Medical Image Computing and Computer-Assisted Intervention - MICCAI 2015, 2015, pp. 234–241.
25. Farajzadeh, Z.; Saadatseresht, M.; Alidoost, F. Automatic building extraction from UAV-based images and DSM using deep learning. *ISPRS Ann. Photogramm. Remote Sens. Spatial Inf. Sci. GeoSpatial Conf.* **2022**, *X(4)*, 171–177.

JOURNAL OF
HYDRO-METEOROLOGY

Research Article

Saltwater damage in the Vietnamese Mekong Delta: A case study of agricultural livelihoods in Hung My commune, Tra Vinh province

Hung Tan Nguyen[1], Van Hiep Huynh[2]*, Kiet Anh Ly Ngo[1]

[1] Sustainable Urban Development (SUD) program - Vietnamese German University (VGU); hung.nt@vgu.edu.vn; anhkietqh05@gmail.com
[2] Department of Civil Engineering, School of Engineering and Technology, Tra Vinh University; hvhiep@tvu.edu.vn

*Corresponding author: hvhiep@tvu.edu.vn; Tel: +84–963887689

Received: 20 August 2024; Accepted: 26 September 2024; Published: 25 December 2024

Abstract: This study examines the considerable impact of Saline Intrusion (SI) on the livelihoods of households (HH) in Vietnam's Mekong Delta (VMD) which is main rice production powerhouse of the country. As a notable occurrence in the region, its damage has been evaluated through both quantitative and qualitative approaches. The principal conclusions are to the identification of capital elements via the examination of sustained damage and resilience in addressing forthcoming crises. The analysis of gathered data has shown the growing threat to the estuary's agricultural output caused by the incursion of SI. This has particularly affected food production, which is a crucial and longstanding industry in the VMD's economy. Therefore, it is essential to prioritize the implementation of sustainable agricultural practices and develop ways to bolster resilience, which includes enhancing disaster preparedness and promoting sustainable livelihoods. This paper means to setup precedent for future studies, advocating for the inclusion of socioeconomic and ecological factors in policy framework development to mitigate the risks posed by environmental alteration and improve the resilience and adaptability of impacted farmers.

Keywords: Salinity intrusion; Agriculture base; Loss threshold; Household livelihoods; Resilience quality; Adaptive capacity.

1. Introduction

In recent decades, the repercussions of climate change on the environment and humanity have arisen as among the most significant topics of discussion and concern on the international policy agenda [1–3]. A contemporary critical submission, the fifth evaluation publication of the Intergovernmental Panel on Climate Change (IPCC) of the United Nations addresses the devastating impacts of the changing climate on economic sectors such as agribusiness [4, 5]. Southeast Asia's economic output would be marginally impacted by a decline in agricultural productivity [6], given the predicted reduction of the agricultural segment [7, 8]. According to Ministry of Agriculture and Rural Development (MARD), the VMD is a significant rice-producing in the region [9, 10], contributing 18 percent to the overall Vietnam's GDP [11, 12]. However, this area is threatened by the effects of climate crisis and its implications, as the intensity of such crisis has grown over the past decade [13–16]. SI, which closely relates to this dire environmental disaster, is a natural phenomenon caused by water scarcity, upstream dam activity, and rising sea levels [17–20]. This situation has drastically influenced the likelihood of people across the delta, resulting in considerable

losses to material and ecological resources, along with negative impacts on finances, social structure, and communities. In 2016, a vast expanse of rice and aquaculture land, exceeding 215,000 and 68,000 hectares respectively, was profoundly affected by severe drought and salt intrusion, leading to an estimated economic loss of approximately 7,517 billion VND across nine provinces and one municipality in the estuary [14]. In 2020, 685,558 people, 130 thousand of whom were children, were exposed to several health risks, including inadequate drinking water and poor cleanliness [17]. Many men in their working ages have moved to nearby provinces or HCMC to trade their labor in the low-skilled industries as they were said to repay debts from the previous drought-related saltwater intrusion [21]. Furthermore, these adverse outcomes have directly impacted the livelihoods of the residents not only on economic terms but also in land planning level [22], particularly those involved in farming and ranching practice [23, 24]. Consequently, policymakers and scholars have emphasized the investigation of climate variability and its effects on the design of sustainable agriculture strategies [25–29]. While the authorities have implemented numerous adaptation strategies in response to climate change and variability [9, 30]. Nevertheless, the quality of effort is relatively limited and fragmented [8, 31–33].

Firstly, to be plausible resilience against climate change means encompassing the capacity to anticipate, consolidate, and coordinate emergency response [14, 16]. The concept of sustainable livelihoods was initially introduced as a means of integrating socioeconomic and ecological factors into a cohesive, policy-relevant framework by Brundtland commission on environment and development [34]. Then its idea was further elaborated by the 1992 United Nations Conference on Environment and Development, specifically within the framework of Agenda 21, which underscored the significance of income security as a coherent goal for poverty improvement [35]. While several research literatures indicate that flexibility approaches highlight the importance of learning capacity in both individuals and organizations [36–38], education and literacy as well as with information exchange are crucial for community resilience to disasters [39, 40]. Previous case studies in Vietnam determines that identifying dependent factors is the first step in developing adaption strategies to reduce environmental risks [20, 41–43]. It suggests that sustainable living can act as an “integrating part” to address development challenges, resource managing, and poverty relief simultaneously [42, 44]. This research aims to dissect information collected from affected farmers in SI-infested areas to re-evaluate their position in response to environmental challenges.

2. Methodology

This study seeks to provide a better insight on the topic by integrating the systematic, data-oriented approach of quantitative research with the detailed, interpretative analysis typical of qualitative research. Thus, allowing a more distinct examination, using the advantages of addressing the study problems from different points of view.

2.1. Overview of studied area

The case study was performed in Hung My Commune in Tra Vinh Province, one of the most adversely affected spots of salt intrusion in the Mekong outlet [45, 46]. In a typical dry season, the maximum saltwater incursion ranges from 1,5 million to 2 million hectares [10]. In 2020, approximately 5,177 hectares of rice, cultivated by 6,710 homes, representing 78% of all rice-growing families, were threatened by seawater intrusion [47].

Findings from the “Mekong Futures” envision indicate that households categorized as middle well-off, possessing a farm size of 0.4-0.7 hectares, generated an average monthly revenue of two million VND per laborer [2]. This income level is just above the poverty line issued by Vietnamese government for 2021-2025 period [48], which mean average family in VMD still vulnerable against prospect of climate disaster in term of financial asset. Although

a significant number of individuals in Vietnam have ascended from poverty, many "near poor" homes remain in a vulnerable state and could readily regress into poverty owing to adverse shocks [49].

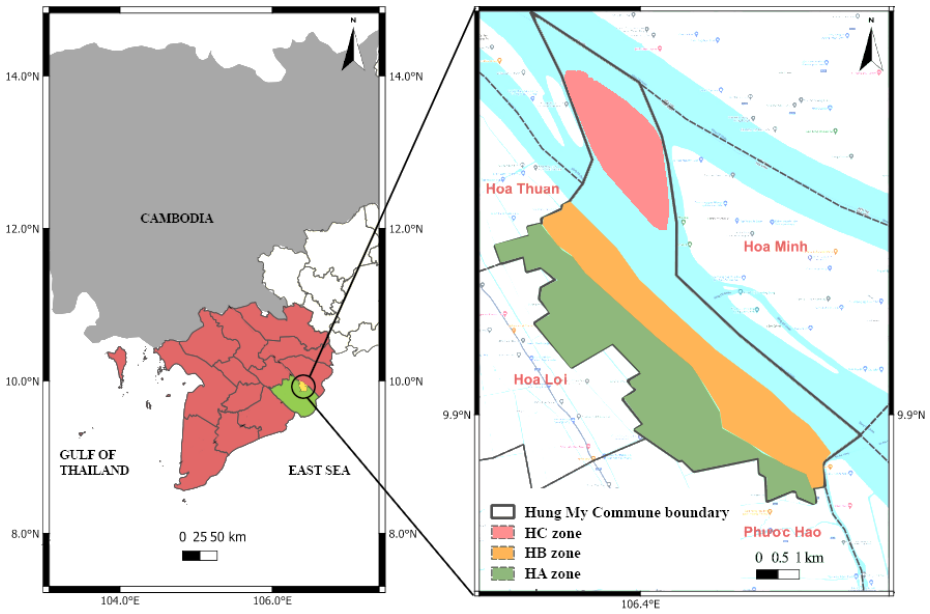

Figure 1. Geographical location of Hung My commune, Chau Thanh District, Tra Vinh Province in the VMD, Vietnam.

Located at the mouth of the Mekong waterways, the terrain of Tra Vinh (Figure 1) is distinguished by its lower, moister terrain. The land is notably irrigated by both natural and man-made canals, with a typical height ranging from 0.6 to 1.0 meters, encompassing two-thirds of the total area [23]. Furthermore, this region is susceptible to sea level rise, as the medium-range emission scenario predicts that by 2030, the sea level could increase by 13 centimeters [13]. Positioned adjoining to the Co Chien River in the Chau Thanh District, Hung My commune encompasses a total extent of 2,829 hectares (28.29 square kilometers), of which 59 percent is agricultural/forest territory.

2.2. Identifying relevant agents

On a local scale, vulnerability assessment is essential for understanding the effects of climate change on individual economy [5], which is beneficial for conducting research on SI damage assessment. Nevertheless, in their findings [37–39] suggested and emphasized that adaptable livelihood approaches may be rendered unsuccessful if they are not accurately assessed and identified in relation to the susceptibility of livelihoods to shifting climates. Investigations from [50, 51] outline that, for people and families, "key capacities" may be seen as assets and representing a pool of resources that individuals and social groups can use to enhance their well-being. Furthermore, the study [50] has recapped those instrument capabilities in accordance with the terms utilized in resilience thinking by his predecessors in this regard (Table 1).

Table 1. The concept of Resilience quality of capital capacities [50].

Quality	Descriptions
Responsiveness	Capability to organize, recognize, foresee, strategize, and ready for an emergency or unexpected occurrence
Resource mobility	Ability to deploy funds and facilities for action. This encompasses the capacity to access monetary and other commodities through collaboration
Learning capacity	Capacity to assimilate prior knowledge, circumvent recurrent mistakes, and improvise to enhance productivity

To assess the vulnerabilities of HH using this theoretical framework, the research needs to determine the main assets of the affected and measuring their capacity against risk is the basis to gauge the risk endurance of said homes. Hence, two sets of parameters have been needed. Firstly, reviewing previous studies of [42–44, 51–52], the common approach frequently evaluates the five primary elements of farmer resource: natural, social, financial, physical, and human. The addition of the components of employment strategy, as well as natural catastrophes endurance, was further analyzed and divided into subsections of each criterion due to their influence on the resilience and economic vulnerability of farming residences (Table 2).

Table 2. Dividing five main capitals to subcomponents and categorize by resilience quality.

Capital	Indicators	Resilience quality
Human	H1: General education	Responsiveness
	H2: Health	Responsiveness
	H3: Knowledge SI-resilient livelihood	Responsiveness
	H4: Knowledge of actions to protect livelihood before SI event	Responsiveness
	H5: Learning from experience	Learning capacity
	H6: Innovation for SI-resilient livelihood	Learning capacity
Social	S1: Knowledge sharing for SI-resilient livelihood	Resource mobility
	S2: Support to recover/overcome after the event of SI	Resource mobility
	S3: Training by local government	Learning capacity
	S4: SI defense measure regulations	Responsiveness
Physical	P1: Early warning system	Responsiveness
	P2: Livelihood preparation before SI events	Responsiveness
	P3: Community-level protection infrastructure	Responsiveness
Natural	N1: Condition of natural system for SI	Responsiveness
Financial	F1: Financial support for SI-resilient livelihood	Resource mobility
	F2: Access to finance sources for SI-resilient livelihood	Resource mobility
	F3: Family savings	Resource mobility

It is essential to identify factors that hinder or facilitate future change and to compare the results with those from conducted survey [58]. The principal benefit of this technique is that the collected knowledge would be essential for preparing precisely targeted adaptation strategies [42].

The second criterion for evaluating the vulnerability of HH is how much damage caused by SI they can sustain. The loss limit is divided to three level:

Total loss: farmhands were forced to sell their land and changed occupations which were interpreted as complete destruction of livelihood.

Heavy: affected who lost more than fifty percent of their investment in agriculture and pushed them to seek external help.

Minimal damage: homes were marginally affected by SI and/or self-sustained thanks to their own capitals.

2.3. Data collection

a) Define a farming household

The “farmer family” assessment entails measuring the total well-being and productivity of those reliant on agricultural activities for their living. This procedure includes not only the members of the agricultural dwelling who own and operate the farm but also those who are hired as a labor force to assist with various tasks. The assessment may involve examining factors such as access to resources, land ownership, income levels, food security, and overall living conditions. By understanding the dynamics of the agriculture residence and the roles of each member, interventions can be developed to encourage flexible agricultural practices and improve the living standard of those involved in the agricultural sector. The individuals selected to represent those residing within the irrigated region have been categorized into

three distinct groups: HA, HB, and HC (HH of zone A, zone B and zone C respectively-figure 1).

b) Define different studied neighborhoods by focusing on water stress

HA is "water stress" level less - because has multiple water supplies (from inner irrigation, public water supply).

HB is "water stress" level medium - has only inner irrigation.

HC is "water stress" level high - no water supply.

HA is composed entirely of landowners with agricultural property situated within the protection canal. On the contrary, the HB group includes farmers whose properties are situated beyond the SI barrier, while the HC group comprises families residing on Con Co island. The placement of each HH was determined to be within a radius of 5 kilometers from the primary irrigation system.

c) The sample size calculation

This approach involves determining a more precise sample size by analyzing the disparity between the population and the sample. Due to the challenges of surveying the entire population within time constraints, a sample was selected from the population, and a comprehensive survey was subsequently performed. With the purpose of determine the sample size, the following Yamane formula was applied [53]:

$$n = \frac{N}{1 + N \times e^2} \quad (1)$$

where n is the experiment amount; N is the number of HHs in the studied area; and e is 10% of N. The sample size necessitated the establishment of a 10% significance level, as the number of individuals meeting the criteria was limited, hence necessitating a higher sample size. In 2019, Hung My Commune had an inhabitant of 10,068 which equivalent to 2,405 homes. While based in dominance rice culture of VMD, agricultural sector had only 43.85 percent of its economy (which consist of 1,057 farming families) [54]. Therefore, the optimal number of sample size for carrying out survey was decided as around 200 households using formula (1).

2.4. Sampling collection

This survey covers the social aspects of the vulnerability of rural communities in the Hung My commune of Tra Vinh province within the project to understand how these vulnerability characteristics affect the extent of damages and impacts experienced by selected houses during salinity intrusion periods, which hit the province. The specific objectives of the work within this survey are:

To assess the demographic characteristics and vulnerability (five-capital analysis) of targets.

To understand the relationship between social vulnerability characteristics of a "farmer family" and how said member built their ability and protected their living environment during the saltwater intrusion (measures, methods, techniques, etc.).

To understand how the above aspects affected the level of impact experienced.

The study employed a quota of 208 HHs as its targets of the assessment, owing to time and financial constraints. In accordance with the research design framework, a series of multi-level interviews with key informants were undertaken to choose the study site within the province. The Five Capital framework (human, physical, social, natural, financial) must be applied for the assessment of the social vulnerability of the targets. In addition, pertinent documents including maps, and the annual report were considered.

A total of 10 individuals, consisting of field personnel from Can Tho University and local partners, were trained extensively before conducting interviews as part of a questionnaire pretest. The surveys were done across two distinct time frames, spanning from September to October and then again in December 2023. Four staff members were sent to each of

the major zones, while the HC received one pair of surveyors. The participants in the study were the head of households or their spouses, whose major source of income was primarily derived from activities related to crop cultivation, ranching, or aquaculture. A systematically structured questionnaire was utilized to gather data on socio-demographic characteristics, employment, community connections, wellness, access to food and water, emergencies, and environmental disparities. The poll item was drafted based on the subsections or measures illustrated in Table 2. This process also utilized the assistance of local leaders in choosing appropriate and suitable indicators that accurately represent the socioeconomic characteristics of the community being examined.

2.5. Benchmarking

Each household survey was thereafter entered into a digital database and assessed according to the established parameters (Table 3). Subsequently, each indicator is arranged according to its mean values, and then it is shown in diagrams for a more comprehensive explanation. Using this technique, an examination of principal patterns about each attribution may either hinder or aid response to saline shocks. The band score from 1 to 5 indicates capital capacity intensity to identify from the insufficient and affluence. These indicators are then classified into 5 divisions in which 1 shows strong weakness while 5 indicates strong ability. The score 3 belongs to the neutral answers and normal tones from the interviewees. Score 2 gives the weak potential and 4 is for strong reactions and perspectives. These segments of capital capacity could cover all the feedback from the interviewees focusing on the concerned issues.

Table 3. Capital capacity score ranges from scarcity to abundancy (self-assessed value).

	0-2	**2-4**	**4-5**
Farmer HH's capital (I-V)	Asset depleted	Transitional	Great capacity

3. Results

3.1. Tendency of main major assets between study zones

All data retrieved from their questionnaire was evaluated by the authors and transformed into a capacity score based on the scale in Table 3, subsequently shown in Figure 2. This graph presents the variations of five major assets of surveyed households in three chosen sites with each household is represented by a specific color.

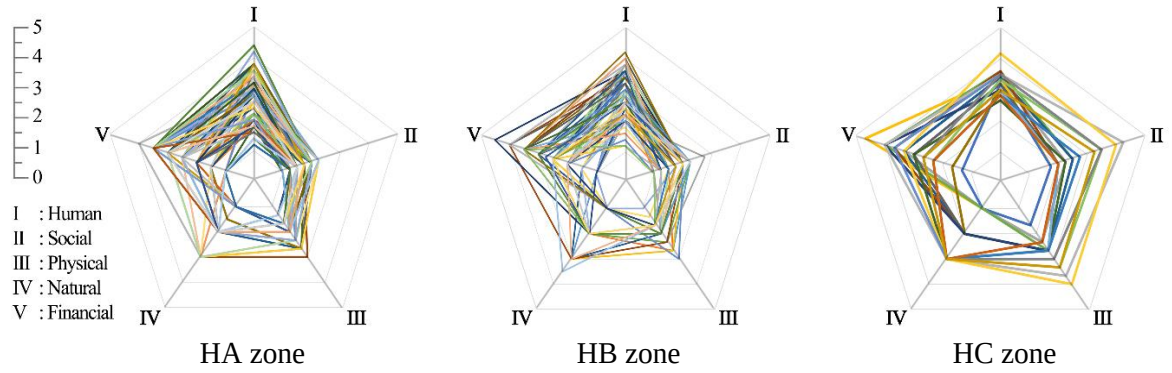

Figure 2. The discrepancies in asset evaluating of farming family between 3 HH groups.

Firstly, these charts illustrate the considerable discrepancy among existing assets. Many of the farmers in question are constrained by Social and Physical resources, since only a small number of families have attained the median value in both domains. The amplest capital could be seen as Human asset which shows a wider distributing tendency than others.

The distribution of HA capitals is highly limited and concentrated, indicating that the scores are generally lower across most metrics. The Human and Financial parts are undoubtedly the most significant, and they are much greater than the other aspects. Unlike HA, the HB zone diagram displays a broader configuration, indicating that scores are enhanced across all indicators. Nonetheless, while the Natural and Financial indicators may be more pronounced, the chart continues to show a similar trend to the previous one. The most extensive shape among the three radar charts is that of HC, signifying the highest output or scores in most data points. The financial, human, and physical qualities in this section are significantly advanced, exhibiting consistently high scores throughout the chart. In general, Figure 2 indicates that "Human" is the predominant capital possessed by Hung My inhabitants, which could be advantageous in mitigating the setbacks of SI.

3.2. Representation of SI damage in different studied neighborhoods

In HA (Figure 3), the scores primarily persist within the "Heavy damage" spectrum, with a small number of them extending to the "No damage" area. The scores of many assessments begin in the "Heavy damage" section and progressively increase as they approach the "No damage" sector. Like HA, HB (Figure 4) also demonstrates a consistent trend throughout the assessments. In contrast to HA, the scores are slightly lower overall, with a greater number of individuals falling within the "Heavy damage" and a smaller number reaching the "No damage" zone. The aggregate score levels indicate that HB presents less favorable conditions than HA, despite the consistent trend. However, HC (Figure 5) exhibits a markedly distinct pattern, with certain landowners having a "Capitals score" that is even lower than the "Total loss" range. Nevertheless, the variety of capitals in HC is increased by the fact there are two families in the No-damage zone. In summary, the most favorable trend is demonstrated by HC, as a greater number of assessments reach the "No damage" range. While HA has shown improvement, the majority of interviewees' score remains in the "Heavy damage" region, suggesting that this group continues to encounter some obstacles. The most significant challenges confront Zone B, as most scores remain in the "Total loss" and lower "Heavy damage" tiers, indicating severe conditions that impede improvement.

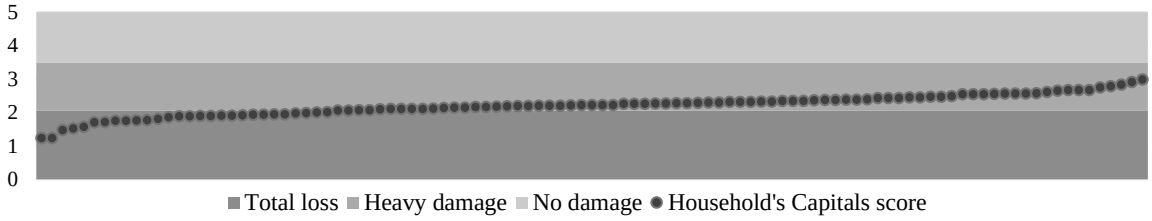

Figure 3. Loss range of studied farmer group in HA.

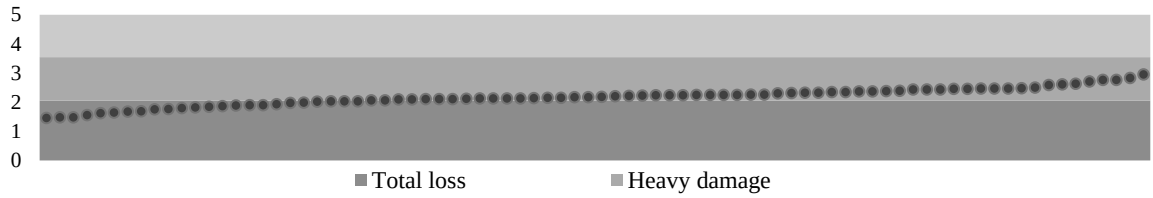

Figure 4. Loss range of studied farmer group in HB.

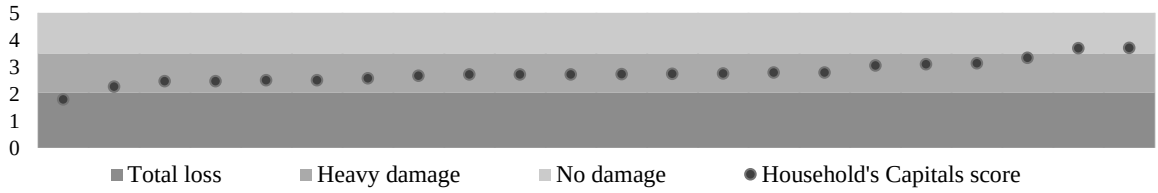

Figure 5. Loss range of studied farmer group in HC.

3.3. Notable revelations from survey

SI had a substantial negative influence on agricultural output, resulting in reduced planted crop areas, damage to rice volume and other products, livestock disease, a drop in agricultural inputs such as nutrients, and contamination of aquaculture cultivation land.

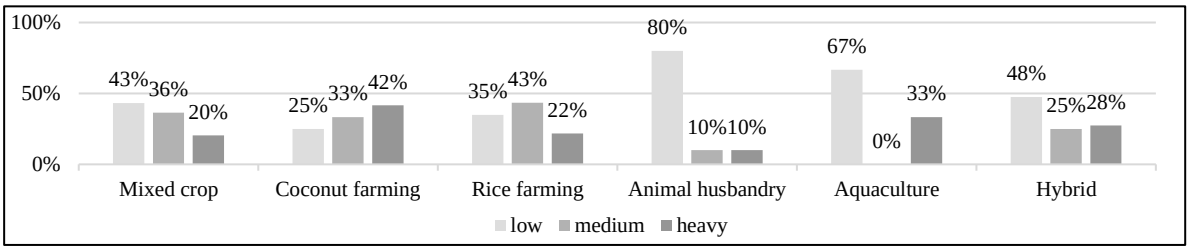

Figure 6. Finance loss by SI of studied Households by means of agricultural activity as main income source.

Collected data reveal significant disparities between different groups of landowners (Figure 6). Damage estimation showed Coconut farming suffered the highest rate of damage with 42 percent in heavy loss range. In contrast, the aquaculture group was less affected by SI as 67 percent of the families sustained no damage. Moreover, financial losses in animal husbandry are overwhelmingly low with very few farmers facing medium (10%) or heavy (10%) losses respectively. Mixed cropping and other hybrid agricultural practices also showed resilience in the face of saline water challenges. The data suggests that specific farming activities, such as animal husbandry, demonstrate greater resilience and reduce financial losses. Conversely, other agrarian forms, such as vegetation planting like rice or coconut, have a more diverse effect on interviewee's finance.

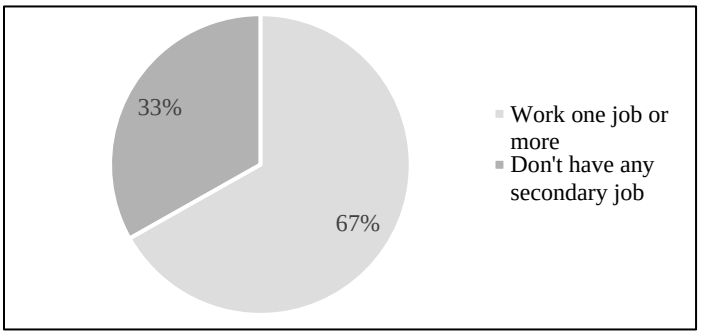

Figure 7. Demographic of households regarding to secondary job.

Many HH strive to secure employment in two separate works to bolster their income to make ends meet. Most families (67%) have at least one second occupation, according to Figure 7. This pattern might reflect economic pressures, suggesting that people generally need additional sources of income. The minority (33%) of people without a second job may be made up of HHs with alternative lifestyle choices or ones with a sufficient primary income.

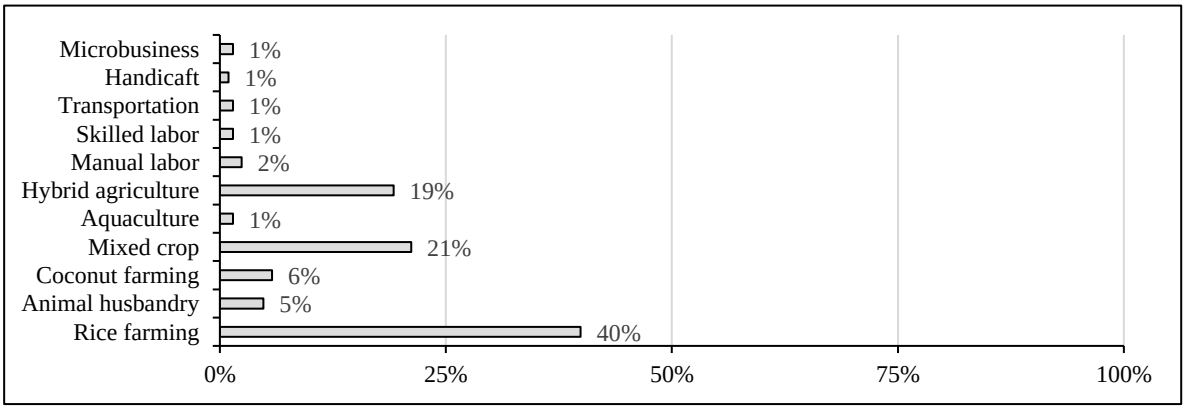

Figure 8. Main earning sources of household from surveyed categorizing by means of occupation.

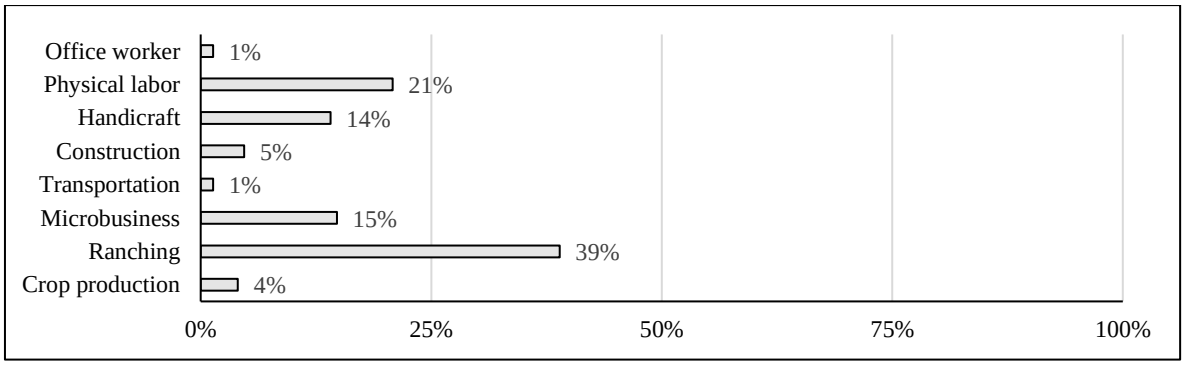

Figure 9. Secondary earning sources of household from surveyed categorizing by means of occupation.

Growing rice is the most common source of income for farmers, accounting for 41% of their earnings, indicating the prominence of rice growing in the surveyed region. The second most common main income source is mixed crop farming (21%) where these families engage in cultivating multiple crops, reflecting diversified agricultural practices. A modest proportion of farmhands rely on manual labor, skilled labor, micro-business, or handicrafts as their primary source of income, with each category accounting for just one percent. The minimal contributions as principal sources of income by concerned groups suggest limited opportunities or engagement in these fields.

At 39%, ranching is the most common secondary source of income, which is like the importance of wet rice as a primary source of income. This could indicate a trend where growers are diversifying by raising both cattle and crops. Physical work is a significant secondary source of income, accounting for 21% of total income, most likely because of seasonal or part-time employment. With 15% of the market, the microbusiness sector is notable for showcasing household-based entrepreneurship as a secondary source of income. Crafts are a common secondary occupation, accounting for 14% of all employment, maybe because they are flexible and enable workers to work from home. Construction and food production which consist of five and four percent respectively, like other small-scale jobs like office work and transportation, contribute relatively little to community economy.

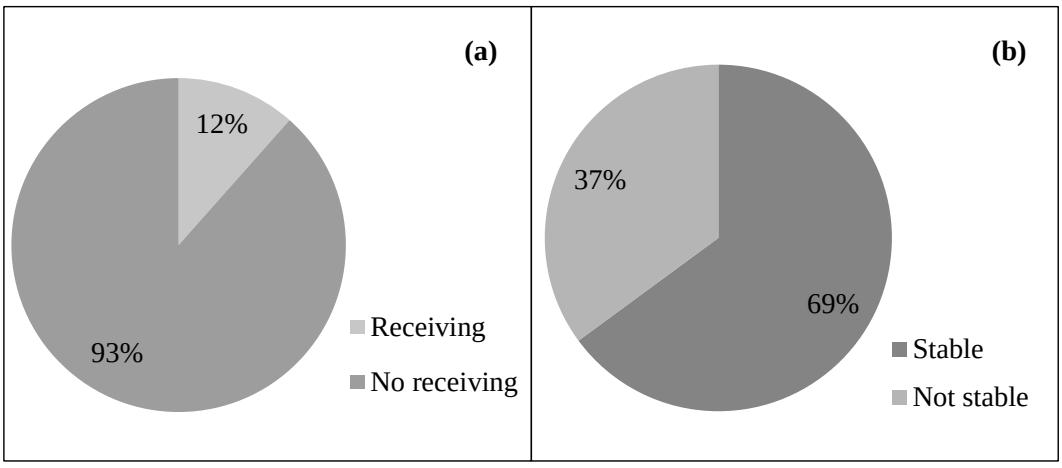

Figure 10. Percentage of farmer has received monetary support compared to percentage of their financial situation: (a) Distribution rate of government financial subsidy; (b) Stable income situation.

Figure 10 illustrates a stark discrepancy in the approach to combat poverty, as it reveals discrepancies between the data on the number of studied individuals experiencing financial difficulties and the allocation of government relief funds. Although two-thirds of the overall interviewees endure acute economic strain, just 12 percent of SI affecters receive monetary aid. If this tendency continues, most families that have not received any types of welfare would face significant challenges when a crisis happens.

4. Discussion

The study verifies the notion that higher levels of livelihood assets (indicators and capitals) correlated with higher levels of adaptive capacity. Farmers with more capital capacity appear to be financially well situated and perform better during a crisis. While there have been other attempts to relate living and adaptability [42, 55–58], the finding helps provide additional insight on the matter and this approach that could be further experimented. The comprehensive interviews unveiled the strategies employed by agrarian cultivators to manage not just the escalating climatic variability and change, but also their reactions to other influencing factors. Reflecting from data reveal that during unfavorable agricultural seasons, some farmhands even sold their fields, got into desperate loans with excessive interest rates, and resorted to leaving to urban area to be better finance. Such extreme cases of loss of livelihoods are not a rare incident as families who deem stable finance is low (Figure 10).

4.1. Shortcoming of the research

This evaluation relies on both quantitative and qualitative data which has been carried out independently. The approach requires direct contact with affected inhabitants in considerable time with dedicated investigators for specific zones to help obtain valuable insights. Such information usually neglects or loses if only relying on government data due to lengthy collecting methods and finances constraints. The subjective nature of surveys is tackled by extensive review and constants organizing. Then, only data deemed to be worthy can be utilized in the assessment process.

However, while time consuming is the main adversary of such tactics, on-field problems also occur regularly. For instance, the absence of farmers who lost all means of income and were forced to relocate makes it difficult to collect their voices and consider the severe of whole situation. Furthermore, most of the interviews took place at farmers' residences, with fewer conducted in the fields. This could have potentially bias on the results obtained also raised concerns from other researchers [22, 40]. A restrained budget also has made it difficult to evaluate the project's impact in terms of limits of the studied sample size. Moreover, as the subject matter and context are intricate, encompassing a vast array of physical, social, economic, and practical variables which necessitate a foundation of knowledge could lead to inadequate answers from interviewees.

4.2. Suggestions

Multiple factors were discovered that impeded affected family’s ability to adjust to environmental challenges. These steps should be enforced to empower examined individuals in efficiently managing and adapting to the effects of ecological change. Improving the value of natural resources is considered essential for agricultural practices across all aspects of cultivation. Landowners with less financial resources, who possess fewer livelihood assets, are more susceptible to the consequences of weather crisis. Although national-sponsored development projects, such as the “Hunger eradicate and poverty relief” initiative, have been crucial and advantageous, they are not enough on their own to enable small holdings to effectively adapt to climate-related changes. Cooperative crop growing promotes social learning and collective assistance, which improves small-scale the ability of landowners to maintain their livelihoods significantly.

Evaluating the feasibility of alternatives involves identifying crops and livestock that exhibit more resilience to the specific climatic circumstances of the location, such as crops that can withstand drought or cattle that can survive in varying temperatures. Promote the amalgamation of crops and livestock to establish a rural system that is more varied and robust. Intercropping and integrated livestock-crop systems can enhance land use efficiency and mitigate dangers linked to monoculture farming. Capacity building and information transfer can

be achieved through a training program for farmers, which aims to educate them on the advantages and methods of crop diversification and animal production. Moreover, ensure convenient availability of essential resources, including seeds, livestock, and technology, along with credit and financial services, to assist in the process of transitioning. Possible measures could encompass subsidies, grants, or tax incentives to encourage the adoption of alternate crops and livestock. Ultimately, it is crucial to involve local communities, agricultural-orientation organizations, and other stakeholders in the decision-making process to guarantee that the transition is in line with their requirements and preferences. By considering these factors, a complete plan may be developed to transition from rice cultivation to more flexible agricultural methods, ultimately strengthening the ability of cultivation communities to withstand the impacts of climate crisis.

5. Conclusions

In conclusion, this research's examination of the destruction that SI inflicts on impacted studied Hung My commune, where the saline rampages, presents significant risks to conventional agricultural activities. The results demonstrate notable discrepancies in household resilience among various zones, with the most susceptible who are experiencing substantial losses and confronting severe financial instability. Although government interventions and local adaptive strategies have offered some relief, their effectiveness is limited when done separately. The review approach employs independent, field-based data collecting to provide insights often overlooked by official sources; yet it encounters problems like time limitations, absent perspectives from displaced families, and budgetary limits. Interviews mostly held at target's home may have impacted the outcomes, and the intricate nature of the topic complicates the acquisition of thorough responses. The research highlights the need for adaptable agricultural strategies in SI-infested areas to strengthen farmers' resilience. It advocates for diverse farming methods to provide additional income sources, reducing dependence on a single livelihood and ensuring that policies address the specific needs of affected communities. The recognition of SI harm to domestic livelihoods provides the foundation for further research aimed at improving the stability and resilience of agricultural communities against escalating climate change problems.

Author contribution statement: Developing research ideas: N.T.H.; H.V.H.; Process data: processing, manuscript writing: N.T.H.; H.V.H.; L.N.A.K.; Reviewed and completed the manuscript: H.V.H.

Acknowledgments: This study is funded by the MOET from the project: Saltwater Intrusion's Impact Assessment on Farming Households in Tra Vinh Province, Vietnam under grant number B2023-VGU-03. The authors gratefully acknowledge this support.

Competing interest statement: The authors declare no conflict of interest.

References

1. UNFCCC. Report of the conference of the parties on its fifteenth session, held in Copenhagen, in Framework Convention on Climate Change, Copenhagen, 2009.
2. DFAT CSIRO Research for Development Alliance. Mekong futures: Regional and local studies, 2008-2014. Available online: https://wp.csiro.au/r4da/projects/long-term-projects/regional-and-local-studies/.
3. WMO. The global climate 2011-2020: A decade of accelerating climate change. World Meteorological Organization, Geneva, 2023.
4. Carter, C.; Cui, X.; Ghanem, D.; Mérel, P. Identifying the economic impacts of climate change on agriculture. *Annu. Rev. Resour. Econ.* **2018**, *10*, 361–380.
5. IPCC. Climate change 2014: Synthesis report. Contribution of Working Groups I, II and III to the Fifth Assessment Report of the Intergovernmental Panel on Climate Change. IPCC, Geneva, 2014.

6. Amnuaylojaroen, T.; Limsakul, A.; Chanvichit, P. Assessing the impact of climate change on agricultural water management in Mainland Southeast Asia. *Adv. Meteorol.* **2024**, *2024(1)*, 1–22.
7. Zhai, F.; Zhuang, J. Agricultural impact of climate change: A general equilibrium analysis with special reference to Southeast Asia. Climate Change in Asia and the Pacific: How Can Countries Adapt? SAGE Publications India Pvt Ltd, 2012, pp. 17–35.
8. Taniushkina, D.; et. al. Case study on climate change effects and food security in Southeast Asia. *Sci. Rep*. **2024**, *14(1)*, 16150.
9. Ministry of Agriculture and Rural Development (MARD). Regional environmental assessment on Mekong Delta integrated climate resilience and sustainable livelihoods project, Hanoi, 2016.
10. Mackay, P.; Russell, M. Socialist Republic of Viet Nam: Climate change impact and adaptation study in the Mekong Delta, Sinclair Knight Merz (SKM), 2011.
11. GSO. Planted area of cereals by province. General Statistics Office (GSO) of Viet Nam, 2022. Available online: https://www.gso.gov.vn/en/pxweb/?pxid=E0609&theme=Agriculture%2C%20Forestry %20and%20Fishing.
12. Piesse, M. The Mekong Delta: Land subsidence threatens Vietnam's "Food Basket". Future Directions International Pty Ltd. Nedlands, 2019.
13. Ministry of Natural Resources and Environment (MoNRE). Climate change and sea level rise scenarios of Viet Nam. IMHEN-MONRE, Hanoi, 2016.
14. World Bank. Toward integrated disaster risk management in Vietnam, Washington DC. 2017.
15. Sutton, W.R.; Srivastava, J.P.; Rosegrant, M.; Thurlow, J.; Sebastian, L. Striking a balance: Managing El Niño and La Niña in Vietnam's agriculture. World Bank, Washington DC. 2019.
16. Ministry of Natural Resources and Environment (MoNRE). Proceedings of the Third Conference on Climate Resilient and Sustainable Development of the Mekong River Delta of Viet Nam. Hanoi, 2021.
17. International Federation of Red Cross and Red Crescent Societies (IFRC). Vietnam - drought and saltwater intrusion emergency plan of action (EPoA) DREF operation n° MDRVN019 Final Report, Geneva, 2020.
18. Nguyen, N.A. Historic drought and salinity intrusion in the Mekong Delta in 2016: Lessons learned and response solutions. *VN J. Sci. Technol. Eng*. **2017**, *29(1)*, 93–96.
19. Mai, N.P.; Kantoush, S.; Tetsuya, S.; Thang, T.D. Proposed adaptation measures for saltwater intrusion in the Vietnamese Mekong Delta. Proceedings of the 4th International Conference on Sustainability in Civil Engineering, December 25 to 27, 2022, Singapore, 2024.
20. Nguyen, T.A.; Nguyen, T.; Mac, T.; Nguyen, H. Assessing impacts of saltwater intrusion on social groups in the coastal areas of Mekong Delta and proposing amendments and improvements to social security policies, school of training and fostering cadres and civil servants in Labor - Social Affairs, Hanoi, 2021.
21. United Nations - Vietnam (UNVN). Vietnam drought and saltwater intrusion in Mekong Delta, United Nations Vietnam, Hanoi, 2020.
22. Dung, D.T.; Van Halsema, G.; Hellegers, J.G.J.P.; Fulco, L.; Wyatt, A. Questioning triple rice intensification on the Vietnamese mekong delta floodplains: An environmental and economic analysis of current land-use trends and alternatives. *J. Environ. Manage.* **2018**, *217*, 429–441. https://doi.org/10.1016/j.jenvman.2018.03.116.
23. Phuong, T.H.; Phung, H.P.; Hung, N.T.; Man, D.B.; Mon, D.; Vinh, D.H.; et al. Assessment of changes in the land use structure in Tra Vinh province under the scenarios of climate change and sea level rise. *VN J. Sci. Technol.* **2020**, *58(1)*, 56–70.
24. Loc, H.H.; Binh D.V.; Park, E.; Shrestha, S.; Dung, T.D.; Son, V.H.; Truc, N.H.T.; Mai, N.P.; Seijger, C. Intensifying saline water intrusion and drought in the Mekong Delta: From physical evidence to policy outlooks. *Sci. Total Environ*. **2021**, *757*, 143919.

25. National Agency for Science and Technology Information NASATI. Salinity intrusion in the Mekong Delta: Causes, impacts and response solutions. in Summary of Science - Technology - Economics 2016, Ministry of Sciene and Technology, Hanoi, 2016.
26. Prime Minister Office of Vietnam. Decision on Issuance of National Action Plan on Climate Change Period 2012 - 2020, Hanoi, 2012.
27. Southern Institute of Water Resource Planning (SIWRP). Irrigation planning in the Mekong Delta in consideration of climate change and sea level rise. Ho Chi Minh, 2012.
28. Prime Minister Office of Vietnam. Approval of Irrigation Planning for the Mekong Delta for 2012 - 2020 Period and Orientation Towards 2050. Hanoi, 2012.
29. Government of Vietnam (VG). Resolution on climate-resilient and sustainable development of the Mekong Delta, Hanoi, 2017.
30. Nguyen, N.T. Vietnamese Mekong Delta, 44 years of economic, social and environmental transformation. Implementation of the Resolution No 120/NQ-CP, 2019.
31. Tri, N.H.; Tien, H.T. Adaption to Salinity Intrusion for Rice Farming Household in the Vietnamese Mekong Delta. Proceeding of the 6th Asian Academic Society International Conference, 2018.
32. UNDP Viet Nam. Viet Nam Drought and Saltwater intrusion: Transitioning from Emergency to Recovery, UNDP Viet Nam, 2016.
33. Vietnamese Government Press (VGP). Preliminary Outcomes of Three-year Implementation of Resolution on Climate-resilient development of Mekong Delta, Government News, 2021. Available online: https://en.baochinhphu.vn/preliminary-outcomes-of-three-year-implementation-of-resolution-on-climate-resilient-development-of-mekong-delta-11140641.htm.
34. Brundtland Commission. Our common future: Report of the World Commission on Environment and Development, Geneva, UN, 1987.
35. UNCSD. AGENDA 21, in United Nations Conference on Environment & Development, Rio de Janerio, 1992.
36. Berkes, F. Understanding uncertainty and reducing vulnerability: Lessons from resilience thinking. *Nat. Hazard* **2007**, *41*, 283–295.
37. Diduck, A. The learning dimension of adaptive capacity: Untangling the multi-level connections. Adaptive Capacity: Building Environmental Governance in an Age of Uncertainty, Springer, 2010, 2, pp. 199–221.
38. Folke, C. Resilience: The emergence of a perspective for social-ecological systems analysis. *Global Environ. Change*. **2006**, *16*, 253–267.
39. Twigg, J. Characteristics of a disaster-resilient community a guidance note characteristics of a disaster-resilient community: A guidance note, London, Department for International Development, 2007.
40. Dung, D.T.; Park, E.; Tuoi, H.T.N.; Thien, D.N.; Tu, H.V.; Ngoc, T.A.P.; Van, C.; Long, P.; Loc, H.; Quang, N.X.C. Climate change impacts on rice-based livelihood vulnerability in the lower Vietnamese Mekong Delta: Empirical evidence from Can Tho City and Tra Vinh Province. *Environ. Technol. Innovation*. **2022**, *28*, 102834. https://doi.org/10.1016/j.eti.2022.102834.
41. Huong, N.T.L.; Yao, S.; Fahad, S. Farmers' perception, awareness and adaptation to climate. *Int. J. Clim. Change Strategies Manage*. **2017**, *9(4)*, 555–576.
42. Brown, P.R.; Ward, J.; Tuan, V.V.; Nhan, K.D.; Dung, C.L. Influence of livelihoods on climate change adaptation for smallholder farmers in the Mekong Delta Vietnam. *Int. J. Agric. Sustainability* **2018**, *16*, 1–17.
43. Huong, N.T.L.; Yao, S.B.; Fahad, S. Assessing household livelihood vulnerability to climate change: The case of Northwest Vietnam. *Hum. Ecol. Risk Assess.: Int. J.* **2018**, *25*, 1–19.
44. Ho, T.D.N.; Kuwornu, J.; Tsusaka, T. Factors influencing smallholder rice farmers' vulnerability to climate change and variability in the Mekong Delta region of Vietnam. *Eur. J. Dev. Res.* **2021**, *34*, 1–31.

45. Toan, T.Q.; Thao, N.D.; Takagi, H.; Esteban, M. Climate change and sea level rise in the Mekong Delta: Flood, tidal inundation, salinity intrusion, and irrigation adaptation methods. Proceeding of the Coastal Disasters and Climate Change in Vietnam, Oxford, Elsevier, 2014, pp. 199–218.
46. Thanh, T.N.; Huynh, H.V.; Vo, H.M.; Tri, V.P.D. Salinity intrusion trends under the impacts of upstream discharge and sea level rise along the Co Chien river and Hau river in the Vietnamese Mekong Delta. *Climate* **2023**, *11*, 66. https://doi.org/10.3390/cli11030066.
47. Hoa, L.T. The impact of saltwater intrusion on rice cultivation and aquaculture in Ham Tan Commune, Tra Cu District, Tra Vinh Province, Mekong Delta, Vietnam. *Eur. Sci. J*. **2023**, *19(22)*, 27.
48. Government of Vietnam (VG). Standard for multi-dimensional poverty in 2021-2025 period, Hanoi, 2021.
49. World Bank (WB). The economics of adaptation to climate change, Vietnam, Washington DC. 2010.
50. Tyler, S.; Moench, M. A framework for urban climate resilience. *Clim. Dev*. **2012**, *4(4)*, 311–326. https://doi.org/10.1080/17565529.2012.745389.
51. Shah, K.U.; Dulal, H.B.; Johnson, C.; Baptiste, A. Understanding livelihood vulnerability to climate change: Applying the livelihood vulnerability index in Trinidad and Tobago. *Geoforum* **2013**, *47*, 125–137.
52. Hahn, M.; Riederer, A.; Foster, S. The livelihood vulnerability index: A pragmatic approach to assessing risks from climate variability and change—A case study in Mozambique. *Global Environ. Change* **2009**, *19*, 74–88.
53. Huynh, L.T.M.; Stringer, L.C. Multi-scale assessment of social vulnerability to climate change: An empirical study in coastal Vietnam. *Clim. Risk Manage*. **2018**, *20*, 165–180.
54. Yamane, Y. Statistics: An introductory analysis 2nd Edition, New York, Harper and Row, 1967.
55. Hung My Commune People's Committee. Approved master plan of Hung My Commune, Chau Thanh District, Tra Vinh province, Tra Vinh, 2019.
56. Dung, L.; Nhan, D.; Vo, V.; Ward, J.; Brown, P. Financial capacity of rice-based farming households in the context of climate change in the Mekong Delta, Vietnam. *Asian J. Agric. Dev*. **2018**, *14(1)*, 73–87.
57. Ward, J.; Varua, M.E.; Maheshwari, B.; Oza, S.; Purohit, R.; Dave, H.S. Exploring the relationship between subjective wellbeing and groundwater attitudes and practices of farmers in rural India. *J. Hydrol*. **2016**, *540*, 1–16.
58. Cong, T.P.; Manh, D.; Huy, H.; Phuong, T.; Tuyen, L. Livelihood vulnerability assessment to climate change at community level using household survey: A case study from Nam Dinh Province, Vietnam. *Mediterr. J. Social Sci*. **2016**, *7*, 358.

JOURNAL OF
HYDRO-METEOROLOGY

Research Article

Occurrence and distribution of pesticide residues in coffee growing soil at Lam Ha district, Lam Dong province

Dang Viet Lam[1,2]*, Vu Duc Toan[3]

[1] Graduate University of Science and Technology, Vietnam Academy of Science and Technology; dangvietlam1980@gmail.com
[2] Chemical and Environmental Laboratory, Quality Assurance and Testing Center 1, Commission for Standards, Metrology and Quality of Viet Nam, Ministry of Science and Technology; dangvietlam1980@gmail.com
[3] ROOM Strong Research, Environmental and Life Science Research Laboratory, Thuyloi University; vuductoan@tlu.edu.vn

*Corresponding author: dangvietlam1980@gmail.com, Tel.: +84–989655589; vuductoan@tlu.edu.vn, Tel.: +84-936027466

Received: 15 August 2024; Accepted: 02 October 2024; Published: 25 December 2024

Abstract: Thirty soil samples from 4 communes of Lam Ha district were collected in May and November 2023. The pH, moisture content, organic carbon and mechanical composition were investigated. Two group of pesticides were analyzed including Organophosphorus (Diazinon, Chlorpyrifos, Profenofos, Fenitrothion, Ethoprophos, Glyphosate) and Carbamate (Carbaryl, Mancozeb, Carbosulfan). Maximum concentration of Chlorpyrifos, Profenofos and Carbosulfan founded in soil samples were 391, 63 and 41 µg/kg, respectively. The risk quotient (RQ) of pesticides in coffee growing soils were evaluated for ecological risk assessment. In this study the order from very low to high risk in ascending order from Phi To, Nam Ha, Dong Thanh and Me Linh, respectively.

Keywords: Pesticides in soil; Soil pollutions; Organophosphorus; Carbamates; Risk assessment.

1. Introduction

Lam Dong is a province with favorable natural conditions for growing coffee. Currently, the whole province has a coffee growing area of 172,000 hectares and an output of 515,000 tons. Although it is the second province in the country to accumulate coffee, Lam Dong coffee has the highest average capacity and product in the country. Lam Dong is developing 5 large coffee cultivation areas in the districts of Di Linh, Lam Ha, Bao Lam, Duc Trong, Da Lat city and Lac Duong to form large-scale raw material areas for processing and export.

The coffee area of Lam Ha district is currently about 40,000 hectares, the harvest output is about 135,000 tons and the average harvest yield is 3.45 tons/ha. Lam Ha district has been converting new varieties of plants, grafting and improving robusta coffee... to help coffee trees increase productivity. Increasingly intensive farming measures are the main cause affecting the emergence and development of harmful pests and diseases. In coffee farming, farmers regularly treat soil before planting coffee and use plant protection chemicals when pests are detected. Most coffee producing households use chemical plant protection chemicals to prevent pests on coffee plants with a frequency of use of 1 to 4 times a year [1].

Carbamate insecticides included in this research are Carbaryl, Mancozeb and Carbosulfan. The functional group inactivating enzyme acetylcholinesterase causing toxicity to kill insects. Organophosphate group also affect cholinergic poisoning [2–4].

Organophosphorus pesticides poison insects by phosphorylation of the acetylcholinesterase enzyme (AChE) at nerve endings. The result is a loss of available AChE so that the effector organ becomes overstimulated by the excess acetylcholine [2–6]. From field surveys and previous research, six Organophosphorus pesticides including Diazinon, Chlorpyrifos, Profenofos, Fenitrothion, Ethoprophos and Glyphosate were investigated.

Organophosphorus and Carbamate pesticides are widely used in coffee growing areas in Lam Ha district showed in Table 1 [1]. They are highly toxic, persistent in the environment, have high bioaccumulation in humans and organisms. Thus, ethoprophos has been banned from use since March 2018 and Diazinon since March 2018. Pesticides containing Chlorpyrifos must not be produced or imported since October 2019, can only be sold and used until February 12, 2021; Glyphosate only be sold and used until June 30, 2021 in Vietnam [7].

Table 1. Structure of pesticides.

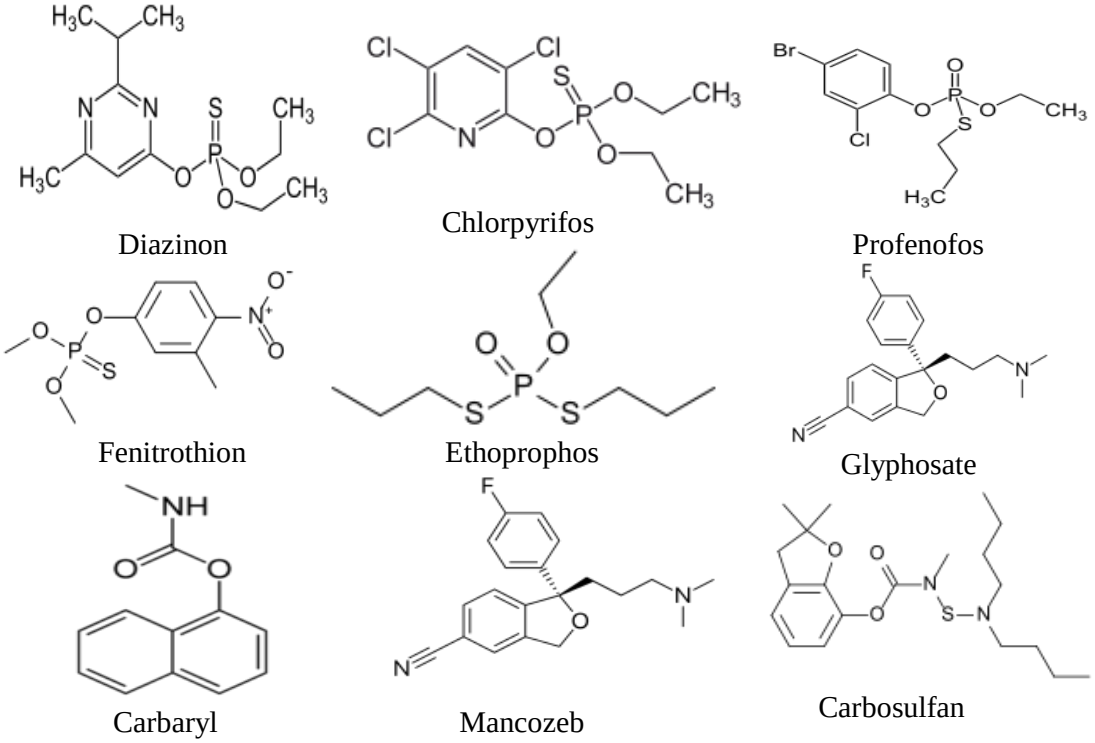

Even though there are specific instructions in the agricultural industry, many farmers still use pesticides incorrectly and at higher doses than allowed, leading to them penetrating and remaining in coffee soil, causing risks and long-term harmful effects on human health [7]. Therefore, assessing the level of environmental risks of pesticides residue in coffee growing soil is very necessary.

The study objectives are: (1) Analysis of physicochemical properties of soil samples; (2) Analysis of six organophosphorus and three carbamate pesticides concentration; (3) Evaluate ecological risk of investigated pesticides.

2. Materials and methods

2.1. Study structure

In this research, thirty soil samples were collected and analyzed for physicochemical properties such as pH, moisture contend, organic carbon and the mechanical composition. Concentration of six organophosphorus and three carbamate pesticides were investigated to assess ecological risk. Figure 1 shown the details of study structure.

2.2. Study area

Samples were taken in May 2023 (rainy season) and November 2023 (dry season), each time 15 surface soil samples with a depth of 0-15cm were taken in Lam Ha district as shown in Figure 2: 3 from Phi To, 5 from Nam Ha, 4 from Me Linh and 3 from Dong Thanh communes.

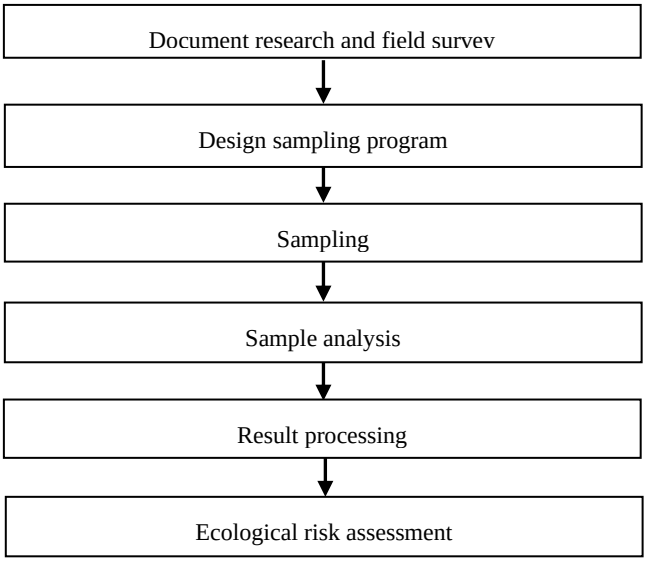

Figure 1. Research diagram.

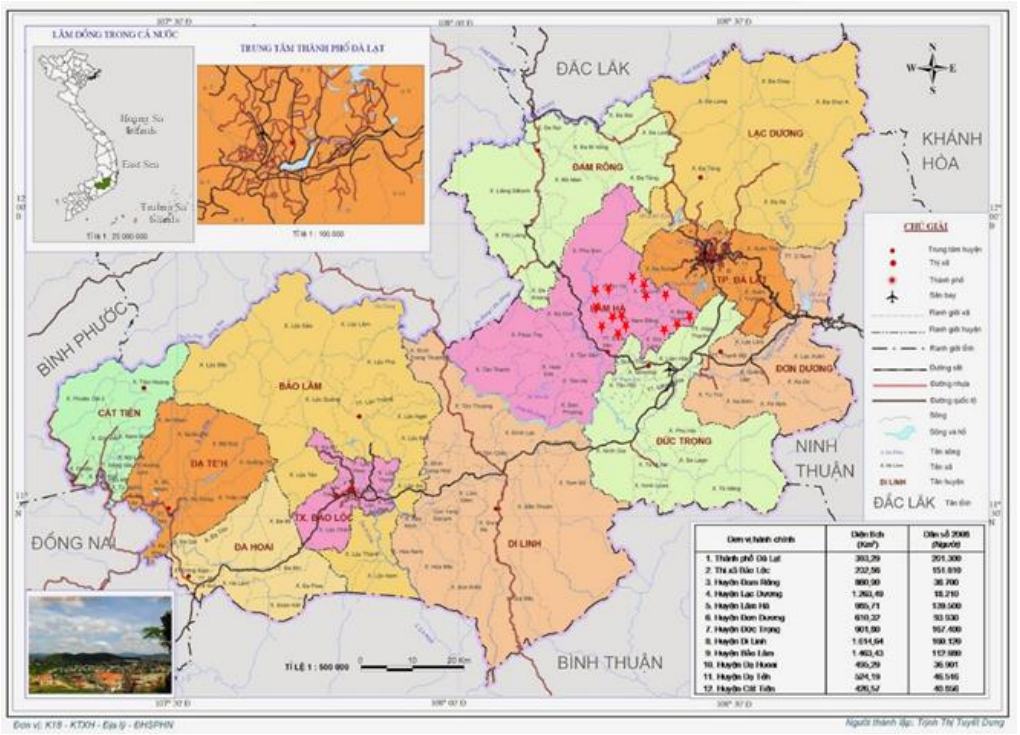

Figure 2. Sampling locations.

2.3. Sampling methods

As a previous research, each coffee garden will take 1 bulk sample with a depth of 0-15cm and a weight of about 1kg. This soil sample is combined from about 5-10 subsamples taken at different locations of the garden to ensure uniformity. These subsamples after removed gravel, leaves, roots were mix well and then followed by the quartering method. Depending on the shape and area of the garden, choose an appropriate sampling method such as the diagonal or zigzag method [8].

2.4. Analysis methods

pH, moisture, organic carbon and mechanical composition of soil samples were determined by Vietnamese standards TCVN 5979:2021, TCVN 4048:2011, TCVN 8941:2011 and TCVN 8567:2010, respectively [8].

There are several extraction methods (shaking, soxhlet, ultrasonic, pressurized liquid extraction, microwave-assisted extraction, solid-phase microextraction and QuEChERS) [10-13], cleaning techniques (SPE, GPC and SFC) [14], and analysis (GC, LC) [15–18] of pesticides in soil, this study chose the soxhlet extraction method, cleaning with Florisil and analysis by GC-MS.

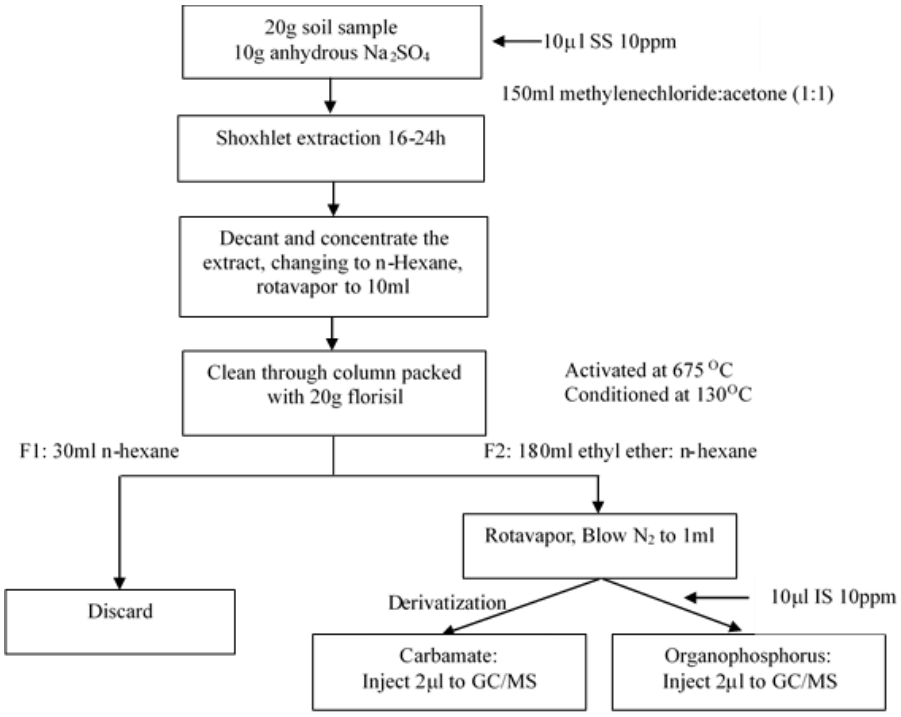

Figure 3. Schematic diagram of pesticides analysis.

Figure 3 describes the diagram of analysis of organophosphorus and carbamate pesticide. 20g of soil samples were extracted with dichloromethane: acetone mixture solvents for 16-24 hours. These extracts were evaporated and transferred to n-Hexane. After cleaned by Florisil column, the eluates were concentrated to 1ml and analyzed by GC-MS.

Derivatization is required for Carbamates before performing analysis. Pesticide concentration of the soil sample is calculated from calibration curve, surrogate standard and internal standard in µg/kg. Soil samples were analyzed according to EPA methods at the chemical and environmental laboratory. The testing laboratory has many years of experience in the field of analysis and has been accredited with ISO/IEC 17025 by the Ministry of Science and Technology and Vimcerts designation by the Ministry of Natural Resources and Environment.

2.5. Ecological risk assessment

To assess the ecological risks of pesticides, in this study, the risk quotient (RQ) is used and calculated according to the following formula:

$$RQ = C/ PNEC \quad (1)$$

where C is the concentration of the pollutant in the sample; PNEC is the concentration value predicted to have no effect on the organism.

$$PNEC = NOEC/ AF \quad (2)$$

where NOEC is the concentration with no effect observed; assessment factor (AF) - factor take into account potential chronic risks.

Assess the levels of ecological risk based on the values of RQ: RQ < 0.01: very low risk; 0.01 ≤ RQ < 0.1: low risk; 0.1 ≤ RQ < 1.0: moderate risk; RQ ≥ 1.0: high risk [8, 19–23].

3. Results and discussion

3.1. Physicochemical properties of soil samples

The pH of 30 soil samples in Lam Ha district in both May and November 2023 was acidic. In general, pH in May (rainy season) is lower than in November (dry season) with lowest in Phi To commune, ranging from 3.52-3.85; then go to Nam Ha commune from 3.90-4.25; Next is Me Linh commune from 4.11-4.36 and the highest is Dong Thanh commune from 4.36-4.58.

Soil moisture in the May was higher than in the November and was not too different between sampling points in the same period. Specifically, the humidity at Phi To ranges from 25.3-34.7%; Nam Ha from 23.7-34.5%; Me Linh from 24.5-38.4% and Dong Thanh from 23.4-33.2%.

Rainwater contains NH_3 which causes the soil to release H^+ and wash away alkaline metals, leading to a decrease in pH. pH and humidity will affect the ability to decompose pesticides in the soil. Organic carbon of 4 communes were ranged of 2.3-3.7%. Phi To ranges from 2.4-2.9%; Nam Ha from 2.3-3.1%; Me Linh from 2.8-3.3% and Dong Thanh from 3.2-3.7%.

Table 2. Physicochemical properties of the soil.

Sample type	pH	Moisture content	OCs	Mechanical components (%)			
				Coarse sand (2-0.2mm)	Fine sand (0.2-0.02mm)	Limon (0.02-0.002mm)	Clay (< 0.002mm)
Rainy seasons	4.05	32.37	2.92	2.85	13.43	28.39	55.33
Dry seasons	4.18	25.37	2.99	2.88	14.23	28.65	54.25

Soil samples in Phi To and Me Linh are clay-rich with the percentage of clay higher than 60% while in Nam Ha and Dong Thanh are mix-clay. There is no significant difference in soil mechanical composition between rainy and dry seasons (Table 2). The average percentages of coarse sand are similar but fine sand, limon and clay are 9.75%, 22.40%, 65.07% in Phi To and Me Linh, and 16.62, 33.67, 46.79% in Nam Ha and Dong Thanh, respectively.

3.2. Pesticide concentration of soil samples

Concentration of Organophosphorus and Carbamate pesticides in soil samples are showed at Table 3 and Table 4.

Table 3. Organophosphorus pesticide concentration.

Sampling time	Sample location	Chlorpyrifos (µg/kg)			Profenofos (µg/kg)		
		Min	Average	Max	Min	Average	Max
May-2023	Phi To	N.D	32.5	61	N.D	N.D	N.D
	Nam Ha	N.D	74.7	158	N.D	N.D	N.D
	Me Linh	119	231	391	N.D	17.3	42.5
	Dong Thanh	129	187	261	N.D	21.0	63
November-2023	Phi To	N.D	29.7	57.5	N.D	9.7	29.0
	Nam Ha	N.D	66.4	129	N.D	N.D	N.D
	Me Linh	78.5	169	294	N.D	7.0	28.0
	Dong Thanh	107	148	195	N.D	17.5	52.5

N.D: Not detected

Table 4. Carbamate pesticide concentration.

Sampling time	Sample location	Carbosulfan (µg/kg)		
		Min	Average	Max
May-2023	Phi To	N.D	N.D	N.D
	Nam Ha	N.D	3.0	15.0
	Me Linh	N.D	14.0	32.0
	Dong Thanh	N.D	12.3	37.0
November-2023	Phi To	N.D	N.D	N.D
	Nam Ha	N.D	4.4	22.0
	Me Linh	N.D	14.8	41.0
	Dong Thanh	N.D	11.0	33.0

N.D: Not detected

In 30 soil samples, 3 pesticides were detected including Chlorpyrifos and Profenofos of the Organophosphorus group and Carbosulfan of the Carbamate group. From Table 3, we found that soil samples in Phi To commune had the lowest Chlorpyrifos concentration with maximum concentration in May and November 2023 were 61 and 57.5 µg/kg, respectively. Nam Ha Commune had the maximum concentration were 158 and 129 µg/kg. The Chlorpyrifos concentrations of soil samples in Dong Thanh communes higher with maximum concentration were 261 and 195 µg/kg and highest in Me Linh with maximum concentration in May and November 2023 were 391 and 294 µg/kg.

Average Chlorpyrifos concentrations in soil samples gradually increased as 32.5, 74.7, 187, and 231 µg/kg in Phi To, Nam Ha, Dong Thanh, and Me Linh in May and 29.7, 66.4, 149, and 169 µg/kg in November. Pesticide concentrations were detected in the rainy season are higher than in the dry season, possibly because there are more pests and diseases in the rainy season, so the amount of pesticides used leads to high residue in the soil.

The highest concentrations of Profenofos were detected in 2 communes Me Linh and Dong Thanh in May at 42.5 and 63.0 µg/kg and in 3 communes Phi To, Me Linh and Dong Thanh in November at 29.0, 28.0 and 52.5 µg/kg respectively. The average concentrations in May were generally higher than in November.

There are 8 soil samples where Carbosulfan was detected in 3 communes: Nam Ha, Me Linh and Dong Thanh, divided equally between two sampling periods in May and November 2023. The highest concentration in Nam Ha, Me Linh and Dong Thanh in May were 15.0, 24.0 and 37.0 µg/kg and the November were 22.0, 41.0 and 33.0 µg/kg, respectively. There is no significant difference of average Carbosulfan concentration in the rainy and dry seasons, suggesting that this may just be the remaining residue in the soil. Chlorpyrifos concentration is showed and compared in Table 5. It was lower than in Lam Ha, February 2023 [8], Iran [23] and Malaysia [16] but higher than others.

Table 5. Chlorpyrifos concentration.

Sample Locations	Sample type	Sampling time	Chlorpyrifos concentration (µg/kg)	Reference
Lam Ha	Soil	2023	N.D - 391	This study
Lam Ha	Soil	2023	N.D - 954	Lam D.V. [8]
Mekong Delta	Land	2019	3.51 - 291	PhD thesis summary
Nepal	Soil	2021	32.5 - 177	Govinda Bhandari [21]
Iran	Soil	2021	240 - 510	Mohsen Hesami Arani [23]
Egypt	Sediment	2022	119 - 241	Eissa [22]
Ghana	Soil	2016	10 - 40	Fosu-Mensah [6]
Malaysia	Land	2010	20 - 2240	Norhayati Mohd Tahir [16]

N.D: Not detected

Table 6 compared Profenofos concentration with previous studies. The results obtained from this research were higher than in Nepal and Ghana. Table 7 showed the Carbosulfan concentration alittle bit lower than in Indonesia.

Table 6. Profenofos concentration.

Sample Locations	Sample type	Sampling time	Profenofos concentration (µg/kg)	Reference
Lam Ha	Soil	2023	N.D – 63.0	This study
Nepal	Soil	2020	1.75	Govinda Bhandari [20]
Ghana	Soil	2016	20-40	Fosu-Mensah [6]

N.D: Not detected

Table 7. Carbosulfan concentration.

Sample Locations	Sample type	Sampling time	Carbosulfan concentration (µg/kg)	Reference
Lam Ha	Soil	2023	N.D – 41.0	This study
Indonesia	Soil	2021	58.2-307.2	Ardiwinata [24]

N.D: Not detected

In the rainy season, soil pH decreases, moisture increases while organic carbon content and soil mechanical composition change little. The decomposition ability of pesticides increases with moderate humidity, mildly acidic to neutral pH, and high organic carbon content [25]. Soil mechanical composition also affects the decomposition ability of pesticides, however analysis results show that there is no obvious difference between soil samples in the dry season and the rainy season. Currently, no clear correlation has been found between the physicochemical properties of soil and the concentrations of pesticides. This may be because these pesticides are partly residual and partly used to kill pests during cultivation.

3.3. Ecological risk assessment

With AF = 10 and NOEC = 65 (µg/kg) for Chlorpyrifos, AF = 50 and NOEC = 50 (µg/kg) for Profenofos [19] and PNEC= 2410 (µg/kg) of Carbosulfan in soil [26], risk index RQ were calculated in Table 8.

Table 8. Risk assessment.

Sampling time	Sample location	RQ of Chlorpyrifos	RQ of Profenofos	RQ of Carbosulfan	Risk assessment
May-2023	Phi To	< 0.01-9.4	< 0.01	< 0.01	Very low risk - high risk
	Nam Ha	< 0.01-24.2	< 0.01	< 0.01	Very low risk - high risk
	Me Linh	18.2-60.0	< 0.01-42.5	0.013	high risk
	Dong Thanh	19.8-40.1	< 0.01-63	0.015	high risk
November-2023	Phi To	< 0.01-8.8	< 0.01	< 0.01	Very low risk - high risk
	Nam Ha	< 0.01-19.8	< 0.01	< 0.01	Very low risk - high risk
	Me Linh	12.1-45.2	< 0.01-28.0	0.017	high risk
	Dong Thanh	16.5-30.0	< 0.01-52.5	0.014	high risk

Table 8 summarizes the results of RQ coefficient in 30 soil samples in 4 communes of Lam Ha district. In general, the ecological risk coefficient is at a very low to high level. Samples detected Chlorpyrifos all had high risk because it is highly toxic and persistent. This is a specific pesticide that was widely used before being banned in 2021. Maybe because people continue to use it, soil samples have RQ coefficients from < 0.01 to 60.0, however it

is lower than the research in February 2023. Profenofos has RQ from < 0.01 to 63.0 and was found in 6/30 soil samples. Other Organophosphorus pesticides were not detected with a detection limit of 1.0 µg/kg and RQ < 0.01. Carbosulfan was found in 8/30 soil samples, however, due to lower toxicity than Chlorpyrifos and Profenofos, the RQ index was ranged from < 0.01 to 0.017. Other Carbamate pesticides were not found and had RQ < 0.01. RQ coefficient is only an initial preliminary assessment of the correlation between residual concentrations and toxicity thresholds. In the following studies, more appropriate evaluation tools will be used to make the most accurate conclusions.

With an ecological risk level < 1.0, no remedial measures are needed. However, with high levels > 1.0, it is necessary to issue warnings and take action to minimize impacts on humans and the environment. Some action that can be taken include propagating and instructing people about the toxicity and usage of some common pesticides, limiting the use of highly toxic and persistent pesticides, and using Personal protective equipment when spraying and cleaning after used to reduce contact.

4. Conclusions

The study was conducted 30 samples of coffee growing surface soil in 4 communes of Lam Ha district: Phi To, Nam Ha, Me Linh, and Dong Thanh. The physicochemical properties and two groups of pesticides, Organophosphorus and Carbamate, were selected for research. Basically, soil in the rainy season has lower pH and higher moisture than in the dry season. Organic carbon content and mechanical composition do not change much with the seasons. Among total 9 Organophosphorus and Carbamate pesticides, 3 were found: Chlorpyrifos, Profenofos and Carbosulfan of a total 30 soil samples. The highest concentrations of Chlorpyrifos, Profenofos and Carbosulfan were 391, 63 and 41 µg/kg, respectively. Using the RQ coefficient, the ecological risk level is assessed with risk results from very low to high and in ascending order from Phi To, Nam Ha, Dong Thanh and Me Linh.

Authors contribution: Constructing research idea: D.V.L., V.D.T.; Select research methods: D.V.L., V.D.T.; Data collection: D.V.L., V.D.T.; Data processing: D.V.L., V.D.T.; Writing original draft preparation: D.V.L.; Writing review and editing: D.V.L., V.D.T.

Acknowledgments: The authors would like to thank the Graduate University of Science and Technology, Vietnam Academy of Science and Technology; Chemical and environmental laboratory, Quality assurance and testing center 1 and ROOM strong research, Thuyloi University for their support during the research.

Conflicts of interest: The authors declare that this article was the work of the authors, has not been published elsewhere, has not been copied from previous research; there was no conflict of interest within the author group.

References

1. Available online: http://khuyennong.lamdong.gov.vn/ky-thuat-trong-trot/ki-thuat-trong-cay2/302-quy-trinh-k-thu-t-canh-tac-cay-ca-phe-che.
2. Pubchem available online: https://pubchem.ncbi.nlm.nih.gov/compound/.
3. Vale, A.; Lotti, M.J.H. Organophosphorus and carbamate insecticide poisoning. *Handb. Clin. Neurol.* **2015**, *131*, 149–168.
4. Degrendele, C.; Klánová, J.; Prokeš, R.; Příbylová, P.; Šenk, P.; Šudoma, M.; Röösli, M.; Dalvie, M.A. Samuel Fuhrimann. Current use pesticides in soil and air from two agricultural sites in South Africa: Implications for environmental fate and human exposure. *Sci. Total Environ.* **2022**, *807*, 150455.
5. Ragnarsdottir, K.V.J.J. Environmental fate and toxicology of organophosphate pesticides. *J. Geol. Soc.* **2000**, *157(4)*, 859–876.

6. Fosu-Mensah, B.Y.; Okoffo, E.D.; Darko, G.; Gordon, C. Organophosphorus pesticide residues in soils and drinking water sources from cocoa producing areas in Ghana. *Environ. Syst. Res*. **2016**, *5(1)*, 1–12.
7. Plant Protection Department. Available online: http://www.ppd.gov.vn.
8. Lam, D.V.; Toan, V.D.; Phuong, T.M. Residual and ecological risk assessment of Chlorpyrifos in coffee growing soil areas: A case study in Lam Ha district, Lam Dong province. *J. Hydro-Meteorol*. **2023**, *3*, 100–108.
9. U.S. Environmental Protection Agency: Operating Procedure. ID: LSASDPROC-300-R5. Soil Sampling.
10. Tadeo, J.L.; Pérez, R.A.; Albero, B.; García-Valcárcel, A.I.; Sánchez-Brunete, C. Review of sample preparation techniques for the analysis of pesticide residues in soil. *J. AOAC Int*. **2012**, *95(5)*, 1258–1271.
11. Falaki, F. Sample preparation techniques for Gas chromatography. IntechOpen, 2019. https://doi.org/10.5772/intechopen.84259.
12. Md Nur, A.N.; Husna, E.K.; Merillyn, V.J.; Rovina, K. Extraction and identification techniques for quantification of carbamate pesticides in fruits and vegetables. Pesticides - Updates on Toxicity, Efficacy and Risk Assessment, IntechOpen, 2022, *2*, https://doi.org/10.5772/intechopen.102352.
13. Pham, T.L.; Phan, T.H.; Nguyen, T.D. Analysis of pesticides in soil using dispersive solid phase extraction coupled to GC-MS. *Soil Sediment Contam: Int. J*. **2013**, *23(3)*, 339–352. https://doi.org/10.1080/15320383.2014.829024.
14. Das, S. Recent developments in clean up techniques of pesticide residue analysis for toxicology study: A critical review. *Univers. J. Agric. Res*. **2014**, *2*, 198–202. https://doi.org/10.13189/ujar.2014.020603.
15. Tat, T.Q.; Vien, D.M. Determination of analytical procedures for the active ingredient chlorpyrifos ethyl from soil. *VNU J. Sci.: Nat. Sci. Technol*. **2017**, *33(2S)*, 156–161.
16. Tahir, N.M.; Soon, K.H.; Ariffin, M.M.; Suratman, S. Chlorpyrifos and malathion residues in soils of a terengganu golf course: A case study. *Malaysian J. Anal. Sci*. **2010**, *14(2)*, 82–87.
17. João, B.; Paula, G.; Marco, G.S.; Mateus, E.P.; Ribeiro, A.B. Analysis of pesticide residues in soil: A review and comparison of methodologies. *Microchem. J*. **2023**, *195*, 109465. https://doi.org/10.1016/j.microc.2023.109465.
18. Mdeni, N.L.; Adeniji, A.O.; Okoh, A.I.; Okoh, O.O. Analytical evaluation of carbamate and organophosphate pesticides in human and environmental matrices: A review. *Molecules* **2022**, *27(3)*, 618. https://doi.org/10.3390/molecules27030618.
19. Lan P.T.N.; Hong P.T.; Toan, V.D.; Lan N.T.P. Textbook of soil pollution and treatment measures. Bach Khoa Publishing House, 2023.
20. Bhandari, G.; Atreya, K.; Scheepers, P.T.J.; Geissen V. Concentration and distribution of pesticide residues in soil: Non-dietary human health risk assessment. *Chemosphere* **2020**, *253*, 126594.
21. Bhandari, G.; Atreya, K.; Vašíčková, J.; Yang, X.; Geissen, V. Ecological risk assessment of pesticide residues in soils from vegetable production areas: A case study in S- Nepal. *Chemosphere* **2021**, *788*, 147921.
22. Eissa, F.; Al-Sisi, M.; Ghanem, K.J.J. Occurrence and ecotoxicological risk assessment of pesticides in sediments of the Rosetta branch, Nile River, Egypt. *J. Environ. Sci. Global*. **2022**, *118*, 21–31.
23. Arani, M.H.; Kermani, M.; Kalantary, R.R.; Jaafarzadeh, N.; Arani S.B. Pesticides residues determination and probabilistic health risk assessment in the soil and cantaloupe by Monte Carlo simulation: A case study in Kashan and Aran-Bidgol, Iran. *Ecotoxicol. Environ. Saf*. **2023**, *263*, 115229.

24. Ardiwinata, A.N.; Harsanti, E.S.; Kurnia, A.; Sulaeman, E. The distribution of paraquat and carbosulfan residues in Indonesia. *IOP Conf. Ser.: Earth Environ. Sci.* **2021**, *648*, 012033. https://doi.org/10.1088/1755-1315/648/1/012033.
25. Cink, J.H. Degradation of chlorpyrifos in soil: effect of concentration, soil moisture, and temperature. Retrospective Teses and Dissertations. 1995, 11048. Available online: https://lib.dr.iastate.edu/rtd/11048.
26. Carbosulfan Solution (Solvent: Acetonitrile). Available online: https://www.hpc-standards.com/shop/ReferenceMaterials/Pesticides/Carbosulfan_Acetonitrile4.htm.

JOURNAL OF
HYDRO-METEOROLOGY

Research Article

Mapping hydrological drought under the CMIP6 climate change scenarios in sub-basin scale: A case study in the upper part of Dong Nai river basin

Pham Hung[1]*, Le Van Trung[3,4], Vo Le Phu[3,4]

[1] Department of Natural Resources and Environment Lam Dong Province, Dalat, Vietnam, 54 Pasteur, Ward 4, Dalat City, Lam Dong Province, Vietnam; hungmtk25@gmail.com
[2] Faculty of Environment and Natural Resources, Ho Chi Minh City University of Technology (HCMUT), 268. Ly Thuong Kiet Street, District 10, Ho Chi Minh City, Vietnam; lvtrung@hcmut.edu.vn; volephu@hcmut.edu.vn
[3] Vietnam National University Ho Chi Minh City, Linh Trung Ward, Thu Duc District, Ho Chi Minh City, Vietnam; lvtrung@hcmut.edu.vn; volephu@hcmut.edu.vn

*Corresponding author: hungmtk25@gmail.com; Tel.: +84–886138809

Received: 15 August 2024; Accepted: date; 03 October 2024: 25 December 2024

Abstract: Hydrological droughts have become more severe due to the compounded effects of climate change and anthropogenic activities. This study aims to assess how climate change could impact hydrological droughts at the sub-basin scale for the Upper Part of Dong Nai (UPDN) river basin. The study used the Soil and Water Assessment Tool (SWAT) to simulate hydrological conditions based on climate change scenarios of SSP2-4.5 and SSP5-8.5 from the CMIP6 projections for the future period of 2030s (2021-2040) and 2050s (2041-2060). The streamflow drought index (SDI) was applied to evaluate the drought severity and frequency. The findings indicate a clear increasing trend in minimum (Tmin) and maximum temperatures (Tmax) relative to yearly rainfall. Under the SSP2-4.5 scenario, yearly rainfall shows a slight increase. However, under the SSP5-8.5 scenario, annual rainfall has a slight increase in the West-Southwest and a decrease in the East-Southeast regions. Rainfall trends show a decrease in the dry season and an increase in the rainy season. The frequency and severity of hydrological droughts can vary between sub-basins. Da Tam, Don Duong, Da Quyn, Da Dang, Dak Nong, Dong Nai 2, and Dak R'Keh are the sub-basins that have more extreme drought conditions compared to the rest of the basins. These results emphasize the need for targeted drought management strategies in the UPDN river basin to build resilience against future climate impacts.

Keywords: Climate change; Mapping hydrological drought; SWAT model; CMIP6; The upper part of Dong Nai river basin; Drought management.

1. Introduction

Hydrological droughts, characterized by reduced water availability in rivers, lakes, and reservoirs, pose significant challenges to water resource management. These droughts are not merely the result of short-term weather anomalies but are often linked to broader climatic patterns and long-term changes in rainfall and temperature [1, 2]. Climate change scenarios suggest that many regions, including Southeast Asia, are likely to experience more severe drought conditions due to shifts in precipitation patterns and rising temperatures [3]. In addition, drought patterns are also driven by seasonal fluctuations in precipitation, temperature, and other hydro-meteorological conditions [4]. Along with climate change,

human-driven activities such as the construction and operation of reservoirs have significantly altered flow patterns [5]. These modifications in flow impact drought conditions by changing the timing and distribution of water availability, thereby exacerbating drought severity and frequency [6, 7].

According to the IPCC, climate change has caused varying increases and decreases in rainfall at high and low latitudes of the Earth [8], and these shifts in precipitation have altered drought conditions. Global climate change scenarios for the future are often based on estimates from General Circulation Models (GCMs). GCMs have relatively coarse resolutions, most of which are around 100km or more [9]. Therefore, it is necessary to suitable downscaling techniques to be able to forecast climate change at the local or regional scale. Up to now, IPCC has six times of accessing and updating climate change scenarios and the most recent was the sixth assessment report (AR6) [10]. Therein, the Coupled Model Intercomparison Project Phase 6 (CMIP6) climate model benchmarking project was used to support the IPCC's AR6 [11]. Compared to the fifth assessment report (AR5) known as Representative Concentration Pathways (RCPs), the AR6 was built based on the Shared Socio-economic Pathways (SSP) approach with 5 main scenarios including SSP1, SSP2, SSP3, SSP4, and SSP5 with respectively name: (i) "Green growth", (ii) "Middle-of-the-road", (iii) "Regional rivalry", (iv) "Inequality" or "A road divided", and (v) "Fossil fuel-based development" [12]. These scenarios are crucial for understanding how different climate futures might influence regional hydrological patterns. In the context of the UPDN river basin, applying CMIP6 scenarios allows for a more precise prediction of hydrological drought risks, offering insights into the spatial and temporal variability of drought across sub-basins.

The upper part of Dong Nai (UPDN) river basin plays a crucial role in the ecological and socio-economic sustainability for the whole Dong Nai river basin. It supports diverse ecosystems, including protected forests and biodiversity hotspots like Cat Tien National Park. The river's natural flow sustains wetlands, fisheries, and agriculture, and maintains the region's ecological balance. Additionally, the UPDN river basin is essential for water supply, energy production, and agriculture. It provides water to millions of people, especially in downstream areas such as Ho Chi Minh City. The basin also hosts major hydropower plants, such as the Dong Nai hydropower system (2, 3, 4, 5), which supplies a significant portion of the region's energy needs. However, rapid urbanization, deforestation, and agricultural activities have placed increasing pressure on water resources and ecosystems. These challenges, combined with climate change, have made the basin more vulnerable to extreme events such as droughts and floods, threatening both its ecological integrity and socio-economic sustainability. Previous studies have primarily focused on basin-wide assessments [13–16], often overlooking the drought impacts for sub-basin. Mapping hydrological drought at the sub-basin scale is crucial for identifying areas most at risk and implementing effective mitigation strategies. Therefore, understanding the impacts of climate change on droughts, especially hydrological droughts following the spatial and temporal aspects at the sub-basin scale, in the UPDN river basin is essential for effective adaptation and mitigation strategies.

This study aims to map hydrological drought across the sub-basins of the UPDN river basin under the CMIP6 climate scenarios SSP2-4.5 and SSP5-8. The comprehensive analysis has been employed by integrating GIS, remote sensing (RS), and the Soil and Water Assessment Tool (SWAT) model, which has been widely used for climate change impacts on hydrology and droughts [4, 13, 14, 17, 18]. In addition, the frequency and intensity of drought events has also analyzed following temporal and spatial distribution in the sub-basin scale. The findings could offer valuable insights for regional water resource management, particularly in planning for drought resilience and adaptation under the conditions of ongoing climate change.

2. Materials and Methods

2.1. Study area

The Dong Nai river basin, the longest inland river in southeastern Vietnam, extends over 586 km and encompasses a catchment area of approximately 36,530 km², spanning across ten provinces and Ho Chi Minh City. This region is a significant economic hub, accounting for approximately 48% of Vietnam's gross domestic product in 2022 [19]. The basin has over 200 irrigations and hydropower reservoirs, regulating nearly 6 billion cubic meters of water. It also has a hydropower capacity of around 3,000 MW. The forest cover rate of the whole basin is about 28%, but it is mainly located upstream in the provinces of the Central Highlands. Hence, this study focuses on the UPDN basin, which spans an area of 11,036 km², with 70% situated in Lam Dong province compared to 30% of the rests of Dak Nong, Binh Phuoc, Dong Nai, and Binh Thuan provinces [20]. The characteristics of the UPDN river basin and its 18 sub-basins are detailed in Table 1 and Figure 1.

Table 1. Properties of the UPDN river basin's sub-basins.

No.	ID	Sub-basin	Main reservoir	Sub-basin mean elevation (m)	Land use (the largest area % first)	IYRES	CHP (MW)	$RES_{\_EVOL}$ (10^4 m^{4-})	Area (km²)
1	DN1	Da Nhim	Da Nhim	1500	Forest, perennial agri.	1965	240	16500	729
2	DN2	Da Tam	Tuyen Lam	1321	Forest, annual agri.	1987	-	2785	227
3	DN3	Don Duong	-	1141	Forest, annual agri.	-	-	-	372
4	DN4	Da Quyn	Dai Ninh	978	Forest, annual agri.	2008	300	31977	562
5	DN5	Suoi Vang	Dankia	1550	Forest, perennial agri.	1998	4.6	90	314
6	DN6	Da Dang	Da Dang	987	Forest, industrial crops	2016	34	760	1283
7	DN7	Dong Nai 2	Dong Nai 2	907	Perennial crops, forest	2013	70	28100	332
8	DN8	Dong Nai 3	Dong Nai 3	847	Forest, perennial agri.	2011	180	169010	495
9	DN9	Dong Nai 4	Dong Nai 4	714	Forest, perennial agri.	2012	340	33210	159
10	DN10	Dak Nong	Dak R'tih	757	Perennial crops, forest	2011	144	13710	1120
11	DN11	Dong Nai 5	Dong Nai 5	637	Forest, perennial agri.	2014	150	10633	592
12	DN12	Dak R'Keh	Dak Sin	567	Perennial crops, forest	2015	28	1609	321
13	DN13	Dong Nai 6	-	372	Forest, perennial agri.	-	-	-	483
14	DN14	Cat Tien	-	285	Forest, perennial agri.	-	-	-	773
15	DN15	Da Teh	Da Teh	414	Forest, perennial agri.	1990	-	2400	630
16	DN16	Da Huoai	Dam B'ri	592	Forest, perennial agri.	2013	75	5630	909
17	DN17	Ta Lai	-		Perennial crops, rice	-	-	-	431
18	LN1	La Nga	Dai Nga	140	Perennial crops, forest	2015	10	46	1304
All of the UPDN									11036

*CHP is the capacity of hydropower plants (MW); YRES is the year the reservoir became operational; $RES_{\_EVOL}$ is the quantity of water needed to raise the reservoir to the emergency spillway (10^4 m^4); agri. is agriculture).

The UPDN river basin is subdivided into 18 sub-basins across two tributaries including the main tributary of the UPDN river basin and the sub-tributary La Nga river basin [21]. The main tributary has 17 sub-basins (from DN1 to DN17) terminating at the Tri An reservoir. The sub-tributary has just one sub-basin (LN1) ending at the Dami hydropower reservoir. The basin's terrain ranges from the Lang Biang plateau (1,300-2,000 above sea level) in the North, through the Di Linh plateau (700-1,000 m) in the center, to a transitional zone with elevations of 200-500 m in the South-Southwest. The region experiences a tropical monsoon climate varying with terrain elevation with a rainy season from May to November and a dry season from December to April of the following year. The average annual rainfall was nearly 2500 mm. The average annual temperature was approximately 22°C. Total rainfall accounts for approximately 87% in the rainy season compared to 13% in the dry season. The total flow in the basin is about 18.5 billion cubic meters, and the rainy season accounts for approximately 85% compared to only 15% in the dry season [22]. These distinct seasonal

rainfall patterns play a critical role in the occurrence of hydrological droughts. During the dry season, reduced precipitation and high evaporation rates can significantly lower river flows and water levels in reservoirs, intensifying drought conditions. Conversely, during the rainy season, heavy rainfall can lead to uneven water distribution, leaving some areas more prone to flooding.

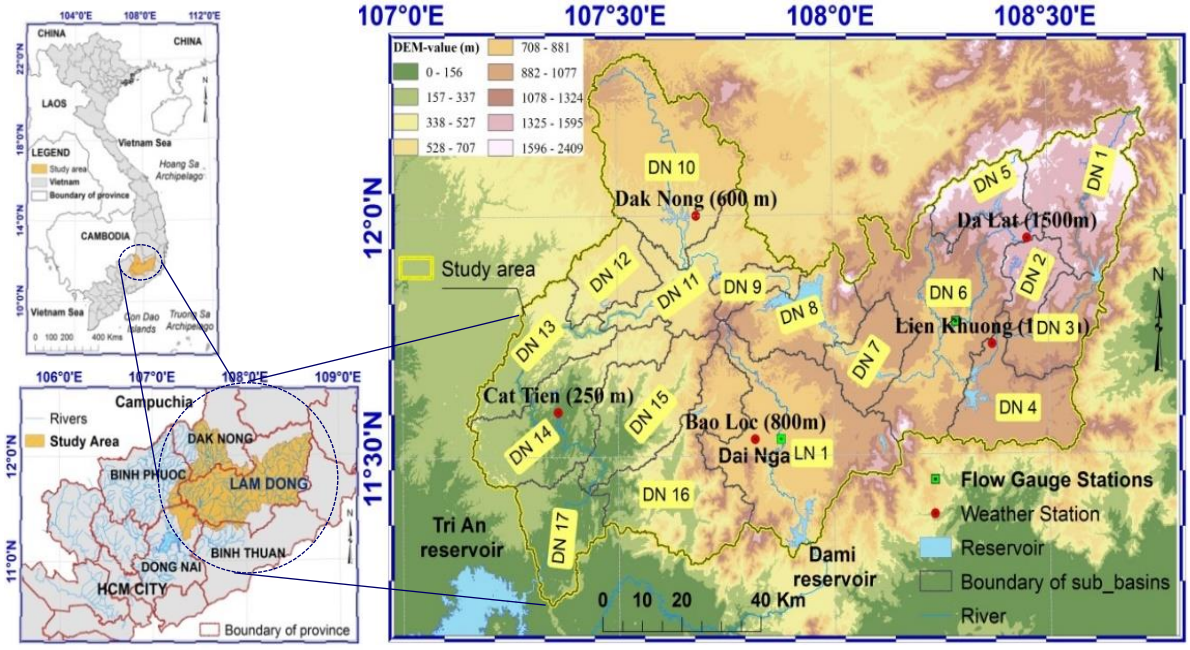

Figure 1. Location of the study area and its sub-basins based on DEM.

2.2. Methodology

The methodological framework for this study is illustrated in Figure 2.

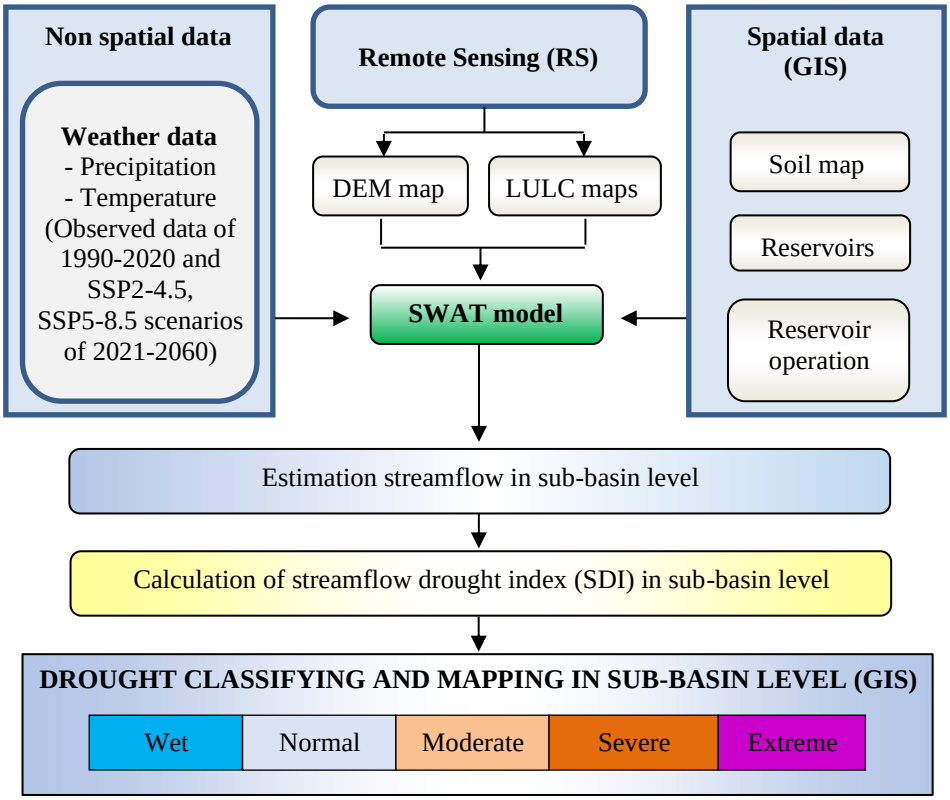

Figure 2. Flowchart of the methodology used for mapping hydrological drought.

2.2.1. Data collection and input preparation

a) Hydro-meteorology data collection

Daily rainfall and temperature data (T_{max}, T_{min}) in the past for the 30-year period (1990-2020) serving as input for the SWAT model as well as for comparison and evaluation purposes have been collected at 5 stations, including Da Lat (1509 m), Lien Khuong (1100 m), Bao Loc (800 m), Dak Nong (600 m), and Cat Tien (300 m) with corresponding altitudes in the areas of about 1,500 m, 1,100 m, 800 m, 600 m and 250 m, as shown in Table 2. These data have been gathered from local management agencies (Department of Natural Resources and Environment of Lam Dong Province, Highland Regional Hydro-meteorological Center). The distribution of these 5 monitoring stations is evenly dispersed across the basin with different elevations, so they can cover the climatic conditions of the study region. Information on the monitoring stations is shown in Table 1 and Figure 1.

Table 2. Descriptions of meteorological monitoring stations in the basin.

No	Name of the monitoring station	Station altitude (m)	Height of zone (m)	Longitude	Latitude
1	Da Lat station	1509	1500	108.45	11.95
2	Lien Khuong Station	939	1100	108.37	11.73
3	Bao Loc Station	840	800	107.82	11.54
4	Dak Nong Station	631	600	107.68	12.00
5	Cat Tien	250	300	107.36	11.59

b) Climate change scenarios in the future

Selecting appropriate General Circulation Models (GCMs) is crucial for enhancing downscaled result accuracy and optimizing computational resources. Five GCMs available in the CMIP6_VN dataset, namely EC-Earth3-Veg, EC-Earth3, CanESM5, HadGEM3-GC31-LL, and CNRM-CM6-1-HR, were chosen based on their suitability and effectiveness for the region [23, 24]. These models were downscaled using the Bias Corrected Spatial Disaggregation (BCSD) method, resulting in a spatial resolution of 10×10 km (~ 0.1°×0.1°) and daily temporal resolution [25, 26]. These climate data are available at: http://remosat.usth.edu.vn/~thanhnd/Download/dat_GEMMES_WP1.

As mentioned above, the Shared Socioeconomic Pathways (SSP) approach in CMIP6 is more up-to-date than the previous CMIP5's Representative Concentration Pathways (RCPs), offering better accuracy in rainfall and temperature projections [8, 11, 18, 25, 27]. The SSP2-4.5 and SSP5-8.5 scenarios from CMIP6 represent "moderate" and "extreme" emissions, respectively, and are recommended by the IPCC to quantify varying levels of greenhouse gas emissions and associated socioeconomic factors [18]. Therefore, the study utilizes climate change scenarios of SSP2-4.5 and SSP5-8.5 to project future hydrological drought conditions for this study. Climate projections are analyzed in the future period of 2021-2060 for minimum temperature, maximum temperature and precipitation. Hydrologic droughts are more deeply assessed periods of the 2030s (2021-2040) and the 2050s (2041-2060). To facilitate localized analysis at specific monitoring stations and to input prepare for SWAT model, datasets in "netCDF.NC" were converted to point data ("Excel.xls") by using ArcGIS's "Multidimension Toolbox".

c) Operation of reservoirs

Reservoirs play an important role in the region's water management, as depicted in Figure 1 and detailed in Table 1. To evaluate the impact of reservoir operations on drought conditions, key reservoir characteristics such as hydropower capacity, operational start year, storage volume etc. were collected from the local Departments of Industry and Trade (DIT) and Agriculture and Rural Development (DARP). Current and future operations are established according to the inter-reservoir operation procedures for the Dong Nai river basin, as stipulated in Decision No. 1895/QD-TTG [28]. Furthermore, the maintenance of

minimum environmental flows downstream of reservoirs follows Circular 64/2017/TT-BTNMT [29].

2.2.3. Setup SWAT model

a) SWAT model description

The Soil and Water Assessment Tool (SWAT) is a hydrological model founded on physical principles, designed by Jeff Arnold for the USDA-ARS [30]. It partitions a watershed into sub-watersheds and Hydrological Response Units (HRUs), linking them through stream networks. SWAT operates in two phases: the land phase, which calculates water, sediment, nutrient, and pesticide loads from each HRU, and the routing phase, which tracks these quantities through the channel network to the watershed outlet. The model uses the water balance equation:

$$SW_t = SW_0 + \sum_{i=1}^{t}(R_{day} - Q_{surf} - E_a - w_{seep} - Q_{gw}) \quad (1)$$

where SW_t is the final soil water content; SW_0 is the initial soil water content on day i; t is the time (days); R_{day} is the amount of precipitation on day i; Q_{surf} is the amount of surface runoff on day i (mm H_2O); E_a is the amount of evapotranspiration on day i; w_{seep} is the amount of water entering the vadose zone from the soil profile on day i; Q_{gw} is the amount of return flow on day I (all water units are in mm H_2O).

- Dataset

Essential datasets for the SWAT model include Digital Elevation Model (DEM), soil and Land Use/Land Cover (LULC) maps, and weather data [30]. This study utilized a 12.5-meter resolution DEM that was downloaded from the NASA website: https://urs.earthdata.nasa.gov/users/new. This website provides access to a broad range of Earth observation data, including DEM, satellite imagery, and climate data. The LULC map was inherited from 2020 classified Landsat OLI-TIRS images with seven categories WATR, URML, AGRR, FRSE, FRST, PINE, and AGRC [20, 31]. Historical daily rainfall and temperature data from 1990 to 2020 from five weather stations (Bao Loc, Da Lat, Lien Khuong, Cat Tien, and Dak Nong) were used to input for the SWAT model. Monitoring flow at Thanh Binh, Dai Nga, and Tai Lai gauges in the same period of 1990-2020 were used to calibrate and validate the SWAT model. While missing solar radiation, wind speed, and humidity data were auto-generated by SWAT [32]. Future climate projections were derived from CMIP6 scenarios. Table 3 summarizes the datasets for the applied SWAT model.

Table 3. Input data used to simulate and evaluate the SWAT model.

Data	Resolution	Source
Digital Elevation Model (DEM) map	12.5 m	Downloaded from the NASA website: https://urs.earthdata.nasa.gov/users/new
Soil map	30 m	Obtained from the local Department of Natural Resources and Environment (DONRE)
LULC	30 m	Landsat OLI-TIRS images in 2020, downloaded from the website: http://earthexplorer.usug.gov
Weather	Five stations	Obtained from 5 weather stations (Lien Khuong, Da Lat, Bao Loc, Cat Tien and Dak Nong)
Streamflow	Three stations	Derived from 3 gauges (Thanh Binh, Dai Nga, and Ta Lai)

- Model evaluation

The SWAT model could be evaluated by using several key indices such as the coefficient of determination (R^2), Nash-Sutcliffe efficiency (ENS), the Root Mean Square Error (RMSE) and Percent Bias (PBIAS). In this study, R^2 and ENS were specifically chosen for evaluation due to their strong relevance in assessing model performance in hydrology. The R^2 provides a clear measure of the proportion of variance explained by the model, while

ENS effectively captures the model's predictive accuracy in relation to observed data. Together, these indices offer a comprehensive view of the model's performance, essential for validating its reliability in simulating hydrological processes. R^2 ranges from 0 to 1, with 1 indicating a perfect simulation. ENS ranges from -∞ to 1, with values above 0.5 considered satisfactory; values from 0.5-0.65, 0.65-0.75, and 0.75-1.0 are acceptable, good, and very good, respectively [33]. Streamflow data from 1990-2020 from Dai Nga, Thanh Binh, and Ta Lai gauges were used for the model calibration and validation. Calibration used data from 1990-2000, and validation used data from 2001-2010. The SUFI-2 algorithm, a suitable method implemented in SWAT-CUP 2012 and ArcGIS 10.2 [34], was used for these steps of model calibration and validation. Notably, the missing meteorological data such as solar radiation, wind speed, and humidity can impact model performance by introducing bias or reducing the accuracy of simulations. However, the auto-generation method employed by SWAT is appropriate as it uses established algorithms and relationships to estimate these missing variables based on available data, thereby maintaining the integrity of the model outputs.

2.2.2. Drought indices

The temporal variation in hydrological drought can differ across various time scales, including short-term (1 or 3 months), medium-term (6 months), and long-term (12, 24, and 48 months) accumulation periods. The medium-term time scale of 6 months (SPI6, SDI6) is appropriate for portraying hydro-meteorological regimes and is suitable for monitoring hydro-meteorological drought [35]. Thus, this study uses the streamflow drought index in a 6-month scale (SDI6) for assessing hydrological drought in the UPDN river basin due to its effectiveness, as popularly applied by previous research [14, 17, 35]. Monthly streamflow data in the future periods of the 2030s (2021-2040) and 2050s (2041-2060) were calculated using the DrinC software, a tool widely adopted in drought research [36, 37], and freely accessed at the website: (https://drought-software.com). Drought classifications are based on SDI values as follows: Drought classifications are based on SDI values as follows: $SDI \geq 2.0$: Extremely wet; $1.5 \leq SDI < 2.0$: Very wet; $1.0 \leq SDI < 1.5$: Moderately wet; $-1.0 \leq SDI < 1.0$: Normal; $-1.5 \leq SDI < -1.0$: Moderate drought, $-2.0 \leq SDI < -1.5$: Severe drought, $SDI \leq -2.0$: Extreme drought [14, 38].

3. Results and discussions

3.1. Performance evaluation of the SWAT model

The SWAT model was calibrated and validated by using simulated and observed flows from 1990-2000 and 2001-2010, respectively. The hydrological stations were selected based on their geographic distribution, data availability, and representativeness of the UPDN river basin. Thanh Binh and Dai Nga stations, located upstream, and Ta Lai, downstream, were chosen to capture the natural flow patterns across different sections of the basin. Additionally, the data from these stations during the selected periods of 1990-2000 for calibration and 2001-2010 for validation were considered reliable and minimally impacted by anthropogenic activities (hydropower operation). This ensured stable hydrological conditions, allowing for accurate and robust model calibration and validation. The study used the Sequential Uncertainty Fitting, version 2 (SUFI-2) method for model calibration and verification, as it typically yields good results [34]. The SUFI-2 method efficiently narrows parameter ranges with few iterations, making it ideal for complex models like SWAT [14, 18], where capturing variability and reducing uncertainty are crucial for accurate streamflow predictions. The SWAT model's performance was assessed by using R^2 and ENS statistical values, both of which exceeded 0.70 (Table 4). These values demonstrate the model's good suitability based on criteria in previous studies [33, 39]. Therefore, it can be concluded that

the SWAT model is appropriate for predicting streamflow in the UPDN river basin. Accordingly, it can be reliably used to project the impacts of hydrological drought conditions in the sub-basin scale for the study area in the future.

Table 4. The values of R^2 and NSI in the calibration and validation periods of the SWAT model.

Gauging station	Calibration		Validation	
	R^2	NSI	R^2	NSI
Thanh Binh	0.810	0.757	0.811	0.809
Dai Nga	0.812	0.780	0.781	0.809
Ta Lai	0.731	0.712	0.771	0.759

3.2. Projected changes in minimum, maximum temperature, and precipitation

Figure 3 illustrates the yearly average trends of minimum temperature (T_{min}), maximum temperature (T_{max}), and precipitation from 2021 to 2060. These trends are based on ensemble means from five selected Global Climate Models (GCMs) under the SSP2-4.5 and SSP5-8.5 scenarios for five areas: Da Lat (DL), Lien Khuong (LK), Bao Loc (BL), Dak Nong (DN), and Cat Tien (CT). The results show that T_{max} and T_{min} have similar increasing trends across the entire UPDN river basin, with nearly parallel trend lines. Both SSP2-4.5 and SSP5-8.5 scenarios indicate a more pronounced increase in yearly mean T_{min} and T_{max} compared to yearly precipitation. The temperature increases of the SSP5-8.5 scenario project higher from 0.5°C to 1.0°C compared to the SSP2-4.5 scenario across the UPDN river basin.

Under the SSP2-4.5 climate change scenario, the temperature increases in Da Lat, Lien Khuong, Bao Loc, Dak Nong, and Cat Tien are approximately 0.80°C, 0.81°C, 0.82°C, 0.83°C, and 0.84°C for T_{max}, and 0.75°C, 0.75°C, 0.76°C, 0.76°C, and 0.77°C for T_{min}, respectively. Figure 4 (a1, a2) illustrates the spatial distribution of these temperature increases. Under the SSP5-8.5 climate change scenario, both T_{min} and T_{max} show similar increasing trends from 2021 to 2060 across all areas. The increases in T_{min} at Da Lat, Lien Khuong, Bao Loc, Dak Nong, and Cat Tien are approximately 1.21°C, 1.22°C, 1.24°C, 1.27°C, and 1.29°C. Meanwhile, the values for T_{max} are 1.20°C, 1.23°C, 1.26°C, 1.28°C, and 1.32°C, respectively. The spatial distribution of temperature increase is less in the East-Northeast regions compared to the South-Southwest regions, as Figure 4 (b1, b2).

Regarding rainfall factors, the SSP2-4.5 scenario graph and trend function in Figure 3 show no clear increasing or decreasing trend for yearly rainfall from 2021 to 2060. The results show a distinct upward trend in both minimum (T_{min}) and maximum (T_{max}) temperatures compared to vague and unclear fluctuation trends in annual rainfall. These findings are also consistent with previous reports [2, 17, 18, 40, 41]. The average rainfall across the UPDN river basin during this period is 2138 mm. Under the SSP5-8.5 scenario, the average annual rainfall is 2096 mm, lower than the SSP2-4.5 scenario. Specifically, under the SSP2-4.5 scenario, the rainfall in Da Lat, Lien Khuong, Bao Loc, Dak Nong, and Cat Tien is approximately 1692 mm, 1688 mm, 2490 mm, 2462 mm, and 2359 mm respectively. Under the SSP5-8.5 scenario, these values are 1633 mm, 1631 mm, 2447 mm, 2438 mm, and 2331 mm respectively. Similar to temperature factors, the spatial distribution of yearly rainfall increase in East-Northeast regions is less pronounced than in South-Southwest regions under the SSP2-4.5 scenario. Moreover, under the SSP5-8.5 scenario, Da Lat, Lien Khuong, and Bao Loc show yearly rainfall decrease trends ranging from -6.73% to -1.23% per year. Meanwhile, Dak Nong and Cat Tien regions show yearly rainfall increase trends ranging from 1.53% to 7.03% per year, as shown in Figure 4 (b3). The relative stability of annual rainfall under the SSP2-4.5 and SSP5-8.5 scenarios suggests that water availability may not fluctuate drastically throughout the years, allowing for more consistent irrigation practices and crop management strategies. However, the distribution of rainfall involves uncertainty [25, 42], so stakeholders must remain vigilant in monitoring rainfall patterns to adapt to potential shifts in climate conditions.

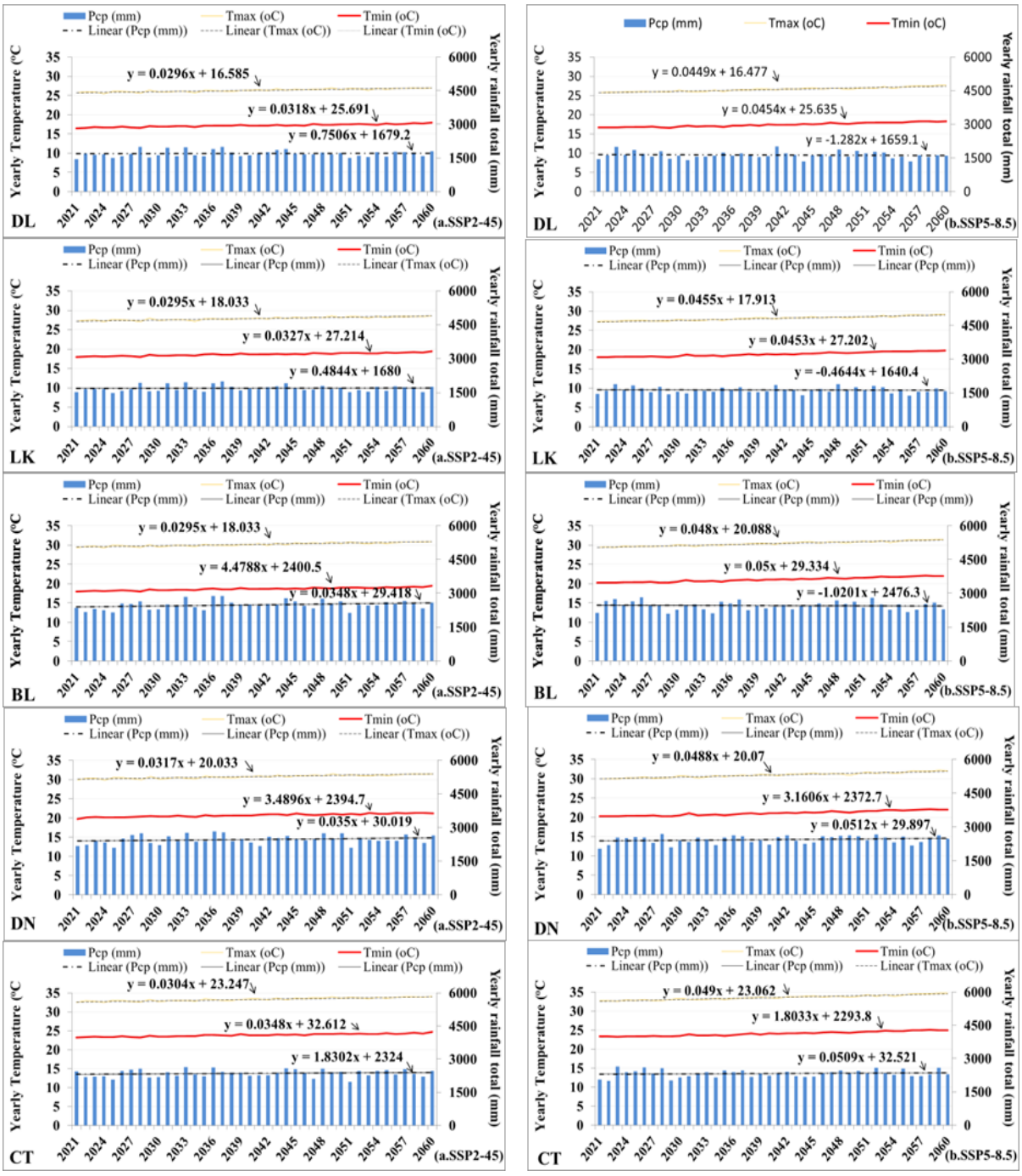

Figure 3. Projected changes in yearly minimum temperature, maximum temperature, and precipitation in the period of 2021-2060 in Da Lat (DL), Lien Khuong (LK), Bao Loc (BL), Dak Nong (DN), Cat Tien (CT): (a) SSP2-45 scenario; (b) SSP5-8.5 scenario.

Because rainfall volumes and changes significantly impact drought conditions [1], this study analyzed rainfall in more detail to assess its effect on drought in the basin. Average monthly precipitation for 2021-2060 was examined in two periods: 2021-2040 (near future) and 2041-2060 (mid-century), under SSP2-4.5 and SSP5-8.5 scenarios. This analysis provides crucial information for developing short-term and long-term adaptation strategies. Figure 5 shows changes in average monthly rainfall for the 2030s and 2050s under the SSP2-4.5 scenario, compared to the 1990-2020 historical period. Monthly rainfall tends to increase from mid-rainy season to the early dry season (August to December). Conversely, monthly rainfall tends to decrease from the mid-dry season to the early rainy season (February to May) for both SSP2-4.5 and SSP5-8.5 scenarios. These results are also similar

to the previous study in Ca river, a basin located in North Central Vietnam with a climate divided into four distinct seasons (autumn, winter, spring, and summer), the spring MAM (March, April, May) precipitation in the future could be decreased, while the autumn (September, October, November: SON) precipitation could be increased [41, 43]. Clearly, the trend of increasing and decreasing rainfall in the study area has the distinctly dry-rainy seasonal characteristics of the Central Highlands region.

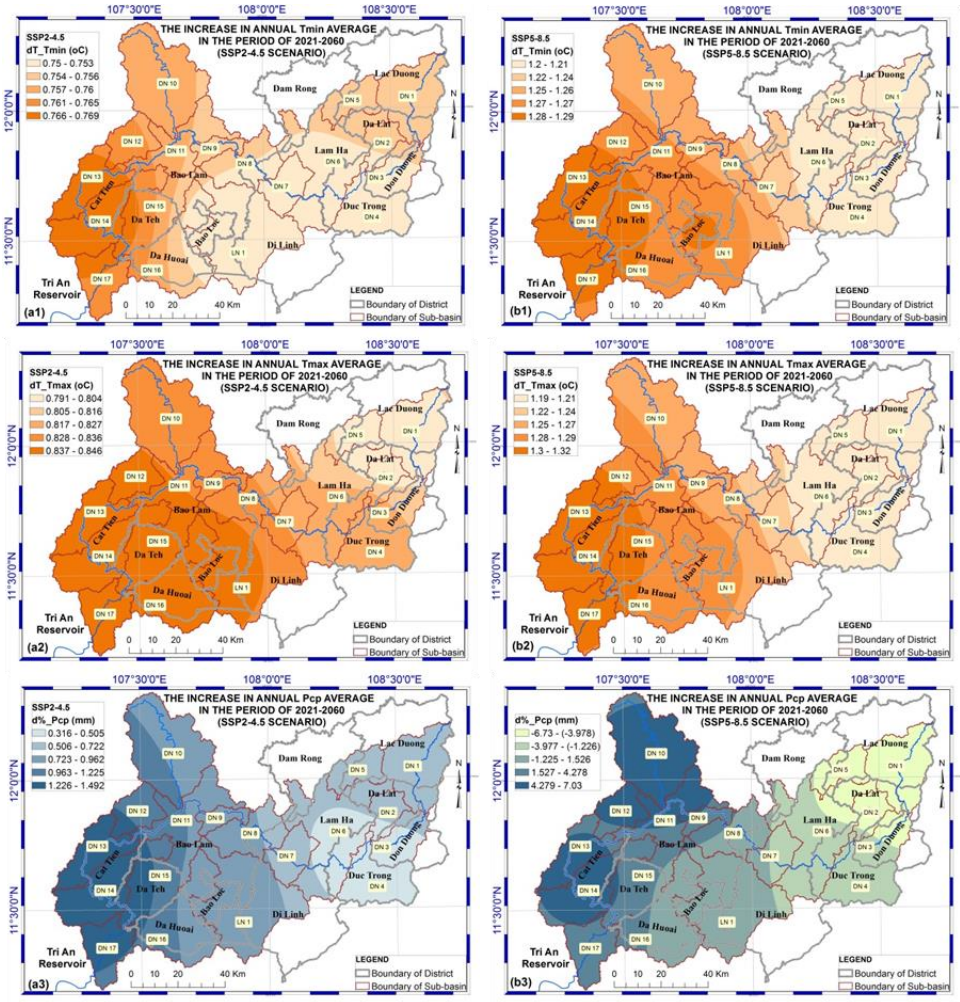

Figure 4. Spatial changes and trends in (1) annual minimum temperature average (T_{min}, ^oC), (2) annual maximum temperature average (T_{max}, ^oC) and (3) annual precipitation (P%, mm) in the period of 2021-2060 in the UPDN river basin: (a) SSP2-4.5 scenario; (b) SPP5-8.5 scenario.

Compared with the SSP2-4.5 scenario, the average monthly rainfall of the SSP5-8.5 scenario is more erratic and unpredictable. In the period 2022-2041, rainfall decreases in the dry season months including January, February, April, May, June, and July. While rainfall increases in the months of September, October, November and December. In the period 2041-2060, rainfall decreases in February, March, April, May, and June but increases in the months of January, June, August, September, October, November, and December. Thus, the SSP5-8.5 scenario can cause irregular monthly rainfall changes, no longer following the seasonal pattern (dry season and rainy season) in the basin.

Generally, under the influence of climate change, the results show that in both SSP2-4.5 and SSP5-8.5 scenarios, rainfall tends to increase in the rainy season months and decrease in the dry season months, especially in the last months of the dry season and the early rainy season (from April to May). It can be predicted that climate change will cause droughts and floods to become more and more unusual in the near future in the basin. Therefore, to

effectively mitigate the risk of extreme drought events during the dry season, managers and policymakers must implement proactive measures focused on prevention and preparedness. Upgrading reservoirs and improving irrigation efficiency are essential for optimizing water management and ensuring that agricultural and domestic needs are met during times of water scarcity.

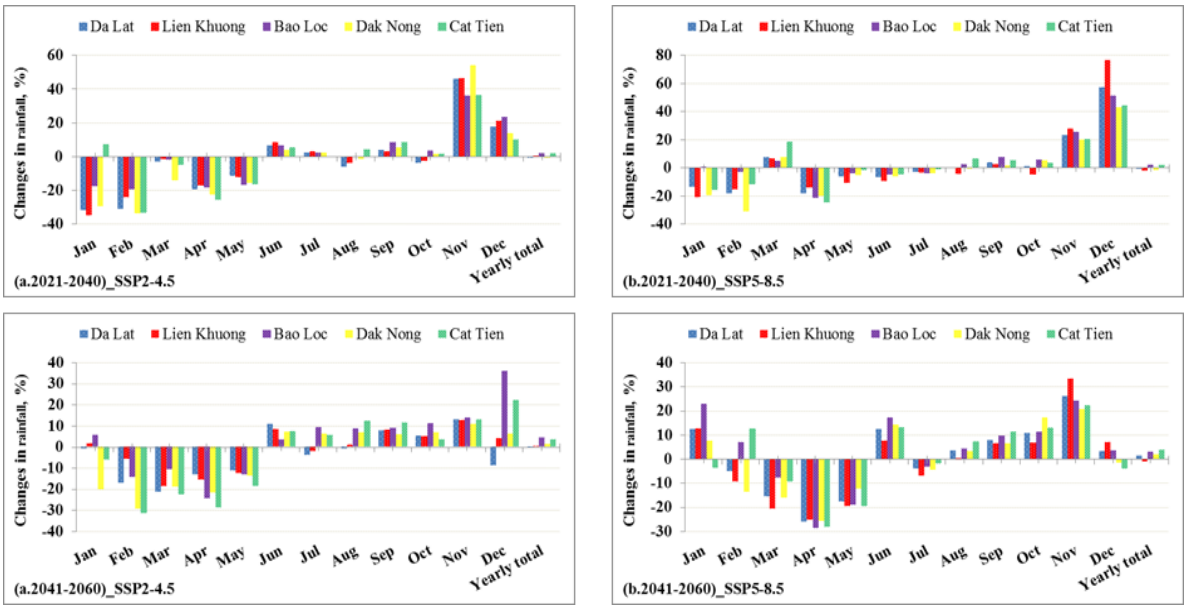

Figure 5. Projected changes in monthly and yearly rainfall mean in Da Lat, Lien Khuong, Bao Loc, Dak Nong, and Cat Tien in the period of 2021-2040 and 2041-2060: (a) SSP2-4.5 scenario; (b) SSP5-8.5 scenario.

3.3. Projected changes in the hydrological droughts

3.3.1. Drought frequency analysis

The frequency of hydrological drought for 18 sub-basins ranked from the highest to the lowest for the period 2021-2040 and 2041-2060 according to the SSP2-4.5 scenario is shown by the bold values in the "Sum of D" column in Table 5. The spatial distribution of hydrological drought (SDI6) for the two periods 2021-2040 and 2041-2060 for the two scenarios SSP2-4.5 and SSP5-8.5 on the UPDN river basin is shown in Figure 6. In general, in the basin, the normal condition (NC) is still the most common, accounting for over 67% compared to the rest being drought (D) and wet condition (WC). At the same time, there is a relatively equal balance between wet (WC) and drought (D) in the basin, which reflects the current reality in the basin, which is local drought and flooding all appear in the basin. Overall, UPDN river basin, wet condition (WC) is 10.5% vs. 11.0% of D over 2021-2040 and 16.5% of WC vs. 15.6% of D over 2041-2060 for the SSP2-4.5 scenario. These figures for the SSP5-8.5 scenario are 14.6% of WC and 15.6% of D in 2021-2040 and 16.3% of WC and 14.7% of D in 2041-2060, respectively. Furthermore, for the SSP2-4.5 scenario, the period 2041-2060 has a higher frequency of drought than the period 2021-2040 (15.6% compared to 11.0%). At the same time, in the near future period 2021-2040, the SSP5-8.5 scenario has a higher frequency of drought than SSP2-4.5 (15.6% compared to 11.0%). However, in the period 2041-2060, the frequency of drought does not differ much between these two scenarios with 15.6% of SSP2-4.5 compared to 14.7% of SSP5-8.5. This is also consistent with the average monthly rainfall forecast for the period 2041-2060 of these two scenarios shown in Figure 5.

At the sub-basin level, according to the SSP2-4.5 scenario, in the period 2021-2040, the three sub-basins with the highest frequency of hydrological drought (SDI6) are respectively

Dong Nai 4 (DN 9), Dong Nai 3 (DN 8) in Di Linh, Bao Lam districts of Lam Dong province and Dak Nong (DN 10) in Dak Glong district, Gia Nghia city of Dak Nong province with corresponding values of 13.6%, 13.2%, and 13.2%. During the period 2041-2060, the three sub-basins Da Huoai (DN 16) in Da Huoai district, La Nga (LN 1) in Di Linh district, and Don Duong (DN 3) in Don Duong district of Lam Dong province will have a high frequency of occurrence. Hydrological drought (SDI6) is the highest with corresponding values of 18.75%, 17.9%, and 17.4%. However, the sub-basin with extreme drought (ED) status belongs to DN2 (Da Tam) in Duc Trong district, DN6 (Da Dang) in Lam Ha district and DN 3 (Don Duong) in Don Duong district for the period 2021-2040 and DN 10 (Dak Nong), DN 12 (Dak R'Keh) of Dak Glong district, Gia Nghia city of Dak Nong province and DN 1 (Da Nhim) in Don Duong district, as italic values shown in Table 5. Therefore, in the future, there needs to be adaptive solutions for these areas where extreme drought (ED) occurs.

Table 5. Ranking from the highest to the lowest the frequency of hydrological drought according to sub-basins under the SSP2-4.5 scenario.

No.	The near future period of 2021 - 2040								Mid-century period of 2041 - 2060							
	ID	WC	NC	Drought (D)			Sum of D	Total	ID	WC	NC	Drought (D)			Sum of D	Total
				MD	SD	ED						MD	SD	ED		
1	DN 9	11.1	75.3	10.2	3.4	0.0	**13.6**	100	DN 16	16.6	64.7	13.2	2.6	3.0	**18.7**	100
2	DN 8	11.1	75.7	9.4	3.8	0.0	**13.2**	100	LN 1	17.0	65.1	9.8	6.4	1.7	**17.9**	100
3	DN 10	9.4	77.4	11.9	1.3	0.0	**13.2**	100	DN 3	16.6	66.0	9.4	6.0	2.1	**17.4**	100
4	DN 16	15.7	71.5	11.9	0.9	0.0	**12.8**	100	DN 6	17.4	66.4	10.2	3.0	3.0	**16.2**	100
5	*DN 2*	8.1	79.1	10.6	1.3	*0.9*	**12.8**	100	DN 7	17.4	66.4	9.8	3.4	3.0	**16.2**	100
6	*DN 6*	11.5	75.7	6.0	6.4	*0.4*	**12.8**	100	DN 8	17.0	67.2	8.9	4.3	2.6	**15.7**	100
7	DN 7	11.5	75.7	6.0	6.4	0.4	**12.8**	100	DN 9	16.6	67.7	8.5	4.3	3.0	**15.7**	100
8	DN 11	10.2	77.0	10.6	2.1	0.0	**12.8**	100	*DN 10*	16.6	67.7	9.8	1.7	*4.3*	**15.7**	100
9	LN 1	14.9	72.8	11.9	0.4	0.0	**12.3**	100	DN 17	18.3	66.0	8.9	3.8	3.0	**15.7**	100
10	DN 4	12.3	75.3	6.4	5.5	0.4	**12.3**	100	DN 4	17.0	67.7	8.9	4.7	1.7	**15.3**	100
11	DN 12	9.4	78.7	8.5	3.0	0.4	**11.9**	100	*DN 12*	17.0	67.7	9.4	1.7	*4.3*	**15.3**	100
12	DN 13	9.8	79.6	9.4	1.3	0.0	**10.6**	100	*DN 1*	13.6	71.5	8.1	3.0	*3.8*	**14.9**	100
13	DN 14	8.9	80.4	9.8	0.9	0.0	**10.6**	100	DN 11	17.0	68.1	6.4	6.0	2.6	**14.9**	100
14	DN 15	8.9	80.4	9.4	1.3	0.0	**10.6**	100	DN 5	15.3	70.2	8.5	4.7	1.3	**14.5**	100
15	DN 17	8.9	80.4	10.2	0.4	0.0	**10.6**	100	DN 13	17.9	67.7	6.4	5.5	2.6	**14.5**	100
16	*DN 3*	11.5	79.1	6.4	2.1	*0.9*	**9.4**	100	DN 14	17.9	67.7	6.4	5.1	3.0	**14.5**	100
17	DN 1	8.9	85.1	5.1	0.4	0.4	**6.0**	100	DN 15	17.9	67.7	6.4	5.1	3.0	**14.5**	100
18	DN 5	6.8	92.8	0.4	0.0	0.0	**0.4**	100	DN 2	10.2	75.7	8.9	4.3	0.9	**14.0**	100
For the UPDN		10.5	78.4	8.6	2.3	0.2	**11.0**	100		16.5	67.8	8.8	4.2	2.7	**15.6**	100

(*) ID: identification; WC: wet condition; NC: normal condition; MD: moderate drought; SD: severe drought; ED: extreme drought; D: drought condition.

Analysis of the SSP5-8.5 scenario reveals significant spatial and temporal variations in hydrological drought frequency across the study area. For the period 2021-2040, Da Huoai (DN 16), La Nga (LN 1), and Cat Tien (DN 14) are the highest frequency of hydrological drought sub-basins, with respective values of 20.0%, 19.6%, and 17.9%. The period of 2041-2060 shows Ta Lai (DN 17), Da Huoai (DN 16), and La Nga (LN 1) are the highest drought sub-basins with frequencies at 18.3%, 17.0%, and 17.0%, respectively. Notably, the occurrence of extreme drought conditions does not necessarily correlate with overall drought frequency. For the 2021-2040 period, extreme drought events are predominantly observed in DN4 (Da Quyn), ND7 (Dong Nai 2), and DN6 (Da Dang). In contrast, the 2041-2060 period sees a geographical shift in extreme drought occurrences, with ND10 (Dak Nong), ND4 (Da Quyn), and DN3 (Don Duong) being the most severely affected. These findings, as illustrated in Table 6, underscore the complex spatial dynamics of hydrological drought in the region and highlight the importance of sub-basin scale analysis in drought management strategies.

Table 6. Ranking from the highest to the lowest the frequency of hydrological drought according to sub-basins under the SSP5-8.5 scenario.

No.	The near future period of 2021 - 2040								Mid-century period of 2041 - 2060							
	ID	WC	NC	Drought (D)			Sum of D	Total	ID	WC	NC	Drought (D)			Sum of D	Total
				MD	SD	ED						MD	SD	ED		
1	DN 16	18.7	61.3	10.2	8.5	1.3	**20.0**	100	DN 17	17.4	64.3	14.0	4.3	0.0	**18.3**	100
2	LN 1	16.6	63.8	11.5	6.4	1.7	**19.6**	100	DN 16	15.7	67.2	9.8	7.2	0.0	**17.0**	100
3	DN 14	18.7	63.4	12.3	4.3	1.3	**17.9**	100	LN 1	18.3	64.7	10.6	6.4	0.0	**17.0**	100
4	DN 15	18.7	63.4	12.3	3.8	1.7	**17.9**	100	DN 15	16.2	67.7	11.9	4.3	0.0	**16.2**	100
5	DN 13	18.3	63.8	10.2	6.8	0.9	**17.9**	100	DN 14	16.2	67.7	11.1	5.1	0.0	**16.2**	100
6	DN 12	15.3	67.2	9.8	4.7	3.0	**17.4**	100	DN 12	17.9	66.8	8.9	3.4	3.0	**15.3**	100
7	DN 11	18.7	65.1	9.4	4.7	2.1	**16.2**	100	*DN 10*	17.4	67.2	9.4	2.6	*3.4*	**15.3**	100
8	DN 17	17.4	66.4	11.5	3.4	1.3	**16.2**	100	DN 13	19.1	65.5	9.8	5.1	0.4	**15.3**	100
9	DN 9	14.5	69.4	9.8	4.7	1.7	**16.2**	100	DN 11	19.1	66.0	10.2	4.7	0.0	**14.9**	100
10	DN 8	14.0	70.6	9.4	3.8	2.1	**15.3**	100	DN 7	15.3	70.6	6.8	4.7	2.6	**14.0**	100
11	*DN 4*	11.5	73.6	9.4	1.7	*3.8*	**14.9**	100	DN 8	17.0	68.9	8.1	3.8	2.1	**14.0**	100
12	DN 2	12.8	73.2	8.5	3.4	2.1	**14.0**	100	DN 9	16.6	69.4	8.1	4.7	1.3	**14.0**	100
13	*DN 7*	10.6	75.3	8.5	1.7	*3.8*	**14.0**	100	DN 6	14.5	71.9	6.4	4.7	2.6	**13.6**	100
14	*DN 6*	11.1	75.3	7.7	1.7	*4.3*	**13.6**	100	DN 1	14.5	72.3	6.0	5.5	1.7	**13.2**	100
15	DN 3	12.3	74.5	6.8	4.7	1.7	**13.2**	100	*DN 4*	14.5	72.3	6.0	3.8	*3.4*	**13.2**	100
16	DN 1	12.3	74.5	7.7	3.4	2.1	**13.2**	100	*DN 3*	14.9	72.3	5.5	4.3	*3.0*	**12.8**	100
17	DN 5	10.2	77.9	6.8	3.4	1.7	**11.9**	100	*DN 2*	14.5	73.2	5.5	3.4	*3.4*	**12.3**	100
18	DN 10	12.3	77.0	8.1	0.4	2.1	**10.6**	100	DN 5	14.5	73.2	5.5	5.5	1.3	**12.3**	100
For the UPDN		14.7	69.8	9.4	4.0	2.2	**15.6**	100		16.3	69.0	8.5	4.6	1.6	**14.7**	100

(*) ID: identification; WC: wet condition; NC: normal condition; MD: moderate drought; SD: severe drought; ED: extreme drought; D: drought condition.

3.3.2. Spatial variability of drought

The spatial and temporal variability of drought conditions within the basin is influenced by a complex interplay of factors, including climate change scenarios, precipitation patterns, sub-basin distribution (upstream and downstream), and hydroelectric plant operations. Under the SSP2-4.5 scenario, drought frequency exhibits a higher prevalence in the sub-basins situated in the East-Northeast upstream region of the basin (Figure 6a). These areas, as previously analyzed, receive comparatively less precipitation than the West-Southwest region. Furthermore, hydroelectric projects within the basin exert a significant influence on drought conditions, particularly in cases of extreme drought (ED). Two noteworthy hydroelectric projects that divert water to external basins warrant particular attention: (1) Da Nhim hydrologic plant with a capacity of 120MW transfers approximately 0.7 billion m^3 of water to the Cai river basin in Phan Rang province, situated between DN1 (Da Nhim) and DN3 (Don Duong); and (2) Dai Ninh hydrologic plant with a capacity of 160MW diverts approximately 1.3 billion m^3 of water to the Luy river basin in Binh Thuan province, located between DN4 (Da Quyn) and DN6 (Da Dang). These projects have a substantial impact on the hydrological drought conditions within the basin. Of particular note, the watersheds DN3 (Don Duong) and DN6 (Da Dang), which are situated downstream of these water-diverting hydroelectric projects, exhibit a higher frequency of extreme drought (ED) conditions compared to other sub-basins. Consequently, these two watersheds should be accorded priority in drought prevention and mitigation efforts within Lam Dong province.

Analysis of the drought conditions under the SSP5-8.5 scenario reveals a higher frequency of drought events in the downstream regions of the basin (DN 15, DN16, DN17) compared to the upstream areas (Figure 6b). Paradoxically, wet conditions (WC) also exhibit greater prevalence in the downstream regions. This dichotomy suggests that the SSP5-8.5 scenario introduces a higher degree of unpredictability in both drought and flood occurrences relative to the SSP2-4.5 scenario. The total annual precipitation does not significantly differ between the two scenarios however there are substantial variations in monthly rainfall

patterns between dry and wet seasons. Consequently, the temporal and spatial distribution of hydrological drought conditions varies markedly between the SSP2-4.5 and SSP5-8.5 scenarios, and therefore there will be a difference in the spatial distribution of drought in the basin.

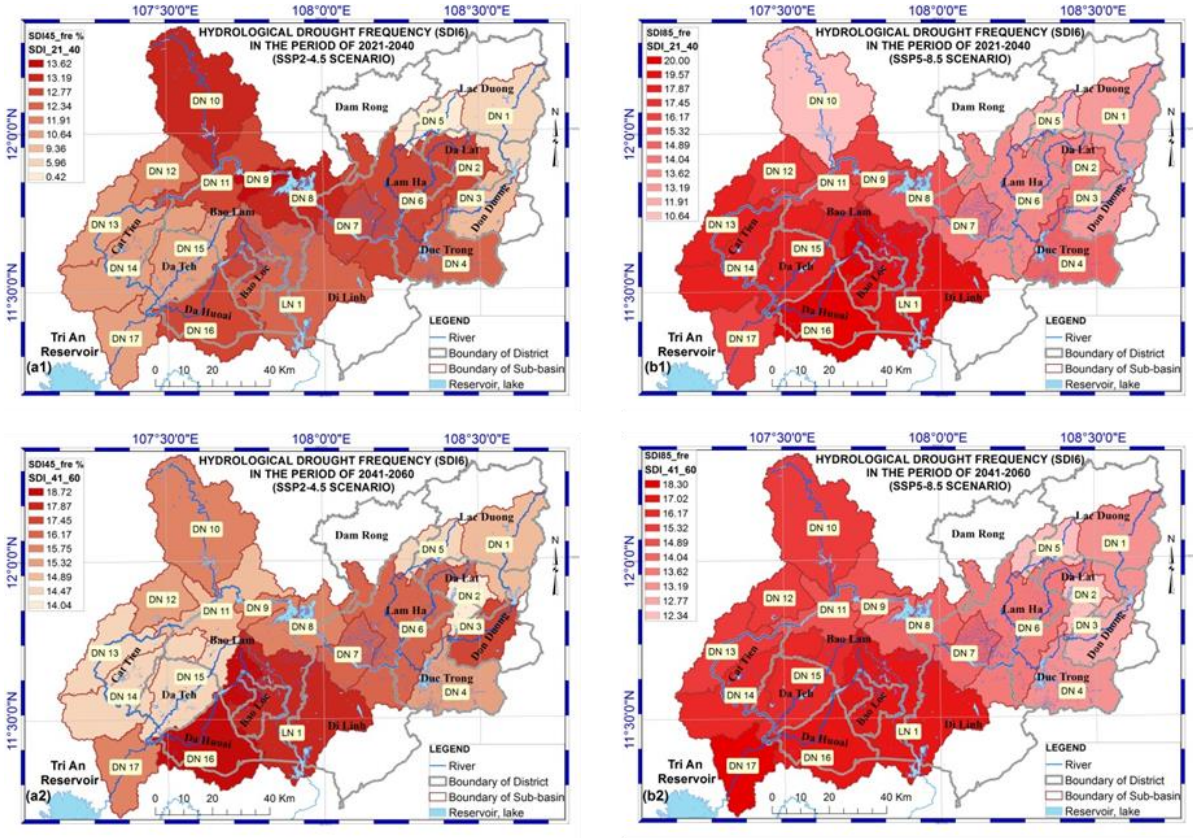

Figure 6. The spatial frequency of hydrological drought according to sub-basins level in the period of (1) 2021-2040 and (2) 2041-2060: (a) SSP2-45 scenarios; (b) SSP5-8.5 scenarios.

3.4. Changes in hydrological drought in future scenarios compared to the historical period

The results of calculating historical hydrological drought are based on monitoring data from three hydrological stations in the basin, including Thanh Binh in the Da Dang sub-basin (ND6), Dai Nga in the La Ngai sub-basin (LN1), and Ta Lai in the Ta Lai sub-basin (DN17). Streamflow data spanning the 30-year period (1990-2020) were utilized to calculate SDI6 for the Thanh Binh and Ta Lai stations. While streamflow data of the 24-year period (1990-2014) were employed for the Dai Nga station, because the Dai Nga station has not operated normally since 2014 due to the water diversion caused by the Dai Nga hydropower plant. Overall, for both the historical and future periods, the NC (normal conditions) still predominates, accounting for more than 63%, compared to the WC (wet conditions) and D (drought) (Table 7). Additionally, the percentage of D and WC is nearly equal, reflecting the climate characteristics of the UPDN basin, which has a five-month dry season (December to April), followed by a seven-month rainy season (May to November). However, under the influence of climate change, extreme drought (ED) is projected to occur more frequently in the future. For example, at Thanh Binh, the ED occurrence was 1.6% during the historical period 1990-2020, compared to 3.0% for the period 2041-2060 under the SSP2-4.5 scenario, and 6.4% under the SSP5-8.5 scenario. At Ta Lai, ED accounts for 4.1% during 1990-2020, rising to 11.5% under the SSP2-4.5 scenario and 14.0% under the SSP5-8.5 scenario for the period 2041-2060, respectively.

Table 7. Comparison of the frequency of hydrological drought historical observation to future predictions at three Thanh Binh, Dai Nga, and Ta Lai gauges under the SSP2-4.5 and SSP5-8.5 scenarios.

Scenarios	Periods	WC	NC	Drought (D)			Sum of D	Total
				MD	SD	ED		
Thanh Binh gauge								
History	1990 - 2020	13.6	73.3	7.4	4.6	1.6	**13.1**	100
SSP2-4.5	2021 - 2040	11.5	75.7	6.0	6.4	0.4	**12.8**	100
	2041 - 2060	17.4	66.4	10.2	3.0	3.0	**16.2**	100
SSP5-8.5	2021 - 2040	11.1	75.3	4.3	1.7	7.7	**13.6**	100
	2041 - 2060	14.5	71.9	2.6	4.7	6.4	**13.6**	100
Dai Nga gauge								
History	1990 - 2020	12.8	76.8	5.0	2.0	3.4	**10.4**	100
SSP2-4.5	2021 - 2040	14.9	72.8	11.9	0.4	0.0	**12.3**	100
	2041 - 2060	17.0	65.1	9.8	6.4	1.7	**17.9**	100
SSP5-8.5	2021 - 2040	16.6	63.8	1.7	6.4	11.5	**19.6**	100
	2041 - 2060	18.3	64.7	0.0	6.4	10.6	**17.0**	100
Ta Lai gauge								
History	1990 - 2020	12.5	73.3	7.4	2.7	4.1	**14.2**	100
SSP2-4.5	2021 - 2040	18.3	66.0	8.9	3.8	3.0	**15.7**	100
	2041 - 2060	17.4	66.4	1.3	3.4	11.5	**16.2**	100
SSP5-8.5	2021 - 2040	17.4	66.4	1.3	3.4	11.5	**16.2**	100
	2041 - 2060	17.4	64.3	0.0	4.3	14.0	**18.3**	100

(*) WC: wet condition; NC: normal condition; MD: moderate drought; SD: severe drought; ED: extreme drought; D: drought condition.

In general, the observed spatial patterns in hydrological drought occurrence within the UPDN river basin can be attributed to a combination of climatic, geographical, and anthropogenic factors. The interplay of these factors results in complex spatial patterns of drought occurrence within the UPDN river basin. The basin's topography has influenced local climate patterns. The distribution of precipitation across the basin is uneven, with certain areas receiving less rainfall than others. For example, the East-Northeast upstream regions with high elevation often experience lower precipitation compared to the West-Southwest areas, contributing to various drought frequency and severity. The presence of hydroelectric plants and water diversion projects has impacted local hydrology. For instance, the Da Nhim and Dai Ninh plants have diverted substantial water to other basins, potentially leading to reduce water availability downstream, especially during dry periods. Hydropower reservoirs upstream can significantly modify the natural flow regime by altering the timing and magnitude of water release. These regulated flows, often designed to meet energy demands, exacerbate drought and flood conditions in downstream sub-basins.

Based on these results, there is a relatively equal balance between wet and drought conditions, reflecting the current reality in the basin, where localized droughts and flooding events frequently occur. These changes in droughts can be reduced by upgrading reservoirs and improving irrigation system efficiency. Moreover, agricultural practices need to adapt to the changing rainfall patterns. Agricultural activities need to shift to more drought-resistant crop varieties, adjust planting schedules, and implement soil moisture management techniques to maintain productivity during drier periods. In addition, the drought mitigation solutions should be prioritized for sub-basins that have high drought frequency and severity such as Da Tam, Don Duong, Da Quyn, and Da Dang.

4. Conclusions

The findings suggest that climate change could lead to more significant increases in temperature than changes in precipitation. In the future, increases in temperature and precipitation are anticipated to vary spatially and temporally across the basin. The trend shows greater temperature and precipitation increases in the West-Southwest than in the

East-Southeast of the basin. Under the SSP2-4.5 scenario, annual rainfall slightly increases in most areas of the basin for the period 2021-2060. However, the SSP5-8.5 scenario projects a slight rainfall decrease in the East-Southeast region and a slight increase in the West-Southwest. Additionally, rainfall tends to decrease in some months of the dry season (February to May) and increase some months of the rainy season (August to December). These changes in rainfall patterns contribute significantly to variations in drought frequency and severity across the basin.

The frequency of drought occurrence varies between the upstream and downstream areas of the basin, depending on climate change scenarios, rainfall distribution, and hydroelectric project operations. According to the SSP2-4.5 scenario, drought frequency is more common at sub-basins located in the upstream part belonging to the East-Northeast of the basin. Conversely, the SSP5-8.5 scenario suggests that the downstream part of the basin (DN 15, DN16, and DN17) experiences more frequent hydrological droughts than the upstream part.

The frequency and severity of droughts can vary between sub-basins. Da Tam (DN2), Don Duong (DN3), Da Quyn (DN2), Da Dang (DN6), Dong Nai 2 (ND7), Dak Nong (DN10), and Dak R'Keh (DN12) are the sub-basins having more frequent extreme drought (ED) conditions compared to the rest of the basins. These sub-basins should be prioritized for drought prevention in the coming years. The research results can provide valuable information for policymakers in planning, management, and sustainable development of the UPDN river basin. These findings highlight the need for targeted adaptive management strategies, such as prioritizing water conservation and storage infrastructure in sub-basins with higher drought frequency and severity, and adjusting hydroelectric project operations to mitigate downstream drought risks.

The study has proposed the useful solution in integrate GIS, remote sensing (RS), and the SWAT model to simulate and analyze the spatiotemporal dynamics of hydrological droughts in the UPDN river basin. However, this study also has some limitations, such as the lack of detailed reservoir operation data. The weather data input for the SWAT model, derived from GCMs with a 10 km × 10 km resolution, can cause uncertainty. Thus, further research should focus on integrating high-resolution climate data and exploring the impacts of land-use changes and human activities on drought dynamics to provide a more comprehensive understanding of future water resource challenges.

Author Contributions: Developed ideas, conceptualized framework, and methodology: P.H., V.L.P.; selected methods, techniques, and processed data: P.H.; wrote the draft article: P.H., L.V.T.; Edited and reviewed the article: V.L.P.

Acknowledgments: The authors would like to thank you Department of Science and Technology (DOST), and Department of Natural Resources and Environment (DONRE) of Lam Dong provinces as well as the Research Institute for Innovation and Sustainable Development (RIFISD) for their supports to this study by providing statistical data and implementation resources. We also acknowledge the support of time and facilities from Ho Chi Minh City University of Technology (HCMUT), VNU-HCM for this study.

Conflicts of Interest: The authors declare no conflict of interest.

References

1. Liming, G.; Yaonan, Z. Spatio-temporal variation of hydrological drought under climate change during the period 1960–2013 in the Hexi Corridor, China. *J. Arid. Land* **2016**, *8(2)*, 157–171.
2. Benyoussef, S.; Arabi, M.; Yousfi, Y.E.; Cheikh, B.B.; Abdaoui, A.; Azirar, M.; Mechkirrou, L.; Ouarghi, H.E.; Zegzouti, Y.F.; Boughrous, A.A. Climate Change and Water Resources Management in the Ghis-Nekor Watershed (North of Morocco) – A Comprehensive Analysis Using SPI, RDI and DI Indices. *Ecol. Eng. Environ. Technol.* **2024**, *25(2)*, 196–209.

3. Li, Q.; Ye, A.; Wada, Y.; Zhang, Y.; Zhou, J. Climate change leads to an expansion of global drought-sensitive area. *J. Hydrol.* **2024**, *632(130874)*, 1–9.
4. Tri, D.Q.; Dat, T.T.; Truong, D.D. Application of meteorological and hydrological drought indices to establish drought classification maps of the Ba river basin in Vietnam. *Hydrology* **2019**, *6(49)*, 1–20.
5. Ngan, T.T.K.; Khoi, D.N. Analysing the impact of hydropower dams on streamflow in the Be river basin. *VN J. Sci. Technol. Eng.* **2019**, *16(4)*, 35–39.
6. Wu, J.; Chen, X.; Gao, L.; Yao, H.; Chen, Y.; Liu, M. Response of hydrological drought to meteorological drought under the influence of large reservoir. *Adv. Meteorol*. **2016**, *16(2197142)*, 1–11.
7. Langen, S.C.H.; Costa, A.C.; Neto, G.G.R.; Oel, P.R. Effect of a reservoir network on drought propagation in a semi-arid catchment in Brazil. *Hydrol. Sci. J.* **2021**, *66(10)*, 1567–1583.
8. IPCC. Climate Change 2022: Impacts, adaptation and vulnerability - working group II contribution to the sixth assessment report of the intergovernmental panel on climate change. New York, USA, 2022.
9. Thanh, N.D.; Nguyen, M.H.; Pannier, E.; Woillez, M.N.; Drogoul, A.; Huynh, T.P.L.; Le, T.T.; Nguyen, T.T.H.; Nguyen, T.T.; Nguyen, T.A.; Thomas, F.; Truong, C.Q.; Vo, Q.T.; Vu, C.T. Climate change in Viet Nam: Impacts and adaptation. A COP26 assessment report of the GEMMES Viet Nam project. Paris, 2021.
10. IPCC. The physical science basis. New York, USA, 2021.
11. Huong, N.T.; Kim, Y.T.; Kwon, H.H. Evaluation and selection of CMIP6 GCMs for long-term hydrological projections based on spatial performance assessment metrics across South Korea. *J. Water Clim. Change* **2023**, *14(8)*, 2663–2678.
12. Riahi, K.; van Vuuren, D.P.; Kriegler, E.; Edmonds, J.; O'Neill, B.C.; Fujimori, S.; Bauer, N.; Calvin, K.; Dellink, R.; Fricko, O.; Lutz, W. The shared socio-economic pathways and their energy, land use, and greenhouse gas emissions implications: An overview. *Global Environ. Change* **2017**, *42*, 153–168.
13. Sam, T.T.; Khoi, D.N.; Thao, N.T.T.; Nhi, P.T.T.; Quan, N.T.; Hoan, N.X.; Nguyen, V.T. Impact of climate change on meteorological, hydrological and agricultural droughts in the Lower Mekong River Basin: a case study of the Srepok Basin, Vietnam. *Water Environ. J.* **2019**, *33*, 547–559.
14. Khoi, D.N.; Sam, T.T.; Loi, P.T.; Hung, B.V.; Thinh, N.V. Impact of climate change on hydro-meteorological drought over the Be river basin, Vietnam. *J. Water Clim. Change* **2021**, *12(7)*, 3159–3169.
15. Sarwar, A.N.; Waseem, M.; Azam, M.; Abbas, A.; Ahmad, I.; Lee, J.E.; Haq, F.U. Shifting of meteorological to hydrological drought risk at regional scale. *Appl. Sci.* **2022**, *12(5560)*, 1–14.
16. Mahdavi, P.; Kharazi, H.G. Impact of climate change on droughts: a case study of the Zard river basin in Iran. *Water Pract. Technol.* **2023**, *18(10)*, 2258–2276.
17. Pandhumas, T.; Kuntiyawichai, K.; Jothityangkoon, C.; Suryadi, F.X. Assessment of climate change impacts on drought severity using SPI and SDI over the Lower Nam Phong River Basin, Thailand. *Hydrology* **2020**, *47(3)*, 326–338.
18. Tran, T.-N.-D.; KimDo, S.; Nguyen, B.Q.; Tran, V.N.; Grodzka-Łukaszewska, M.; Sinicyn, G.; Lakshmi, V. Investigating the future flood and drought shifts in the transboundary Srepok river basin using CMIP6 projections. *IEEE J. Sel. Top. Appl. Earth Obs. Remote Sens.* **2024**, *17*, 7516–7529.
19. Vietnam MONRE. Report on general planning of Dong Nai river basin period 2021 - 2030, vision to 2050. Ha Noi, Vietnam, 2023, pp. 1–281.
20. Hung, P.; Trung, L.V.; Vo, P.L. Decision support tool for integrated water resources management based on GIS, remote sensing and SWAT model: A case study in the

upper part of Dong Nai river basin, Vietnam. In Advances in Research on Water Resources and Environmental Systems. GTER 2022. Environmental Science and Engineering, Vo, P.L.; Tran, D.A.; Pham, T.L.; Le Thi Thu, H.; Nguyen Viet, N.; Ed. Springer: Gewerbestrasse 11, 6330 Cham, Switzerland, 2023, pp. 361–388.

21. Jolk, C.; Greassidis, S.; Jaschinski, S.; Stolpe, H.; Zindler, B. Planning and decision support tools for the integrated water resources management in Vietnam. *Water* **2010**, *2*, 711–725.
22. Hung, P. Application of GIS, remote sensing and SWAT in integrated water resources management: A case study in the upper part of Dong Nai river basin. Ho Chi Minh City University of Technology (HCMUT) - Vietnam National University Ho Chi Minh City, Ho Chi Minh City, 2022.
23. Nguyen-Duy, T.; Ngo-Duc, T.; Desmet, Q. Performance evaluation and ranking of CMIP6 global climate models over Vietnam. *J. Water Clim. Change* **2023**, *14(6)*, 1831–1846.
24. Hung, P.; Quyen, N.T.N.; Trung, L.V.; Phu, V.L. Performance evaluation of some CMIP6-GCMs in simulating rainfall and temperature in the upper part of Dong Nai river basin. *VN J. Hydrometeorol.* **2024**, *762*, 47–61.
25. Tran, A.Q.; Ngo, D.T.; Espagne, E.; Trinh, T.L. A 10-km CMIP6 downscaled dataset of temperature and precipitation for historical and future Vietnam climate. *Sci. Data* **2023**, *10(1)*, 1–12.
26. Department of Climate Change, V.N.M. National Climate Change Impacts and Adaptation Final Report. Ha Noi, Vietnam, 2022.
27. Eyring, V.; Bony, S.; Meehl, G.A.; Senior, C.A.; Stevens, B.; Stouffer, R.J.; Taylor, K.E. Overview of the coupled model intercomparison project phase 6 (CMIP6) experimental design and organization. *Geosci. Model Dev*. **2016**, *9(5)*, 1937–1958.
28. Vietnam Prime Minister. Decision No. 1895/QD-TTg dated December 25, 2019 on the promulgation of inter-reservoir operating procedures in the Dong Nai river basin. Ha Noi, 2019.
29. Vietnam Ministry of Natural Resources and Environment. Circular 64/2017/TT-BTNMT Regulations on determining minimum flows in rivers, streams and downstream of reservoirs, dams. Ha Noi, Vietnam, 2017, pp. 1–8.
30. Neitsch, S.L.; Arnold, J.G.; Kiniry, J.R.; Williams, J.R. Introduction and history. Soil and Water Assessment Tool Theoretical Documentation Version 2009, Texas Water Resources Institute Technical Report No. 406: Texas A&M University System College Station, Texas 77843-2118, 2011, pp. 6–10.
31. Hung, P.; Le, T.V.; Vo, P.L.; Duong, H.C.; Mostafizurb, R.M. Vulnerability assessment of water resources using GIS, remote sensing and SWAT model – A case study: The upper part of Dong Nai river basin, Vietnam. *Int. J. River Basin Manage.* **2021**, *20*, 1–16.
32. Mango, L.M.; Melesse, A.M.; McClain, M.E.; Gann, D.; Setegn, S.G. Land use and climate change impacts on the hydrology of the upper Mara River Basin, Kenya: results of a modeling tudy to support better resource management. *Hydrol. Earth Syst. Sci.* **2011**, *15*, 2245–2258.
33. Moriasi, D.N.; Arnold, J.G.; Liew, M.W.V.; Bingner, R.L.; Harmel, R.D.; Veith, T.L. Model evaluation guidelines for systematic quantification of accuracy in watershed simulations. *Trans. ASABE* **2007**, *50(3)*, 885–900.
34. Khoi, D.N.; Thom, V.T. Parameter uncertainty analysis for simulating streamflow in a river catchment of Vietnam. *Global Ecol. Conserv.* **2015**, *4*, 538–548.
35. Padhiary, J.; Patra, K.C.; Dash, S.S. A novel approach to identify the characteristics of drought under future climate change scenario. *Water Resour. Manage.* **2022**, *36*, 5163–5189.

36. Tigkas, D.; Vangelis, H.; Tsakiris, G. DrinC: A software for drought analysis based on drought indices. *Earth Sci. Inf.* **2015**, *8(3)*, 697–709.
37. Tigkas, D.; Vangelis, H.; Proutsos, N.; Tsakiris, G. Incorporating aSPI and eRDI in drought indices calculator (DrinC) software for agricultural drought characterisation and monitoring. *Hydrology* **2022**, *9(100)*, 1–14.
38. McKee, T.B.; Doesken, N.J.; Kleist, J. The relationship of drought frequency and duration to time scales. Proceeding of the 8th Conf. Appl. Climatol. Anaheim Calif. **1993**, pp. 179–184.
39. Can, T.; Xiaoling, C.; Jianzhong, L.; Gassman, P.W.; Sabine, S.; José-Miguel, S.P. Assessing impacts of different land use scenarios on water budget of Fuhe River, China using SWAT model. *Int. J. Agric. Biol. Eng.* **2015**, *8(3)*, 95–109.
40. Wang, L.; Shu, Z.; Wang, G.; Sun, Z.; Yan, H.; Bao, Z. Analysis of future meteorological drought changes in the Yellow river basin under climate change. *Water* **2022**, *14(1896)*, 1–20.
41. Shin, J.Y.; Chien, P.V.; Um, M.J.; Kim, H.; Sung, K. Projection of changes in rainfall and drought based on CMIP6 scenarios on the Ca river basin, Vietnam. *Water* **2024**, *14(1914)*, 1–19.
42. Anaraki, M.V.; Kadkhodazadeh, M.; Morshed-Bozorgde, A.; Farzin, S. Predicting rainfall response to climate change and uncertainty analysis: Introducing a novel downscaling CMIP6 models technique based on the stacking ensemble machine learning. *J. Water Clim. Change* **2023**, *14(10)*, 3671–3691.
43. Tran, A.Q.; Ngo, D.T.; Espagne, E.; Trinh, T.L. A high-resolution projected climate dataset for Vietnam: Construction and preliminary application in assessing future change. *J. Water Clim. Change* **2022**, *13(9)*, 3379–3399.

JOURNAL OF
HYDRO-METEOROLOGY

Research Article

Development of geomechanical model for determination of elastic modulus and study on law of caving span induced by mechanized longwall mining

Pham Van Chung[1], Nguyen Quoc Long[1,4]*, Nguyen Dinh Huy[2], Dinh Thanh Tuan[3], Luu Van Huyen[5]

[1] Hanoi University of Mining and Geology, Hanoi, Vietnam; phamvanchung@humg.edu.vn
[2] Hanoi University of Civil Engineering, Hanoi, Vietnam; huynd@huce.edu.vn;
[3] Dong Hai Measurement Company Limited, My Tho City; ktbddonghai@gmail.com
[4] Innovations for Sustainable and Responsible Mining, Hanoi University of Mining and Geology, Hanoi, Vietnam; nguyenquoclong@humg.edu.vn
[5] Hanoi University of Natural Resources and Environment; lvhuyen@hunre.edu.vn

* Corresponding author: nguyenquoclong@humg.edu.vn; Tel.: +84–916196336

Received: 10 August 2024; Accepted: 22 October 2024; Published: 25 December 2024

Abstract: A geomechanical model is developed to determine the elastic modulus, to analyze the rules of rock and surface displacement, and study the caving span caused by mechanized longwall mining. The rules of rock deformation and displacement have been determined, including the stress distribution, the development of the failure zone, the height of the failure zone, the caving span of the longwall, the order of layer arrangement, the displacement deformation vector, the maximum subsidence, and the boundary displacement angle. In this paper, the author uses the Rocdata program to determine the elastic modulus (E), cohesion (C), and internal friction angle (φ) as inputs for the geomechanical model. The software RS2 (Phase 2) from Rocscience Inc. (Canada) is then used to calculate some parameters and displacement quantities. The results showed that the maximum subsidence in the dip direction is η = -2.250 m and in the strike direction η = -0.659 m. The boundary displacement angle is β_0 = 47°. The caving height is H = 10 m. The caving repeats at the span 10th, meaning that the length of the longwall mined in the strike direction reaches 65 m. Afterward, the caving span and the height of the caving zone repeat.

Keywords: Deformation and displacement; Geomechanical model; Elastic modulus; Caving span of the longwall.

1. Introduction

Various methods have been used to study rock deformation and displacement. This includes theoretical methods based on the finite element method to determine the stress-strain state from the geomechanical model. A geomechanical model is used to determine the deformation and displacement parameters as well as the complete destruction of the rock mass within the influence zone of the longwall [1]. During the process of stress redistribution in the rock mass, it can reach a completely stable state or an unstable state at different levels, which can cause a loss of force equilibrium, leading to the bending and collapse of roof strata [1, 2].

In Vietnam, studies on mine deformation are mainly conducted based on observation data [3–5], some recent studies have applied AI technology to predict surface subsidence [6,

7]. These studies show high reliability, but it can only be predicted after observation data is available, meaning that the subsidence process has occurred. To solve the problems, elastic and continuous environment modeling was used in the works of researchers [8–14]. Since 2011, several studies on deformation and displacement using equivalent material models have been done in various documents [15, 16–20], focusing on load-bearing capacity and deformation control in roadways [21]. However, these documents show that the research is labor-intensive and conducted on small models, resulting in a large equivalent coefficient. Theoretical research to predict subsidence has also been carried out by some experts. The study [19] used the Phase2 program to analyze subsidence and mechanical transformation during the combined underground and open-pit mining. The study [1] constructed a geomechanical model due to the impact of mechanized longwall mining in thick seams. The study determined a coefficient KC = 1.2 for the Quang Ninh coal region and found the deformation displacement rules. The prediction of the height of the failure zone and layer separation can be found in many studies [17, 22, 23].

In this paper, the author uses the Rocdata program to calculate the elastic modulus (E), cohesion (C), and internal friction angle (φ) as input data for the geomechanical model. The software RS2 (Phase 2) is then used to study the deformation and displacement rules and caving span of Seam I (12) at Mong Duong coal mine, Quang Ninh coal field, Vietnam.

2. Materials and Methods

2.1. Study area

Mong Duong coal mine is located in Mong Duong ward, Cam Pha City, Quang Ninh province, Vietnam. The exploration area is situated 10 km to the East-Northeast of Cam Pha city. At the mine, Seam I (12) is mined using the partially mechanized longwall mining method with full caving from level -97 to -45. The average depth from the surface to the mining longwalls is 90 m to 120 m. The coordinates of the research area limits are shown in Table 1.

Table 1. Coordinates of the research area limits.

No.	Point name	X	Y
1	H	29600	31200
2	E	29600	31900
3	F	30300	31900
4	I	31300	31200

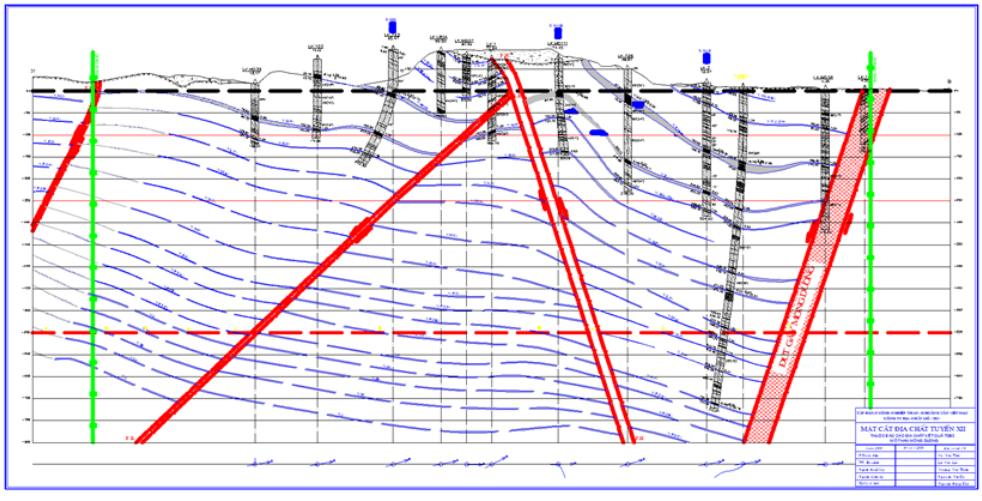

Figure 1. Geological cross-section of line XII [24].

The geological conditions of the seam I (12) are shown in Table 2. The geological line XII passing through the research area is illustrated in Figure 1.

Table 2. Geological conditions of seam I(12).

No.	Parameters of the longwall	m/degree	Seam I(12)
1	Mining level	m	-97 ÷ -45
2	Seam thickness	m	8
3	Seam dip angle	degree	40
4	Overburden thickness	m	5
5	Longwall length in the dip direction	m	60-70
6	Longwall length in strike direction	m	80-120
7	The average depth of the longwall	m	90-120

2.2. Calculation of Elastic Modulus for the Geomechanical Model of Mong Duong Coal Mine

During the geotechnical construction process, in addition to sampling at line XII, additional boreholes LK102, LK103, LK736, LK732, LK2, LK-L2, LK16, LK19, LK24 were taken. The compressive strength (σ) of sandstone ranges from 90 to 126 MPa, with an average of 113 MPa; siltstone ranges from 30 to 55 MPa, with an average of 42 MPa; claystone ranges from 17 to 40 MPa, with an average of 28 MPa; and coal has a strength of 17 MPa [25]. The Rocdata program is used to determine the elastic modulus (E), cohesion (C), and internal friction angle (φ) as shown in Table 3.

To calculate the deformation and displacement of the Mong Duong coal mine, it is necessary to study and build a geomechanical model. The author proposed the elastic modulus EC = KC.ER (where ER is the elastic modulus calculated from Rocdata, KC = 1.24) [1], while other parameters such as cohesion and internal friction angle remain unchanged. The results from RS2 with varying cohesion and internal friction angle show that the deformation does not change significantly in the model. Thus, the determined input parameters E, C, φ for running the geomechanical model of the Mong Duong coal mine are shown in Table 4.

Table 3. Geological conditions of seam I(12).

No.	Type of rock	Compressive strength σ (MPa)	Geological Strength Index (GSI)	Blast damage factor (D)	Material constant (mi)	Elastic modulus E (MPa)	Cohesion C (MPa)	Internal friction angle Φ (dg)
1	Sandstone	113	45	0.8	17	2110	0.805	42.358
2	Siltstone	42	37	0.8	7	691	0.323	23.276
3	Shale	28	11	0.8	4	244	0.40	12.281
4	Coal	17	8	0.8	4	93	0.052	3.5

Table 4. E, C, φ for Mong Duong coal mine.

No.	Parameters	Sandstone	Siltstone	Shale	Coal
1	EC	2532	829.2	292.8	93
2	C	42.358	23.276	12.281	3.50
3	φ	0.805	0.323	0.40	0.052

3. Results

3.1. Calculation diagram

Applying the above geomechanical model, the input parameters E (elastic modulus), C, and φ are entered into the software RS2. The author takes the cross-section of line XII as a representative cross-section for specific calculations. The rock layers are considered to be parallel to each other. The stratigraphy of the rock includes sandstone, siltstone, shale, and

coal. The calculation domain of the model has a width and height of 700×300 m compared to the actual width of the cross-section of 1400×450 m. It should be noted that the area from the observation station of seam I (12) to the outer boundary is 500 m, and the mining level of seam I (12) from -80 to the surface is 250 m, meaning a height of about 330 m. The modeled dimensions of 700×300 m are reasonable compared to reality and are shown in Figure 2.

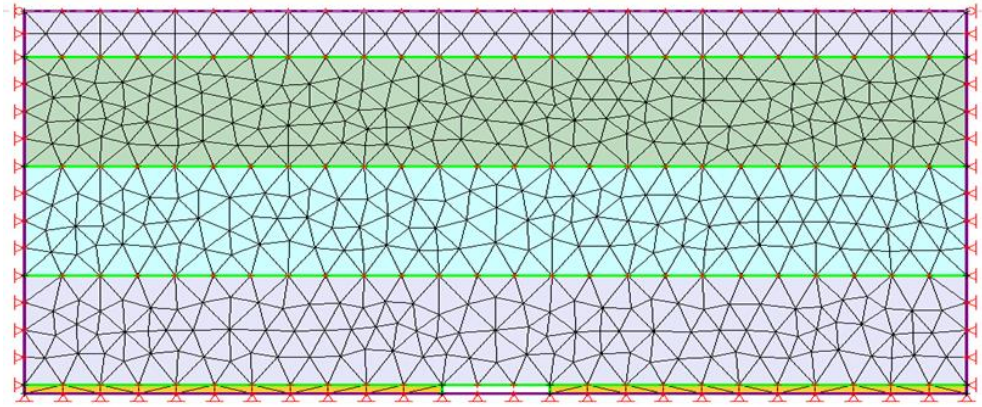

Figure 2. Simulation of soil and rock strata and model dimensions.

3.2. Calculation of deformation and displacement

The longwall mining system uses hydraulic supports. The roof control is managed by full caving, with a coal seam thickness of 8 meters and a longwall length of 80 m. The parameters for sandstone, siltstone, shale, and coal are entered into the model as shown in Figure 3.

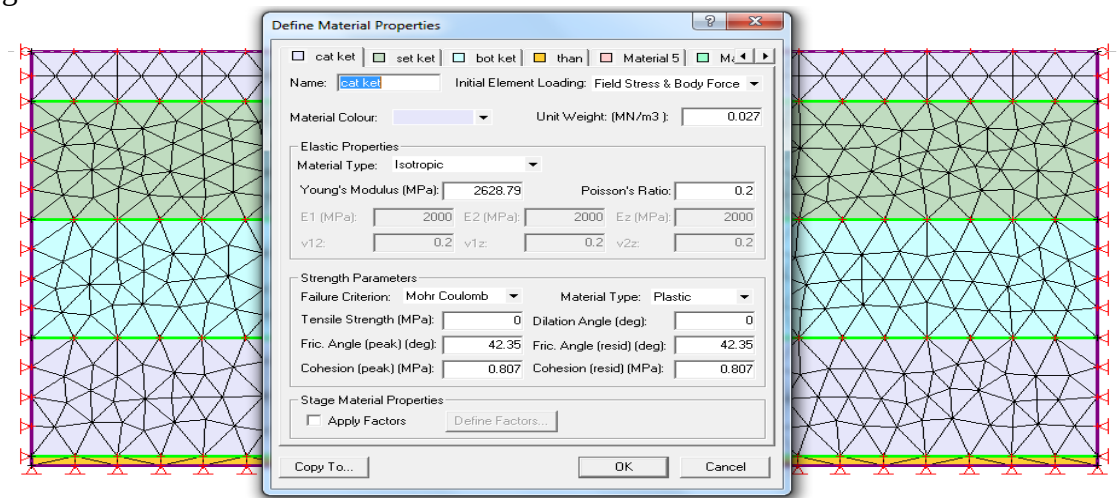

Figure 3. Entering parameters of the model.

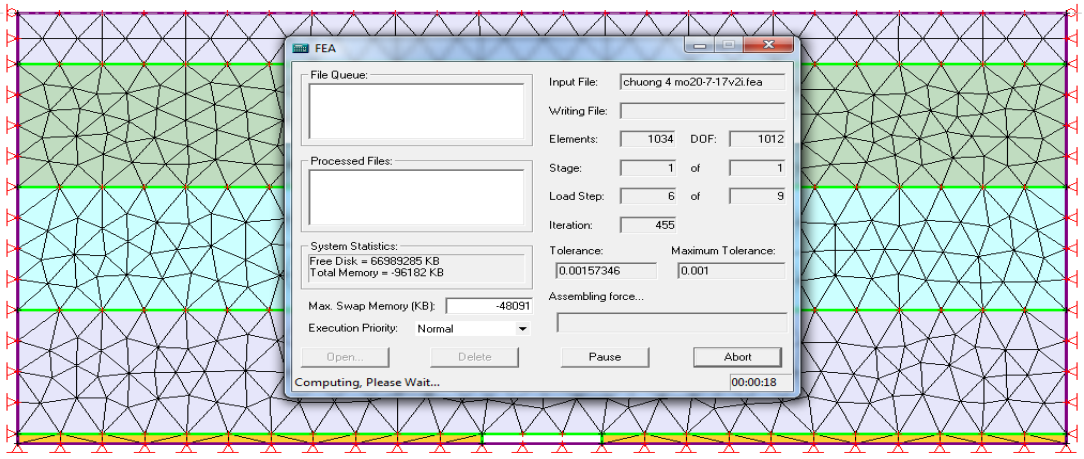

Figure 4. Computing the displacement.

After entering the parameters, the software automatically runs the calculation loop for deformation displacement, as shown in Figure 4. The vertical and horizontal displacements are shown in Figures 5, 6.

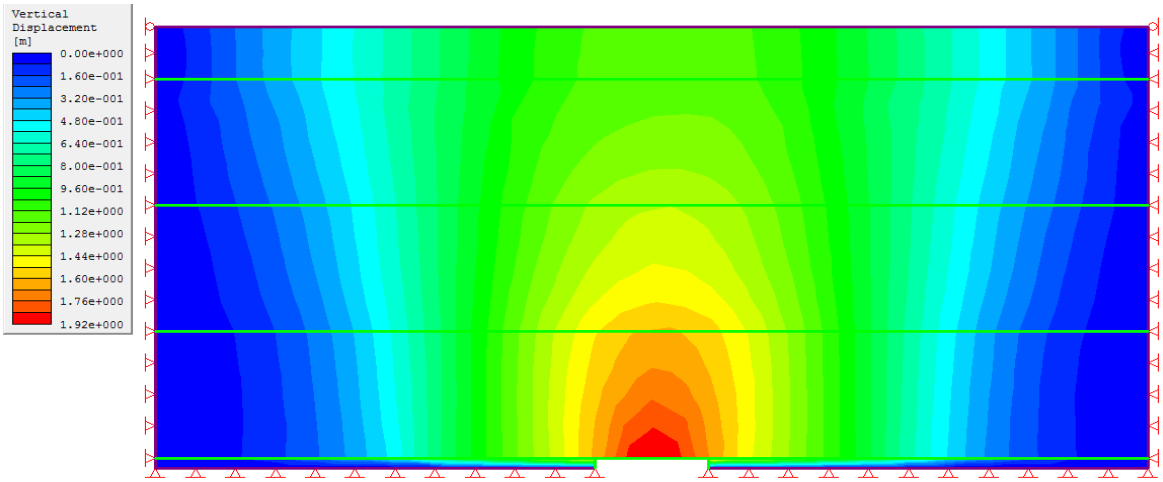

Figure 5. The vertical displacement of rock layers due to underground mining.

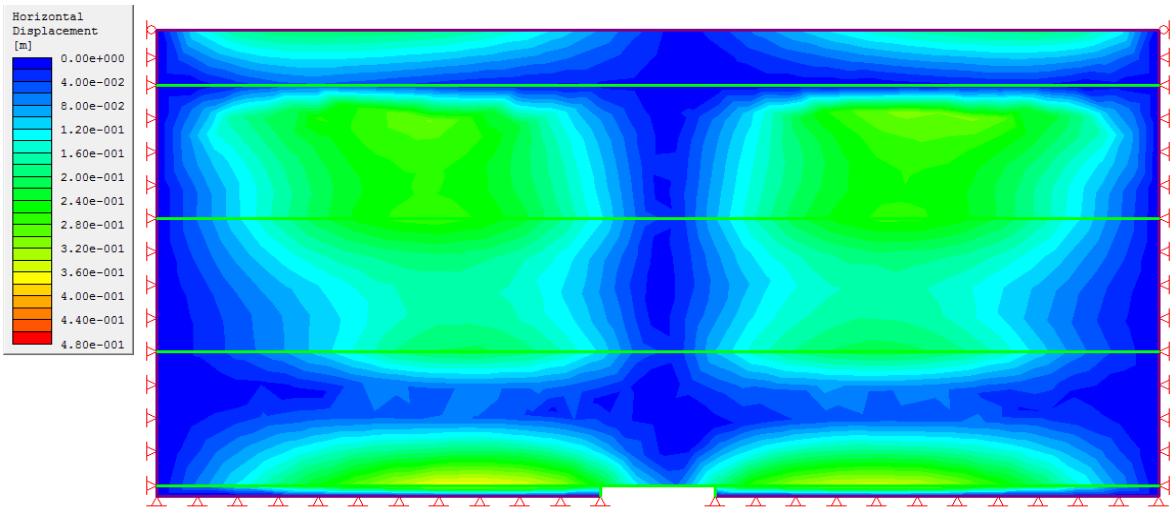

Figure 6. Horizontal deformation.

The determination of subsidence and displacement angle is shown in Figure 7. The graph describing the displacement process of each rock layer is shown in Figure 8.

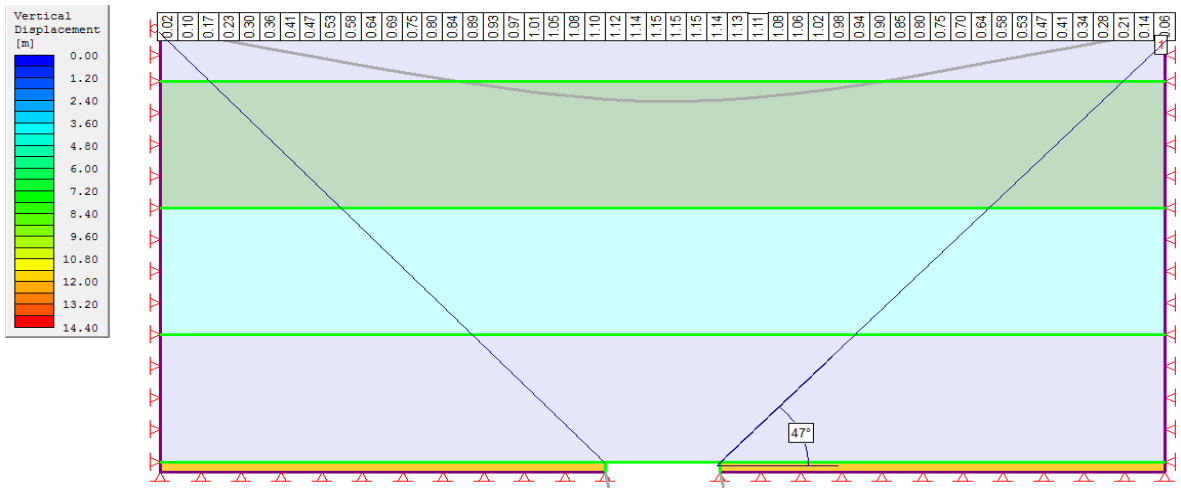

Figure 7. Vertical displacement and displacement angle.

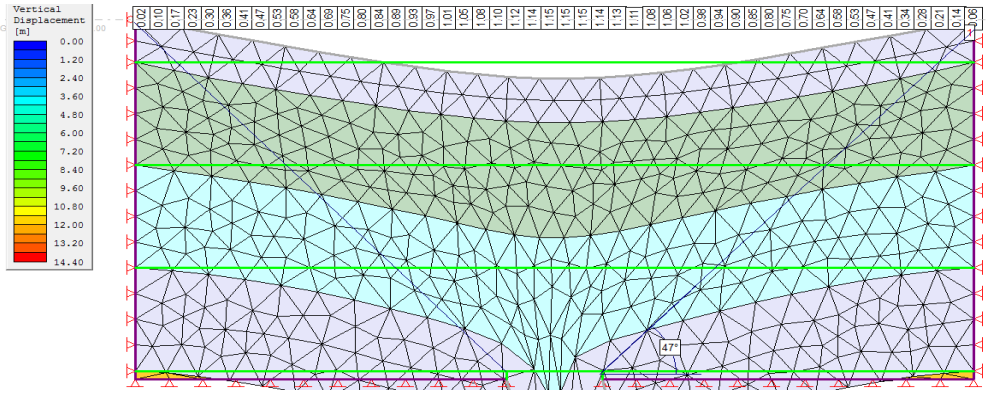

Figure 8. Simulation of displacement of rock layers.

The displacement vectors in the rock layers and the distribution of finite elements in the model are shown in Figures 9 and 10, respectively.

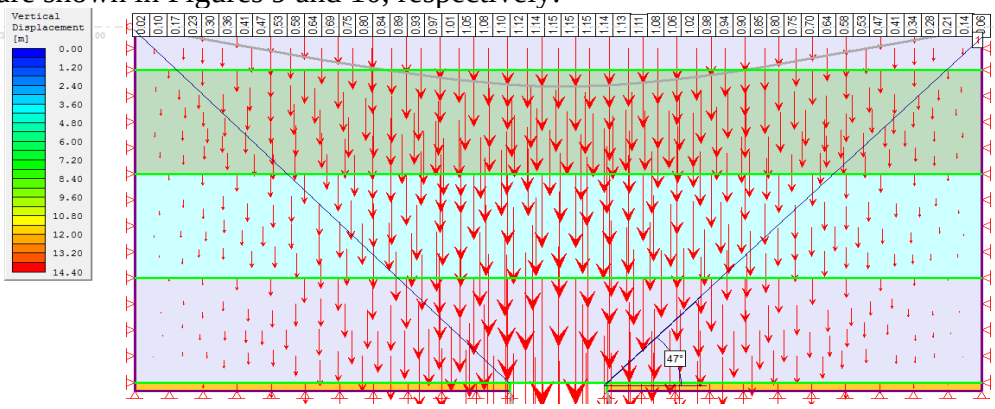

Figure 9. The displacement vectors in the rock layers.

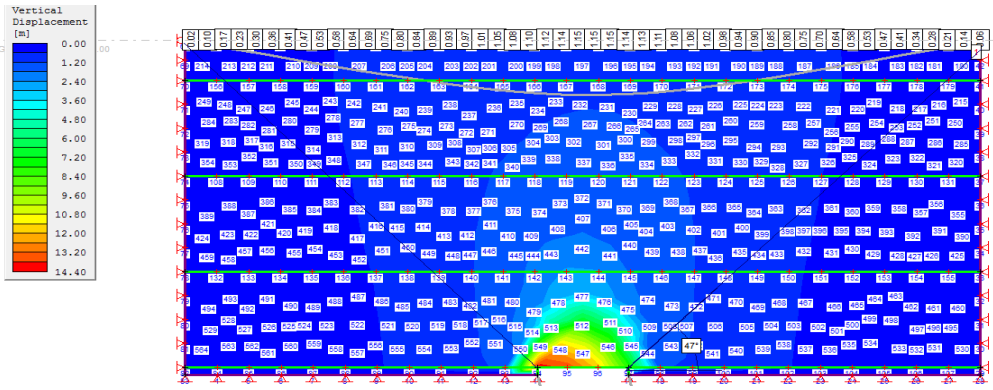

Figure 10. The distribution of finite elements in the model.

3.3. Determination of the caving span of the mechanized longwall I (12)

Calculating the stress-strain state for a mining cycle in the mechanized longwall along the main dip direction is a problem of determining the displacement pattern of the roof coal seam and the overlying strata along the roadway. The displacement of the rock layers due to coal mining originates from the manifestation of mine pressure and abutment pressure in longwall mining. The displacement span of the longwall and the distribution of abutment pressure ahead and behind the longwall face are shown in Figure 11.

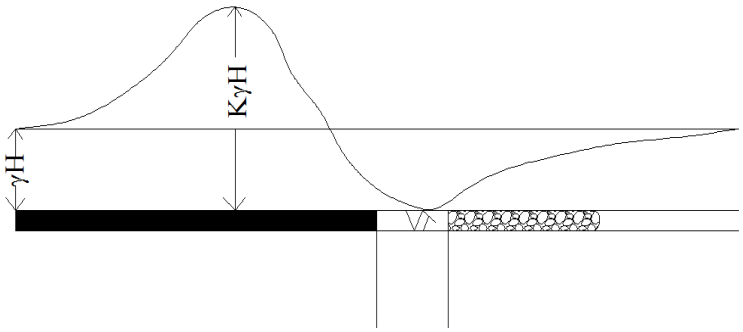

Figure 11. Distribution of abutment pressure ahead and bedind the longwall face.

In the direction of longwall mining, the destruction of the overlying strata gradually develops forward. The process of stress-strain redistribution in the rock strata above the longwall continuously occurs. By analyzing the stress-strain of the rock and coal blocks above the longwall, we can obtain a picture of the destruction (plastic deformation), thereby calculating the caving height (i.e., the height at which the rock strata become plastic - the shear strength reaches residual deformation). The mechanized longwall extracts an 8 m thick seam along the dip direction. The area prepared for installing the support frame is a roadway approximately 6 m wide. Each face advance in each coal-cutting cycle is 0.63 m. The coal cutting height is 2.4 m, followed by full caving of the top coal. The calculation diagram is shown in Figure 12. The physical and mechanical properties of the rock layers are taken according to Table 3. The initial face advance distance is 12.3 m (including 10 caving spans of the longwall and the distance for preparing the support frame installation). To clearly show the stress-strain zone, the author considers 10 mining cycles 6.3 m as one span on the model with 20 spans of the longwall advance to find the distribution pattern of the displacement and deformation zones around the longwall and on the ground surface. The finite element method is applied using the RS2 (Phase 2) software from Rocscience Inc. (Canada).

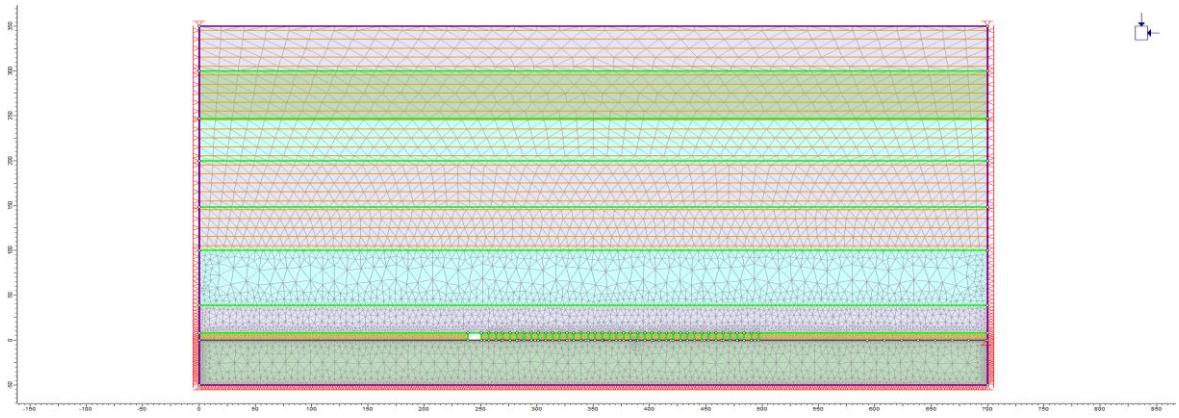

Figure 12. Geomechanical model of the mechanized longwall along the strike direction.

The calculation results of the maximum principal stress values in the caving spans of the longwall mining are shown in Figures 13 to 19.

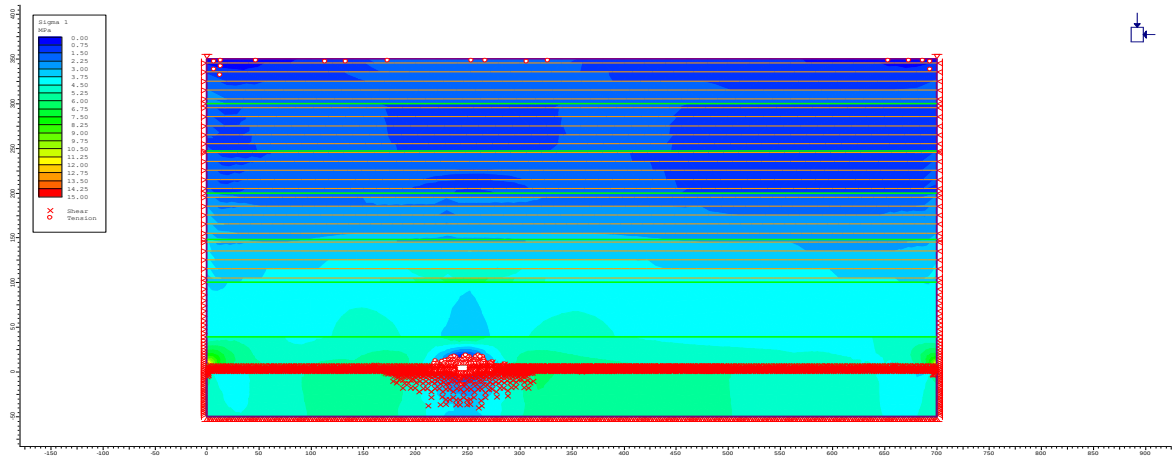

Figure 13. Description of the principal stress σ_1 at the initial longwall.

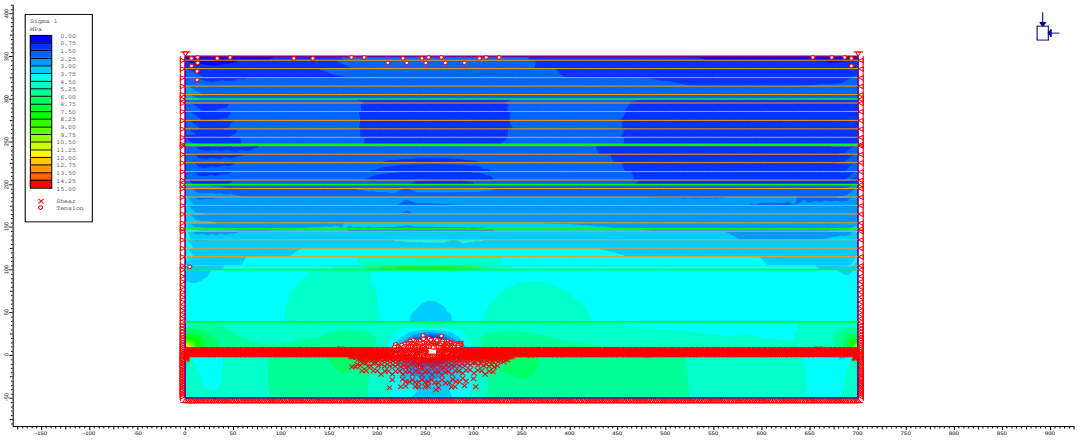

Figure 14. Description of the principal stress σ_1 at the 2nd span.

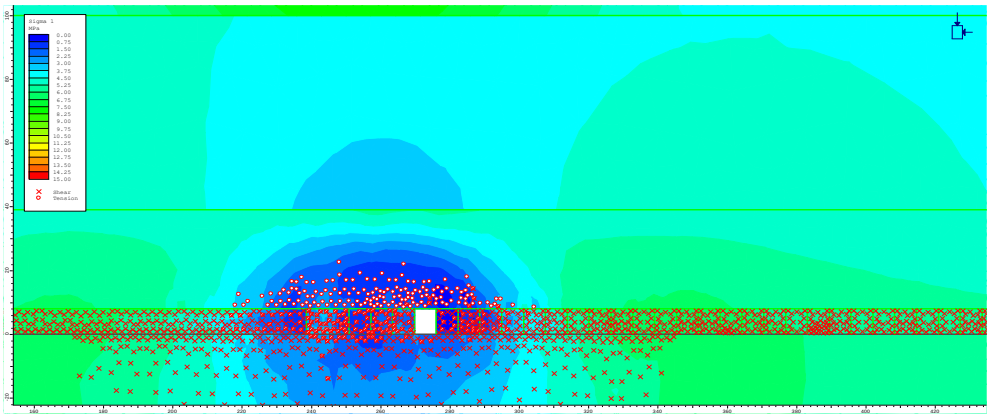

Figure 15. Description of the principal stress σ_1 at the 5th span.

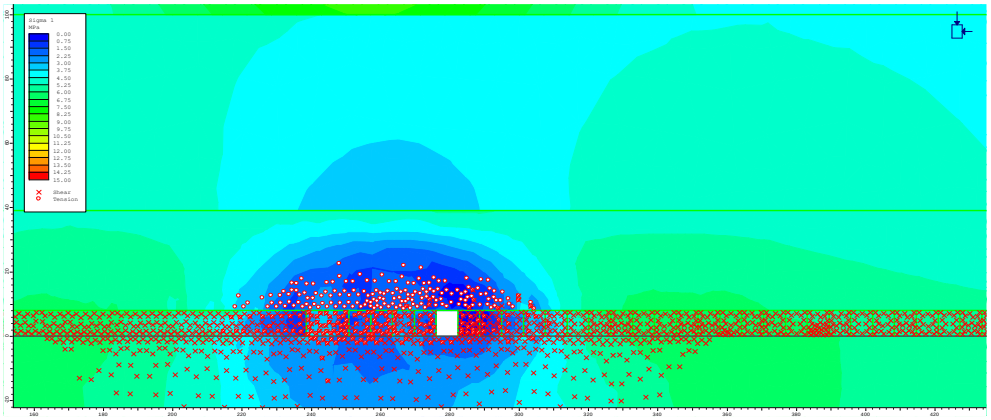

Figure 16. Description of the principal stress σ_1 at the 6th span.

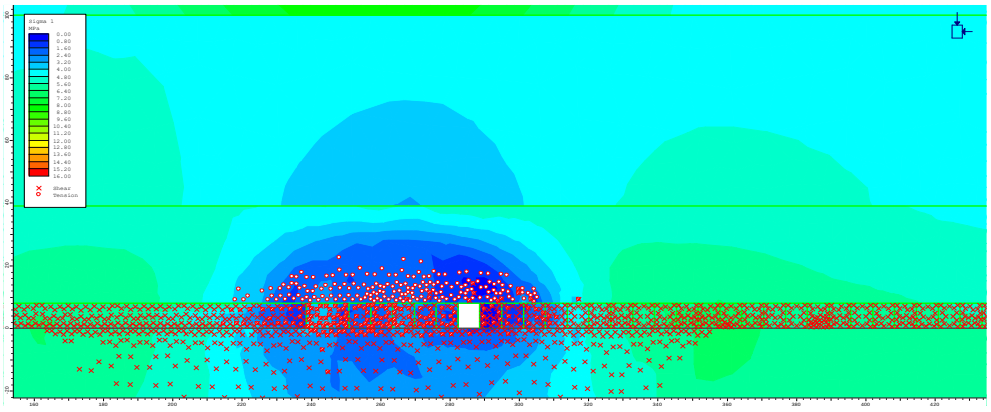

Figure 17. Description of the principal stress σ_1 at the 7th span.

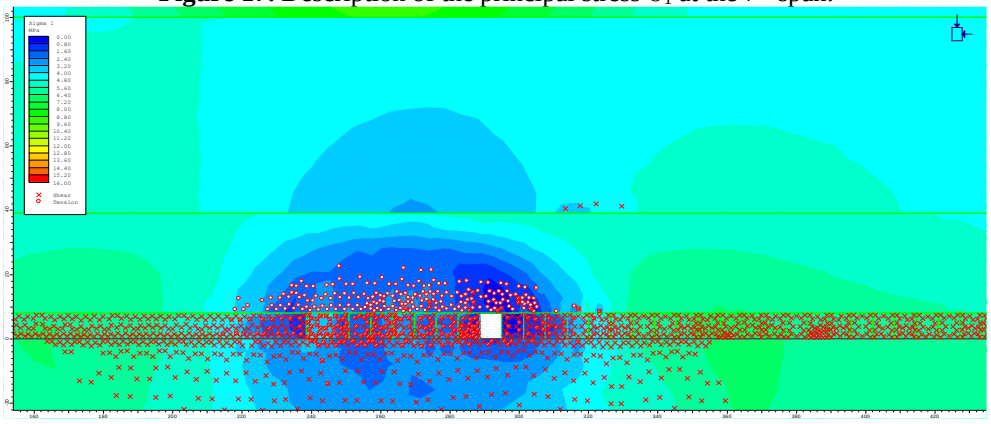

Figure 18. Description of the principal stress σ_1 at the 8th span.

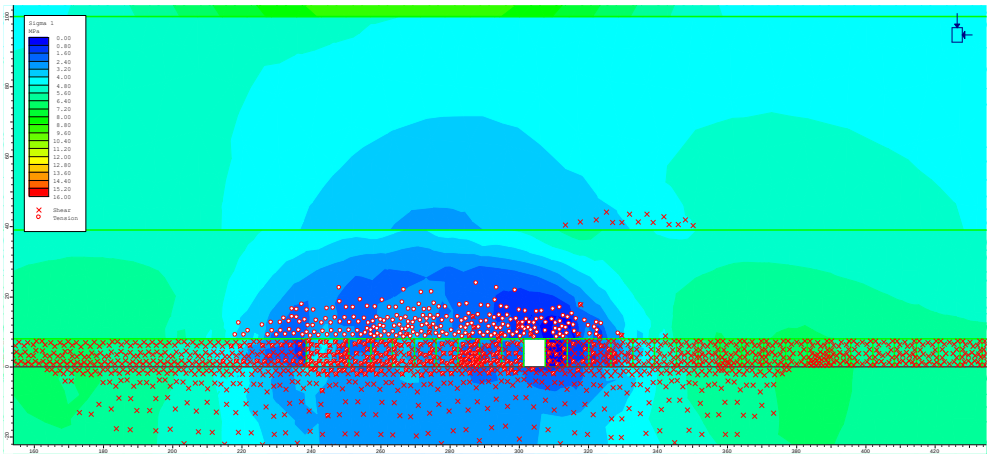

Figure 19. Description of the principal stress σ_1 at the 10th span.

Through the simulations in the above figures, it can be seen that after the face advance, the destruction describes the caving of the rock layers above the longwall. From the figures, the caving height (the distribution area of the circular points) is calculated to be H = 10 m. Thus, at the 10th span, the caving span repeats. This means that the length of the longwall mined along the strike direction reaches 65m, and the caving span and height repeat.

Summarizing the face advances with 10 spans, we see that at the 10th span, the distribution pattern of the principal stress σ_1 returns to the initial state as shown in Figure 20.

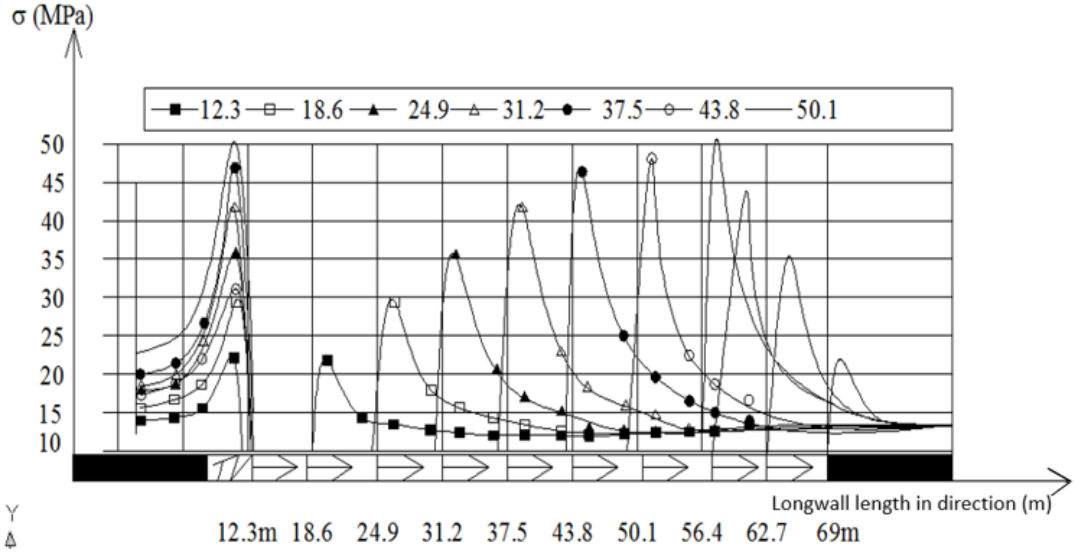

Figure 20. Distribution pattern of the principal stress σ_1 at the spans.

The calculation results of the displacement and deformation of the rock layers on the ground surface and above the longwall are shown in Figures 21–24.

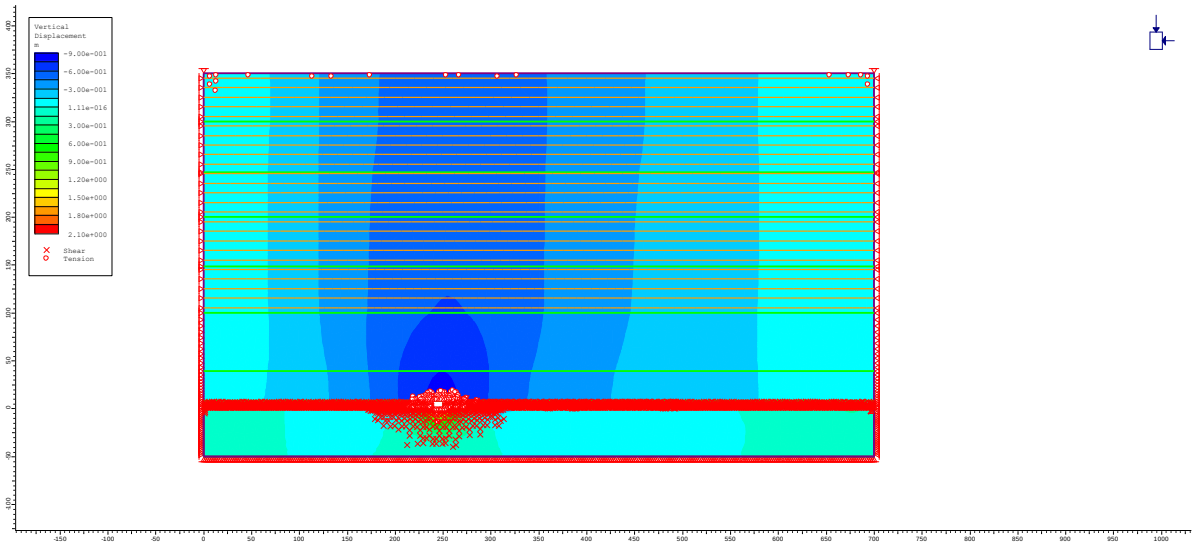

Figure 21. Displacement and deformation of the rock layers during initial longwall mining

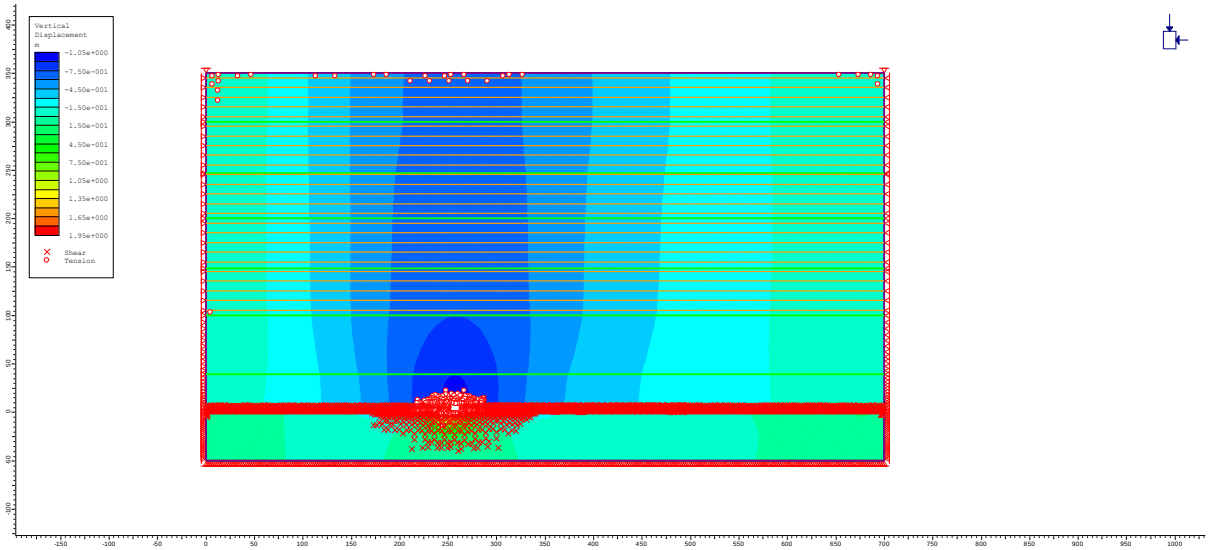

Figure 22. Displacement and deformation of the rock layers at the 5th span.

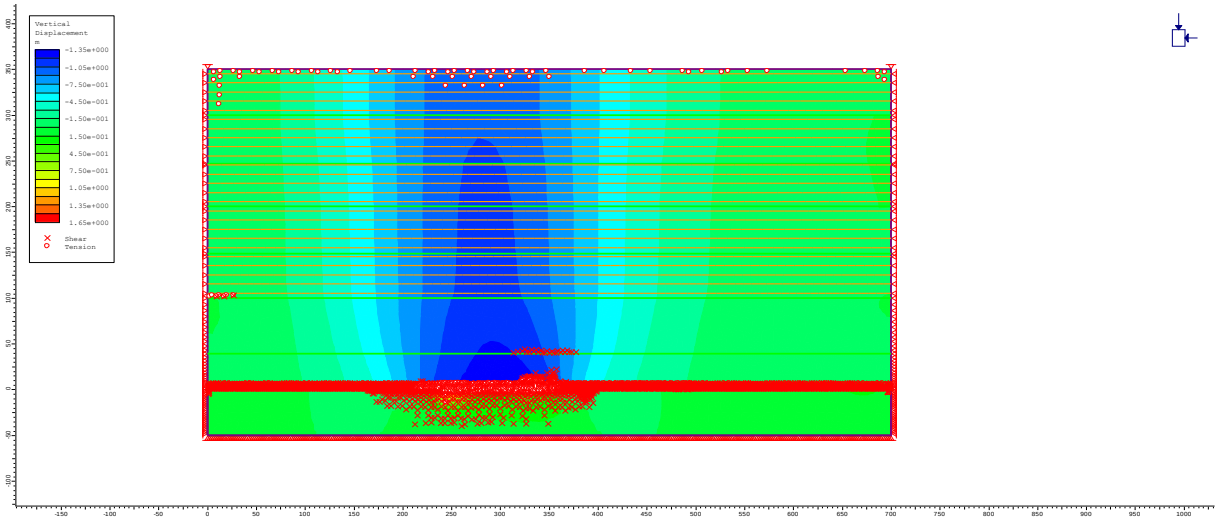

Figure 23. Displacement and deformation of the rock layers at the 10th span.

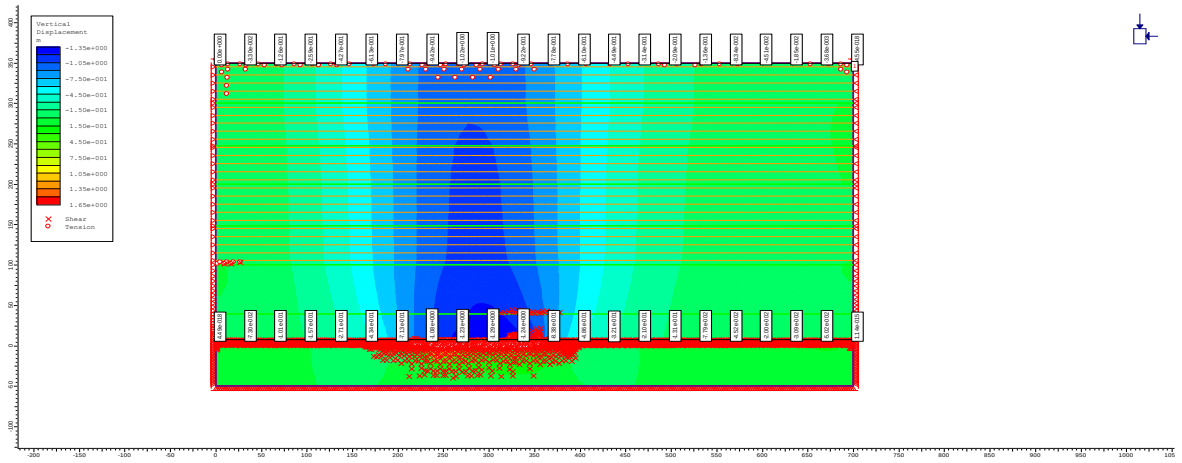

Figure 24. Displacement and deformation on the ground surface and basal rock layer.

The vertical displacement is shown in the cross-section as in Figure 25.

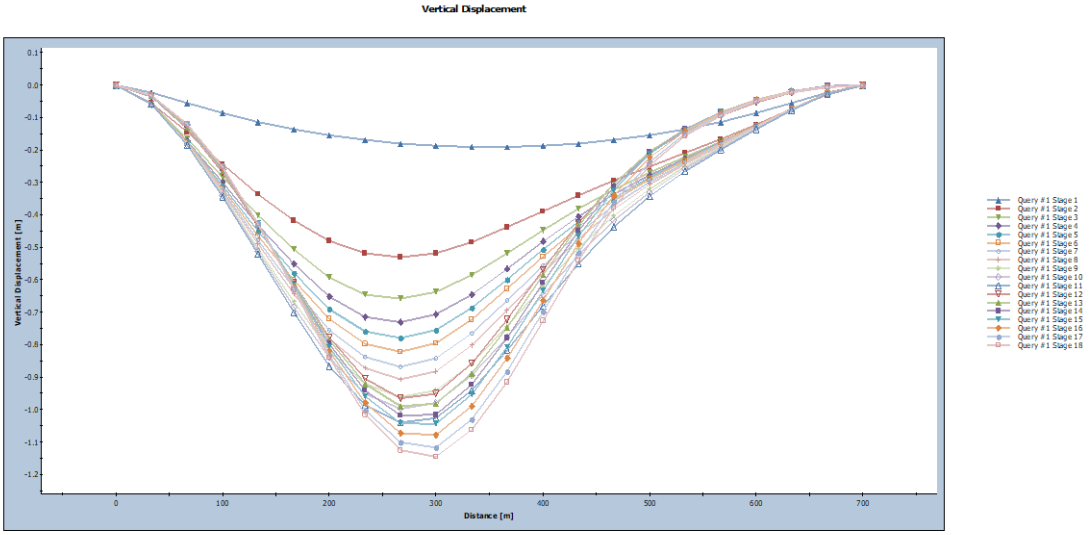

Figure 25. Vertical displacement values on the surface.

The vertical displacement of the surface above the longwall roof is shown in Figure 26.

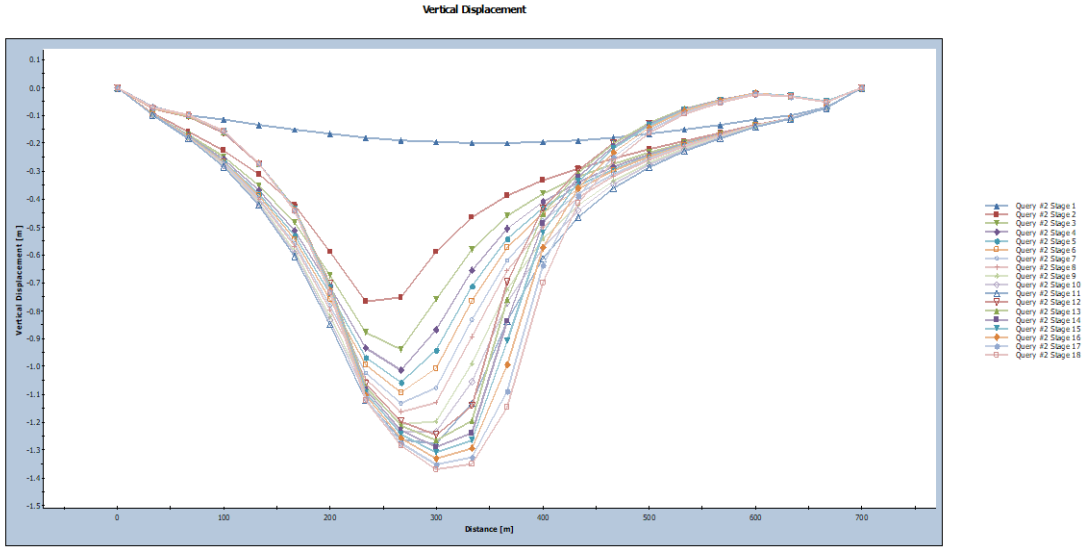

Figure 26. Subsidence curve above the longwall roof.

3.4. Analysis of the geomechanical model

The surface subsidence is shown with the red line representing the maximum value and the blue line representing the minimum value (Figure 5). The calculation result determines the maximum subsidence $\eta = 1.150$ m, with the boundary displacement angle $\beta_0 = 47^o$ (Figure 7).

The results analyzing surface subsidence are shown through the deformation of the finite element mesh (Figures 7, 8). This indicates that when mining at a certain depth, the subsidence area on the surface expands, but the curvature decreases. This means that the deeper the mining is, the less likely it is to cause sliding and collapsing of architectural structures. This also demonstrates that as mining goes deeper and reaches a safe mining depth, the displacement and deformation do not propagate to the surface.

The displacement and deformation of the rock layers show three distinct zones: the complete displacement zone near the roof forming a V-shape, above which is the sagging zone, and the compressed rock zone (Figure 7).

The displacement vector direction is shown, with the vector magnitude increasing from the surface down to the longwall roof, reaching a maximum value at the longwall roof. The further from the center of the longwall, the smaller the displacement vector value is, indicating the compressed rock zone (Figure 9).

The finite elements in the model are uniformly distributed and arranged according to a certain pattern. The destruction zone mainly develops above the roof of the mining area, with the height and shape depending on the dip and the relative distance of the mining area to the surface. It is also noted that during mining, destruction zones may appear on the surface due to overall subsidence and deformation. The tensile failure may appear on the upper boundary of the study area (Figure 10).

The caving height (the distribution area of the circular points) is calculated to be H = 10 m. Thus, at the 10^{th} span, the caving span repeats, meaning that the length of the longwall mined along the strike direction reaches 65 m, and the caving span and height repeat (Figure 20).

Therefore, to ensure the accuracy and reliability of the results from the geomechanical model, the paper determines the maximum subsidence on the model and verifies against the monitoring results at the Mong Duong coal mine, as shown in Table 5. The verification results show that the angle and displacement from the geomechanical model are very close to the actual value.

Table 5. Comparison of subsidence and displacement angle.

Value	Geomechanical model	Field measurement	Note
η	-2.250 m	-2.282 m	Dip direction
η	-0.659 m	-670 m	Strike direction
β_0	47^o	45^o	

4. Conclusion

The geomechanical model accurately determines displacement and deformation parameters at the Nam Mau coal, showing close agreement between field observation and the calculated values for displacement and other parameters.

The model's calculations for the longwall along the dip direction reveal variations in the rock layers surrounding the longwall, including specific strata and surface conditions. The boundary displacement angle was determined to be $\beta_0 = 47^o$, with maximum subsidence values of $\eta = -2.250$ m in the dip direction, and $\eta = -0.659$ m in the strike direction. The caving height was found to be H = 10 m, along with the caving span of the roof rock in thick seams mined using mechanized longwall methods. The model identifies their zone: the

continuous sagging zone, the sagging zone with cracks, and the displacement basin on the surface.

Overall, the geomechanical model provides a comprehensive view of the displacement and deformation processes in rock strata and ground surfaces.

Author contribution statement: Generating the research idea; statement of the research problem; analysis of research results and data preparation; wrote the draft manuscript: P.V.C., N.D.H.; Analyzed and interpreted the data, wrote the draft manuscript: L.Q.N., D.T.T., L.V.H.

Acknowledgments: This research was funded by the Hanoi University of Civil Engineering, grant No: 01-2023/KHXD-TD.

Competing interest statement: The authors declare no conflict of interest.

References

1. Chung, P.V. Research on the construction of a geomechanical fluctuation model in the area of mechanized longwall mining of thick seams in some underground coal mines in Quang Ninh. PhD Thesis, Hanoi University of Mining and Geology (In Vietnamese).
2. Chung, P.V.; Dac, P.M.; Kha, V.T. Building a geomechanical model to determine the elastic modulus for the Quang Ninh coal basin influenced by mechanized longwall mining of thick seams. *J. Min. Ind.* **2018**, *37*, 86–90.
3. Long, N.Q.; Ahmad, A.; Cuong, C.X.; Canh, L.V. Designing observation lines: a case study of the G9seam in the Mong Duong colliery. *J. Min. Earth Sci*. **2019**, *60(3)*, 18–24.
4. Long, N.Q.; My, V.C.; Luyen, B.K. Divergency verification of predicted values and monitored deformation indicators in specific condition of Thong Nhat underground coal mine (Vietnam). *Geoinformatica Polonica* **2016**, *15*, 15–22.
5. Long, N.Q. A novel approach of determining the parameters of Asadi profiling function for predicting ground subsidence due to inclined coal seam mining at Quang Ninh coal basin. *J. Min. Earth Sci*. **2020**, *61(2)*, 86–95.
6. Nguyen, Q.L.; Nguyen, Q.M.; Tran, D.T.; Bui, X.N. Prediction of ground subsidence due to underground mining through time using multilayer feed-forward artificial neural networks and back-propagation algorithm – Case study at Mong Duong underground coal mine (Vietnam). *Min. Sci. Technol.* **2021**, *6(4)*, 241–251.
7. Nguyen, L.Q.; Le, T.T.T.; Nguyen, T.G.; Tran, D.T. Prediction of underground mining-induced subsidence: Artificial neural network based approach. *Min. Depos* **2023**, *17*, 45–52.
8. Авершин, С.Г. Расчет деформаций массива горных пород под влиянием подземных разработок [Текст] / С.Г. Авершин. -Л.: ВНИМИ, **1960**. -87с.
9. Методические указания по определению процесса сдвижения горных пород, охране сооружений и горных выработок на месторождениях цветных металлов [Текст]. Л.: ВНИМИ, **1971**. - 66 с.
10. Behnam, A.; Abbas, M.; Hassan, B.A. Investigating mechanical and geometrical effects of joints on minimum caving span in mass caving method. *Int. J. Min. Geo-Eng*. **2023**, *57(2)*, 223–229.
11. Behnam A., Abbas M., Abbas. M. Evaluation of effective geomechanical parameters in rock mass capability using different intelligent techniques. *Int. J. Min. Geo-Eng*. **2024**, *58(3)*, 307–313.
12. Boltengagen, I.L.; Koren'kov, É.N.; Popov, S.N.; Freidin, A.M. Geomechanical substantiation of the parameters of a continuous chamber system of mining with caving of the roof rock. *J. Min. Sci.* **1997**, *33*, 55–63.

13. Alipenhani, B.; Majdi, A.; Amnieh, H.B. Determination of caving hydraulic radius of rock mass in block caving method using numerical modeling and multivariate regression. *J. Min. Environ.* **2022**, *13(1)*, 217–233.
14. Alipenhani, B.; Amnieh, H.B.; Majdi, A. Application of finite element method for simulation of rock mass caving processes in block caving method. *Int. J. Eng.* **2023**, *36(1)*, 139–151.
15. Anh, T.T. Monitoring ground displacement and surface deformation on an equivalent material model using imaging measurement technology. *J. Min. Earth Sci*. **2012**, *39*, 5–10.
16. Son, N.T. Research on determining the displacement and deformation parameters of rock and soil during the extraction of thick seams using the underground mining method on an equivalent material model. Institute of Mining Science and Technology. 2012. (In Vietnamese).
17. Sy, N.V.; Thanh, T.V.; Dung, L.T. Determining the displacement parameters of rock and soil affected by underground mining on the surface of the Mong Duong-Khe Cham coal deposit using an equivalent model. Proceedings of the 20th Scientific Conference, University of Mining and Geology, Hanoi. 2012. (In Vietnamese).
18. Tuan, N.A.; Nguyen, L.D.; Sy, T.V. Evaluation of research results on the impact of movements in the mixed underground-surface mining scheme using an equivalent material model. *Min. Sci. Technol. Inf.* **2011**, *12*, 1–6. (In Vietnamese)
19. Tuan, N.A.; Nguyen, L.D.; Phuc, L.Q. Research on the impact of movements in the mixed underground-surface mining scheme using numerical modeling. *Min. Sci. Technol. Inf*. **2011**, *11*, 1–6. (In Vietnamese)
20. Tuan, N.A.; Quang, D.H.; Nguyen, L.D. Research on the displacement and deformation of rock and soil in underground coal mining in the Quang Ninh region using an equivalent material model. *Min. Sci. Technol. Inf*. **2012**, *10*, 18–23.
21. Phuc, L.Q.; Zubov, V.P.; Dac, P.M. Improvement of the Loading Capacity of Narrow Coal Pillars and Control Roadway Deformation in the Longwall Mining System. A Case Study at Khe Cham Coal Mine (Vietnam). *Inżynieria Mineralna - Lipiec - Grudzień* **2020**, 115–122.
22. Le, T.D.; Nguyen, C.T.; Dao, V.C. Estimation of coal and rock mechanical properties for numerical modeling of longwall extraction. *J. Pol. Mineral. Eng. Soc.* **2020**, *46(2)*, 41–47.
23. Le, T.D.; Bui, M.T. Numerical modeling techniques for studying longwall geotechnical problems under realistic geological structures. *J. Min. Earth Sci*. **2021**, *62(3)*, 87–96.
24. Geological Report of Nam Mau Coal Min3 (In Vietnamese).
25. Hai, P.D. Research on building a geological database for mining to serve the needs of mechanization and modernization of coal extraction in Vietnam. A key project under the Ministry of Industry and Trade. 2011-2013. (In Vietnamese)

JOURNAL OF
HYDRO-METEOROLOGY

Research Article

Prediction of landslide hazard using LS-RAPID model: A case study in the Tia Dinh area (Dien Bien province, Vietnam)

Nguyen Duc Ha[1]*, Nguyen Hoang Ninh[2], Tran The Viet[3], Nguyen Thanh Tung[2], Le Duc Tho[2], Nguyen Huy Duong[2]

[1] Vietnam Geological Department; nh14vn@gmail.com
[2] Vietnam Institute of Geosciences and Mineral Resources; ninh.dcks@gmail.com; thanhtung.vigmr@gmail.com; glg.tanet@gmail.com; nguyenhuyduong112358@gmail.com
[3] Thuyloi University; trantheviet@tlu.edu.vn

*Corresponding: nh14vn@gmail.com; Tel.: +84–989258025

Received: 25 September 2024; Accepted: 8 November 2024; Published: 25 December 2024

Abstract: Landslides represent a severe natural hazard, particularly in mountainous areas where steep slopes, intense rainfall, and unstable geological conditions frequently trigger destructive ground movements. This study focuses on assessing the potential landslides in Tia Dinh Commune, Dien Bien province, Vietnam, using the LS-RAPID model to simulate and predict potential hazards. By conducting extensive field surveys, geophysical measurements, and applying extreme-case scenario simulations, we identified three high-risk landslide zones (S1, S2, S3) alongside a larger area, zone S, which poses the most significant threat due to its potential for widespread and rapid material displacement. Despite challenges posed by limited geotechnical data in remote regions, the LS-RAPID model effectively predicted movement patterns, velocity, and impact zones of landslides, significantly improving our understanding of landslide dynamics. The results underscore the importance of integrating landslide risk assessments into local land-use planning to ensure safer community development. Additionally, we recommend the installation of groundwater monitoring devices at strategically identified locations within these high-risk zones to support early warning systems and enable timely preventive measures. Our findings highlight the need for a proactive approach to landslide risk management, combining prediction models with comprehensive monitoring strategies. This research provides a valuable framework for disaster preparedness, offering insights adaptable for regions facing similar landslide threats.

Keywords: Landslide hazard; LS-RAPID model; Tia Dinh commune.

1. Introduction

Landslides are among the most devastating natural disasters, particularly in mountainous regions where the convergence of steep slopes, heavy precipitation, and unstable geological conditions often triggers extensive ground movements [1, 2]. These events result in significant damage worldwide, affecting infrastructure, and agricultural lands, and posing severe threats to human safety [3, 4]. Notably, many landslides involve single mass movements characterized by long and wide flow paths, making them difficult to predict and leading to catastrophic consequences. A notable instance is the rock and ice avalanche from the north peak of Nevados Huascarán in Peru in 1970. This event resulted in a mass movement that traveled 16 kilometers, descending about 4,000 meters in elevation, with average speeds reaching 280 km/h, ultimately leading to the tragic loss of approximately

18,000 lives [5]. Similarly, on February 17, 2006, a rapid and long-runout landslide struck the southern part of Leyte Island, Philippines, where the debris flow extended over 1.5 kilometers, causing 154 confirmed fatalities and leaving 990 individuals missing [6].

In Vietnam, the risk of landslides is heightened by its rugged terrain, fractured geological structures, and intense seasonal rainfall, posing serious threats to communities and critical infrastructure [7, 8]. Many landslide incidents have combined with flash floods, impacting areas that extend over several kilometers. Examples include the events recorded in Phin Ngan Commune, Bat Xat District, Lao Cai Province in 2004 and 2016; in various communes of Phuoc Son and Nam Tra My districts, Quang Nam Province in 2020; and more recently in Lang Nu Village, Phuc Khanh Commune, Bao Yen District, Lao Cai Province. These occurrences underscore the destructive potential of landslides. Given landslides' sudden and volatile nature, developing robust prediction and risk management strategies is essential to mitigate their impact on vulnerable regions [9].

Engineering interventions, including retaining walls and slope reinforcements, are widely used to reduce landslide risks; however, these measures often come with significant financial and labor demands and are difficult to apply effectively over extensive areas. The repeated occurrence of landslides in Sichuan, China, highlights the limitations and challenges of structural mitigation approaches, especially in regions with complex and unstable geological landscapes. Despite considerable investments in preventative efforts, the area's vulnerability to seismic activity and variable weather patterns continue to fuel these recurring landslide events. Studies have shown that natural triggers such as earthquakes and intense rainfall are frequently responsible for initiating landslides, thereby complicating the efficiency of conventional engineering solutions in landslide control and management [10, 11].

Numerous dynamic models have been developed to simulate and analyze the runout behavior of landslide materials, including MADFlow [12], RASH3D [13], Particle Flow Code PFC3D [14], DAN3D [15], and the LS-RAPID model [16]. These models have proven to be highly effective in accurately predicting landslide initiation and progression when supported by comprehensive geotechnical data. However, their application is often limited due to the substantial requirement for extensive field data, detailed soil characterization, and meticulous model calibration, all of which can be resource-intensive processes [17]. Additionally, the variability of terrain in landslide-prone areas, marked by differing soil characteristics, rock formations, and hydrological conditions, presents a significant challenge in applying these models universally across diverse regions.

In situations where early indicators of instability, such as ground cracks or subsidence, are observed, the prompt use of predictive models becomes crucial in issuing early warnings and executing preventive measures. Extreme scenario modeling can effectively highlight high-risk areas, enabling timely interventions like evacuations or the enforcement of land-use regulations. The implementation of predictive models for assessing the impact of sliding material flows supports the generation of hazard maps, which play a key role in guiding land-use planning and enhancing disaster preparedness.

In this study, we employed the LS-RAPID model in Tia Dinh Commune to strengthen landslide risk management by simulating extreme-case scenarios. The LS-RAPID model is a 3D software capable of simulating the entire sequence of a landslide event (from identifying the initiation point to tracking the material flow’s movement path). The LS-RAPID model has been applied extensively to simulate numerous landslide events worldwide [18–23], including in Vietnam [24, 25], helping to identify characteristics of landslide masses, such as triggering groundwater levels, material flow thickness, and affected areas. With its proven effectiveness, this model can accurately predict potential landslide movements, providing critical support for construction safety and preventive planning. By offering a rapid and cost-efficient approach to landslide forecasting, our research seeks to enhance the understanding

of landslide dynamics in developing regions, ultimately contributing to the protection of lives and the reduction of economic losses in vulnerable communities.

2. Materials and Methods

2.1. Study area

Tia Dinh Commune, located in Dien Bien Dong district of Dien Bien province in northwestern Vietnam (Figures 1 and 2), lies within a mountainous area that has been identified as a paleo-landslide zone through geological and geomorphological studies, as well as remote sensing analysis. In recent years, the region (referred to as Area A) has shown signs of instability, with multiple ground cracks and subsidence occurring during heavy rainfall events, posing a significant threat to the safety of residents and their infrastructure. Some images of these cracks and subsidence were taken since 2019 and are presented in Figures 3-6. This includes critical structures such as the People's Committee office, health stations, schools, and more than 69 residential houses. Given the evident landslide risks, local authorities have begun the process of relocating the commune center to a safer, lower-lying area (area B) to mitigate potential hazards.

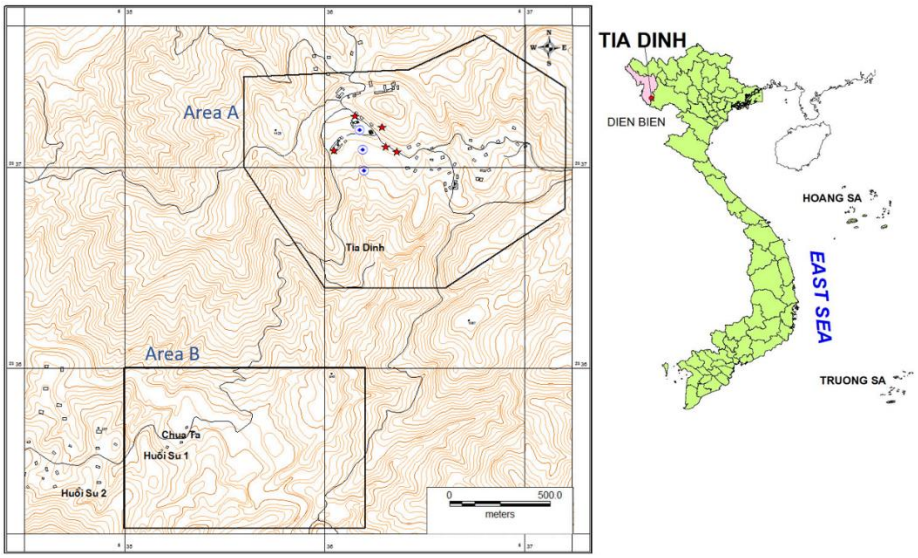

Figure 1. Study areas: The center of the Tia Dinh commune (Area A) and the proposed area for relocation (Area B).

The terrain of the study area is characterized by high mountains, with absolute peak elevations ranging from over 800 m to 1,200 m. In Area A, the terrain features a mixture of steep slopes and relatively rounded peaks. The central part of the commune exhibits distinct elevation levels, with the area above 960 m characterized by steep slopes, while the area below 960 m has significantly gentler slopes. Land cracking and subsidence phenomena are currently mainly observed within the boundaries of this terrain transition. In Area B, the terrain primarily consists of mountain ridges extending in a northeast-southwest direction, interspersed with short, gentle ravines forming part of the Na Hay stream valley. The mountain ridges in this area have relatively gentle slopes and peaks.

Concerning the geological characteristics, the area belonging to the Suoi Bang Formation (T_3n-rsb1) comprises sandstone, siltstone, mudstone, with minor sandstone-conglomerate, conglomerate, and breccia, showing a medium bedding structure. The formation dips southwest, with typical dip angles between 25 and 40 degrees. It belongs to the clastic sedimentary rock group, rich in aluminosilicates, characterized by weak cementation and high porosity. Near faults, the bedding orientation shifts to dip either

southeast or northeast, with dip angles ranging from 60 to 80 degrees. Under humid tropical climate conditions, a thick weathering crust develops, resulting in significant thickness. An ancient landslide mass (Q) (Figure 2) was identified and delineated through topographic analysis combined with field investigation at a scale of 1:5,000, geophysical surveys, and borehole drilling. This landslide covers an area of approximately 15 hectares, extending about 800 meters in length and reaching a maximum width of 340 meters.

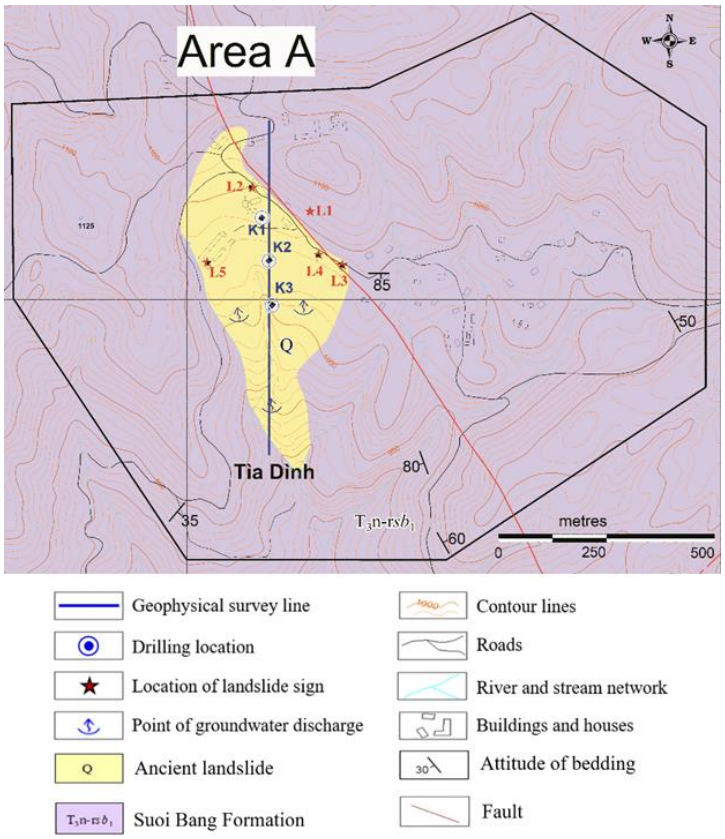

Figure 2. The center of the Tia Dinh commune (Area A).

Figure 3. Instability on the mountain slope (L1 in Figure 3) facing the office building of People's Committee.

Figure 4. Cracks appeared inside the office of the People's Committee (left) (L2 in Figure 3) and in a nearby house (right).

Figure 5. Cracks and subsidence on the foundations of Ms. Sung Thi Pa's house (left) (L3 in Figure 3) and Ms. Giang Thi Chu's house (right) (L4 in Figure 3).

Figure 6. Damages at the primary school (L5 in Figure 3): In the classroom (left) and on the surrounding walls (right).

2.2. Methodology

The LS-RAPID model is a sophisticated tool designed to simulate and predict landslide-prone areas and assess their potential impact. It has demonstrated high accuracy in global applications, particularly when integrated with the undrained dynamic-loading ring-shear apparatus, yielding precise results in various regions. However, in Vietnam, where approximately 75% of the land consists of hilly or mountainous terrain, it is challenging to perform soil sample tests comprehensively across all landslide-susceptible zones due to constraints in resources and time.

Specifically, dealing with large and complex landslide masses poses difficulties, as combining parameters from different locations is often intricate. This complexity arises because physical models are generally more suitable for areas with uniform geological conditions. In regions already identified as at risk for landslides, it is crucial to explore simpler, more practical methodologies that can be rapidly deployed and adapted to predict hazardous zones effectively.

The fundamental concept behind this simulation approach can be visualized through Figure 1, which represents a vertical imaginary column within a moving landslide mass. The forces acting on this column include (1) its self-weight (W), (2) seismic forces (comprising vertical force Fv and horizontal forces Fx and Fy in the x-y direction), (3) lateral pressure on the side walls (P), (4) shear resistance at the base (R), (5) normal stress at the base (N) as a reaction from the stable ground due to the self-weight's normal component, and (6) pore pressure at the base (U). The landslide mass (m) experiences acceleration (a) due to the combined influence of these forces, which include the driving force (composed of self-weight and seismic forces), lateral pressure, and shear resistance.

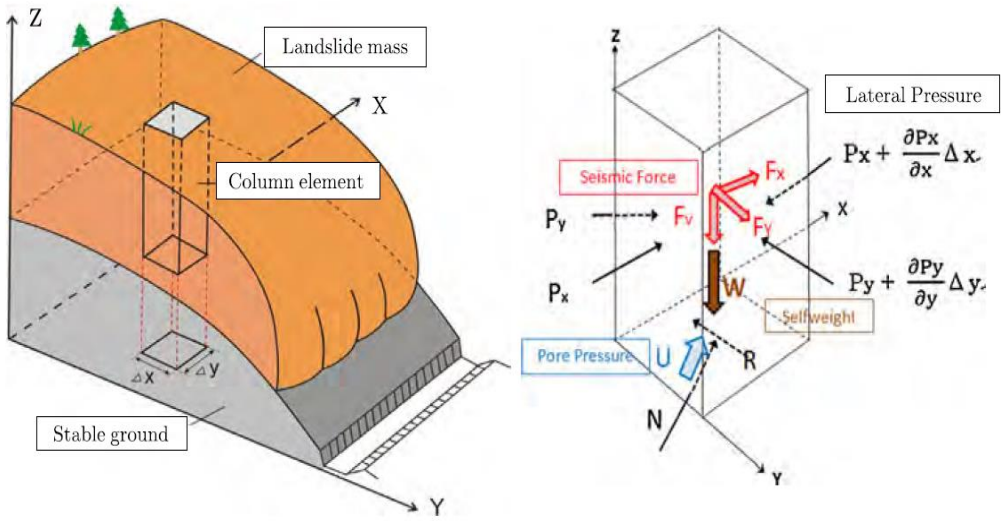

Figure 7. Core principles of the LS-RAPID model. On the left: a column element depicted within the moving landslide mass. On the right: the force equilibrium acting on the column is demonstrated [6].

In this study, the LS-RAPID model was utilized to predict potential landslide hazards, providing valuable insights for land-use planning and infrastructure development. Additionally, groundwater levels that could act as landslide triggers were assessed to enhance monitoring systems and enable early warnings before landslide occurrences. Several geotechnical parameters required for the LS-RAPID model were derived from soil sample analyses. However, due to the limitations in the available equipment in Vietnam, certain parameters could not be directly measured. In these cases, the extreme-case scenarios based on parameter suggestions from the model's developer or data from previous studies were employed to ensure a comprehensive risk assessment. The values of the model's key parameters are presented in Table 1, and detailed information about the parameters can be referred to in [16].

Table 1. The key parameters in LS-RAPID simulations were applied to the Tia Dinh area.

Parameters	Value	Source
Steady-state shear resistance (τ_{ss}, kPa)	5	Extreme value
Friction angle at peak (ϕ_p, degree)	20	Test data (average value)
Friction angle during motion (ϕ_m, degree)	20	Estimation based on ϕ_p
Cohesion at peak (c, kPa)	5	Extreme value
Shear displacement at the start of strength reduction (DL, mm)	6	Extreme value
Shear displacement at the start of steady state (DU, mm)	2500	Extreme value
Pore pressure generation rate (B_{ss})	0.8	Extreme value
Total unit weight of the mass (γ_t, kN/m^3)	20	Test data (average value)
Unit weight of water (γ_w, kN/m^3)	9.8	Standard value

The application process of the LS-RAPID model for predicting landslide hazards involves four key steps as follows:

(1) Data Collection and synthesize relevant information about the study area, including:

- Digital Elevation Model (DEM) data.
- Historical landslide traces and events, identified from satellite imagery and media reports.
- Previous measurement results conducted in the area.

- Research findings from previous applications of the LS-RAPID model, both within Vietnam and internationally.

(2) Field Survey:

- Identify and document visible signs of landslide activity.
- Investigate exposed sections to estimate the thickness of weathered layers (potential slip surfaces).
- Conduct geophysical measurements and drilling to determine the thickness of soil layers, if feasible.

The electrical resistivity sounding method was performed using a multi-electrode approach within a 2D model. Measurement points along each survey line were spaced 10 meters apart, following a dipole-dipole array configuration. Measurements were recorded using an electrical station equipped with a VIP 3000 transmitter and an Elrec Pro receiver by IRIS Instruments, delivering a transmission power of 3KW, with a maximum current of 10A and a peak output voltage of 1500V. For data analysis, we utilized Res2Dinv, a specialized software by Geotomo Software, which supports 2D quantitative analysis and includes terrain correction functions.

The results from the geophysical surveys reveal significant variations in geological units and structures, suggesting that geological features potentially influencing subsidence and landslide activities may extend to depths exceeding 20 meters. Accordingly, boreholes with depths of over 20 meters were drilled to further investigate these subsurface conditions

(3) Model Application: Implement the LS-RAPID model by delineating potential slip surfaces and simulating different scenarios using geotechnical parameters and groundwater levels. These scenarios should be based on both analytical results and data from previous studies.

In LS-RAPID model, the influence of groundwater levels on slope stability due to water rise is shown via the pore water pressure ratio r_u [6]:

$$r_u = \Delta u/\sigma \quad (1)$$

$$\Delta u = h \times \gamma_w \times \cos^2\alpha \quad (2)$$

$$\sigma = H \times \gamma_s \times \cos^2\alpha \quad (3)$$

where Δu: Pore water pressure exerted on the potential sliding surface (kPa); σ: Total normal stress exerted on the potential sliding surface (kPa); h, H: Water depth, soil depth (m); γ_w, γ_s: Unit weight of water, unit weight of soil (kN/m^3); α: Slope angle.

The value of r_u was incrementally adjusted to simulate scenarios of groundwater levels (from dry soil conditions to cases where groundwater levels are at ground level) and thereby predict the locations where landslides are most likely to initially occur.

(4) Report and Hazard Mapping:

- Develop a detailed report and forecast maps that include:
- Areas at risk of landslides and groundwater levels that could trigger such events (identifying locations where groundwater monitoring devices should be installed to support early warning systems).
- Predicted movement patterns of landslide materials (including impact range, average velocity, and thickness of the debris flow).

3. Results

3.1. Results of identifying potential high-risk landslides

Through comprehensive field surveys and analysis of drilling and geophysical data, the research team identified three high-potential landslide zones: S1, S2, and S3 (Figures 8 and 9), along with several other areas at risk. These zones together constitute the largest potential landslide, referred to as S. This extreme-case scenario envisions the simultaneous occurrence

of landslides in all identified zones (S1, S2, S3) as well as other susceptible locations within Area A (Figure 10).

Landslide S1 (Figure 9a): This is the primary arc-shaped sliding surface that governs the movement of the central sliding block in Tia Dinh Commune. It originates from the mountain slope at an elevation of approximately 1070-1080 m. The arc's crest measures about 340 m in width, with the widest portion reaching nearly 400 m. The sliding surface aligns with the boundary between highly fractured rock layers and a significantly weathered zone or the old landslide material. The maximum thickness of the sliding surface in areas at high risk of landslides is estimated to be around 24 m. Cracks and subsidence features have been observed, with crack lengths ranging from a few meters to 30 m, widths up to 20 cm, and subsidence depths reaching up to 1.5 m in some locations.

Landslide S2 (Figure 9b): This large sliding surface is also located in the central area of Tia Dinh Commune. The crest of the sliding arc spans 300 m, with its widest section measuring 380 m. Landslide S2 lies entirely within the old landslide deposit, with its surface coinciding with the boundary between this material and either a highly weathered layer or fractured rocks. The sliding surface is situated approximately 12 m beneath the current terrain surface. Cracks and subsidence are frequently visible on both sides of the road, near the People's Committee office, and at the Primary School, with crack lengths ranging from a few meters to over 20 m and widths from a few centimeters to 10-15 cm. The observed subsidence varies between a few centimeters and up to 25-40 cm.

Landslide S3 (Figure 9c): This sliding surface is present in agricultural fields and around some fishponds, at elevations of 990-1015 m. The crest of this sliding surface measures 70 m, while its widest section reaches 130 m. It is situated within the old landslide material, with an estimated thickness of about 19 m. Signs of cracking and subsidence have been documented along the mountain slope, with lengths ranging from 15 to over 40 m and widths from a few centimeters to 10 cm. The subsidence depth mainly ranges from 20 to 80 cm, with some areas reaching depths of up to 150 cm. Groundwater discharge points are also observed near both the upper and lower sections of this sliding surface.

3.2. Result of LS-RAPID simulations

The LS-RAPID model has been applied to develop a comprehensive landslide risk map, highlighting areas vulnerable to landslide occurrence and their potential impacts by using extreme-case scenario parameters. The process involved generating a 3D model of the study area with a 5 m resolution digital elevation model, compiling detailed data from soil analysis, drilling results, and geophysical measurements, and determining the optimal parameter set

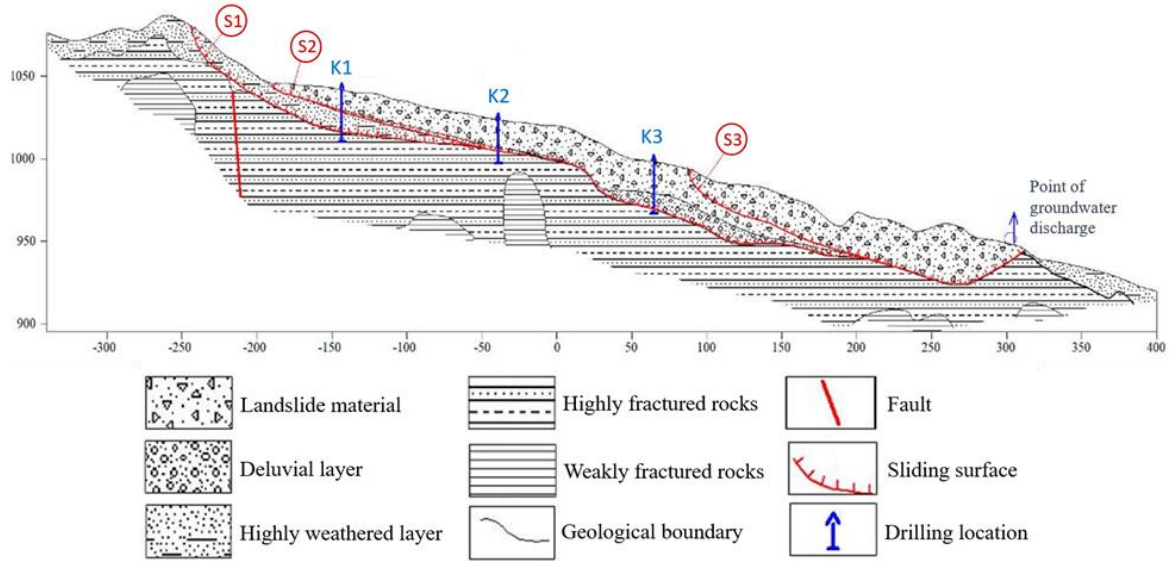

Figure 8. The potential landslides S1, S2, and S3 were determined based on the results of drilling, geophysical measurements, and field surveys.

for the model. The parameter set was based on either direct soil analysis results or extreme-case scenarios derived from recommendations provided by the model's author or from existing published studies. This approach ensures that the model is effectively calibrated to accurately predict landslide risks, taking into account the specific geotechnical conditions of the study area.

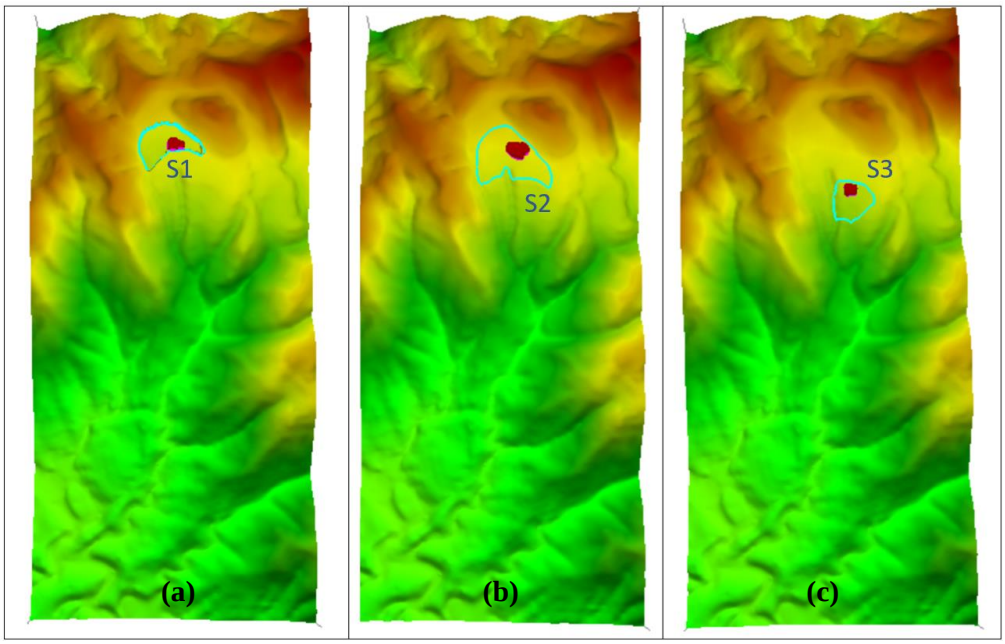

Figure 9. Predicted landslides (S1, S2, S3) (cyan color) and the locations with high potential for initiation (the red blocks inside). The area outside the cyan boundaries represents the elevation of the terrain, which ranges from green to red.

Figure 9 shows three predicted landslides (outlined in green lines) are S1 (a), S2 (b), and S3 (c), with high-risk locations where landslides could initiate (the red blocks inside).

The groundwater levels that are predicted to induce landslides S1, S2, S3 at the potential surfaces:

- Landslide S1 could occur when the groundwater level on the landslide surface is 4.9 m or higher (19.1 m or less from the ground).
- Landslide S2 could occur when the groundwater level on the landslide surface is 2.5 m or higher (9.5 m or less from the ground).
- Landslide S3 could occur when the groundwater level on the landslide surface is 5 m or higher (14 m or less from the ground).

The suggested sites for installing water level monitoring devices, to provide early warnings of landslides, are the locations where the initiation of landslides is predicted (indicated by the red blocks in Figure 9).

The potential hazard of the largest landslide, denoted as S, was simulated for the extreme-case scenario in area A (Figure 10). Figures 10 and 11 present the results of the LS-RAPID model simulations, illustrating the material movement of landslide S originating from area A. The model assumed an average sliding surface thickness of 22 m, consistent with the predicted potential landslides in the region. The simulation forecasted a possible flow path of the landslide material extending over 1.9 km, with a maximum thickness exceeding 40 m. The width of the material flow path progressively narrowed from 370 m at the top of the slope to 50 m at its terminus. Some of the landslide material can travel at high speeds, reaching Area B in just over 2 minutes. This highlights the immediate threat posed to Area B by the fast-moving debris, even as the landslide continues to unfold over a longer period. This indicates that the initial phase of the landslide is extremely fast, posing an immediate

threat to area B, even while the rest of the landslide continues to move more slowly over a longer period.

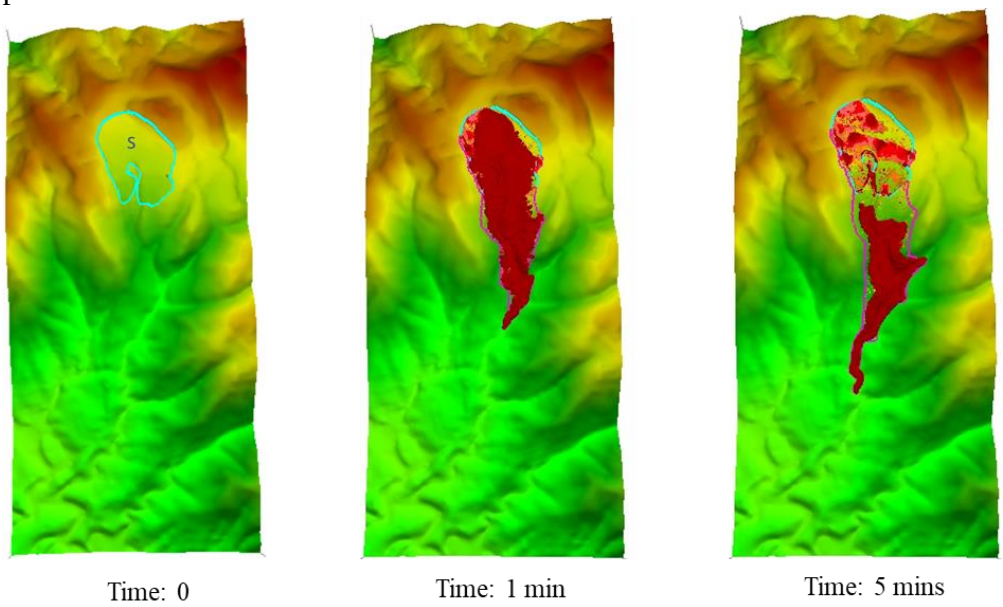

Figure 10. The simulation result of the LS-RAPID model for the movement of landslide S (the cyan color). The purple boundary indicates the range of impact of the sliding material over time, with the red blocks inside representing the masses of sliding material. The area outside the purple and cyan boundaries represents the elevation of the terrain, which ranges from green to red.

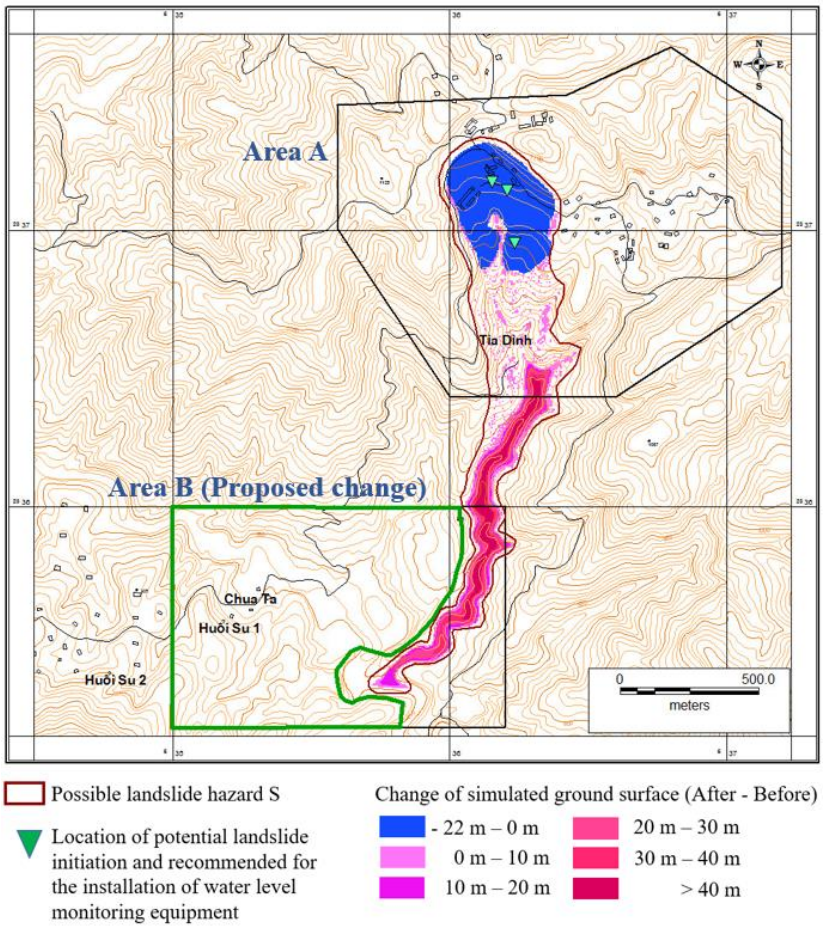

Figure 11. Map of possible landslide hazard S and proposed change for Area B. The red boundary area represents the range of impact from sliding materials, where changes in the topography (post-slide versus pre-slide) are indicated from blue (decreased) to red (increased).

Based on the simulation results, it is recommended to adjust the eastern boundary of area B to mitigate potential impacts from sliding material originating from area A. While the western boundary has been assessed as stable and suitable for further research and possible expansion of the resettlement area, the northern and southern regions appear currently safe from major landslide events. However, additional investigations are advised for these areas to ensure comprehensive risk assessment and mitigation in future developments. Furthermore, considering the potential risk from area A's landslide materials impacting Tia Dinh Commune, local authorities should adopt land-use strategies that prioritize safety. Specifically, high-risk areas might be more suitable for long-term tree planting or agricultural uses rather than residential or public infrastructure development.

Physical models, including the LS-RAPID model, are often praised for their precision in assessing landslide risks and impact extents. However, their applicability tends to be limited to smaller, geologically uniform areas. In larger regions with multiple potential landslide surfaces, geological parameters can vary significantly, which makes it challenging to select a representative sample for the entire area.

To better predict landslide-prone zones for effective land-use planning, the LS-RAPID model was employed using an extreme-case scenario approach for geological parameters. Although this method may not provide an exact simulation of hazard areas, it tends to overestimate the affected zones, thereby ensuring greater safety margins. This approach also offers significant cost and time savings, making it particularly suitable for application in remote mountainous regions of Vietnam. Additionally, if the thickness of the landslide mass can be estimated, the LS-RAPID model can be used to determine the minimum groundwater level required to trigger landslides. Identifying this critical activation level is essential for developing reliable landslide monitoring and early warning systems, thereby enhancing the region's preparedness against such natural hazards.

4. Conclusions

This study has demonstrated the effectiveness of applying the LS-RAPID model for landslide risk prediction in Tia Dinh Commune, Vietnam. Through comprehensive field surveys, soil analysis, and extreme-case scenario simulations, we identified three high-risk landslide zones (S1, S2, S3) within the study area, as well as the larger potential landslide zone S. The results indicate that the movement of landslide material in zone S could spread rapidly, posing immediate threats to both the existing resettlement area and the proposed relocation site, highlighting the need for urgent risk management measures.

The LS-RAPID model has proven to be a valuable tool in accurately simulating landslide dynamics, providing crucial insights into potential flow paths, velocities, and impact ranges of landslides. However, the accuracy of the model heavily depends on the availability of detailed geotechnical data. In regions like Vietnam, where data collection is often limited, there is a need for innovative approaches to estimate geological parameters more effectively.

To enhance early warning capabilities, this study recommends installing groundwater monitoring devices at critical locations identified in zones S1, S2, and S3. These positions were selected based on their potential to trigger landslides when groundwater levels reach specific thresholds. Continuous monitoring at these sites will be essential for issuing timely alerts, enabling preventive actions such as evacuations or structural reinforcements before landslide events occur.

The findings of this study also highlight the importance of incorporating landslide risk assessments into local land-use planning. High-risk areas, including the broader zone S, should be prioritized for non-residential uses, such as reforestation or agriculture, to minimize potential damage to infrastructure and human lives.

This study contributes significantly to the understanding of landslide dynamics in Tia Dinh Commune, providing a framework for effective risk management strategies that can be

adapted to other landslide-prone regions in developing areas. Implementing these strategies, along with the establishment of a robust groundwater monitoring network, will be essential in enhancing community safety and mitigating the devastating impacts of landslides.

Author Contributions: Conceptualization: N.D.H., N.H.N.; methodology: N.D.H., N.T.T.; software: N.D.H.; investigation: N.T.T., L.D.T.; data curation: N.H.N., N.H.D.; writing–original draft preparation: T.T.V., N.D.H.; visualization: N.D.H., N.T.T., N.H.D., T.T.V. All authors have read and agreed to the published version of the manuscript.

Funding: The field surveys and geophysical measurements are part of the project titled "Investigation of the current situation, causes, and risk prediction of subsidence and landslides in the Tia Dinh commune center, Dien Bien Dong district, Dien Bien province, and proposing measures to prevent and mitigate damage". The application of the model was supported by the JASTIP-Net project "Prediction of landslide hazard using the LS-RAPID model. A case study in the Tia Dinh area (Dien Bien province, Vietnam)".

Conflicts of Interest: The authors declare no conflict of interest.

References

1. Wieczorek, G.F. Landslide triggering mechanisms. In: Turner AK, Schuster RL (eds) Landslides: investigation and mitigation (Special Report). National Research Council, Transportation and Research Board Special Report 247, Washington, D.C. USA. 1996, pp. 76–90.
2. Glade, T.; Crozier, M.J. A review of scale dependency in landslide hazard and risk analysis. Landslide Hazard and Risk (eds Glade T, Anderson M, Crozier MJ), 2012, pp. 75–138. https://doi.org/10.1002/9780470012659.ch3.
3. An, H.; Viet, T.T.; Lee, G.H.; Kim, Y.; Kim, M.; Noh, S.; Noh, J. Development of time-variant landslide-prediction software considering three-dimensional subsurface unsaturated flow. *Environ. Modell. Software* **2016**, *85*, 172–183.
4. Tran, T.V.; Alvioli, M.; Lee, G.H.; An, H. Three-dimensional, time-dependent modeling of rainfall-induced landslides over a digital landscape: a case study. *Landslides* **2018**, *15*, 1071–1084. https://doi.org/10.1007/s10346-017-0931-7.
5. Plafker, G.; Ericksen, G.E. Nevados Huascarán Avalanches, Peru. Developments in Geotechnical Engineering (Editor(s): Barry Voight). *Dev. Geotech. Eng.* **1978**, *14*, 277–314. https://doi.org/10.1016/B978-0-444-41507-3.50016-7.
6. Sassa, K.; Nagai, O.; Solidum, R.; Yamazaki, Y.; Ohta, H. An integrated model simulating the initiation and motion of earthquake and rain induced rapid landslides and its application to the 2006 Leyte landslide. *Landslides* **2010**, *7(3)*, 219–236. https://doi.org/10.1007/s10346-010-0230-z.
7. Hung, L.Q.; Van, N.T.H.; Son, P.V.; Ninh, N.H.; Tam, N.; Huyen, N.T. Landslide inventory mapping in the fourteen Northern Provinces of Vietnam: achievements and difficulties. In: Sassa K, Mikoš M, Yin Y (eds) Advancing culture of living with landslides, 2017, pp. 501–510.
8. Ha, N.D.; Quoc, H.L.; Sayama, T.; Sassa, K.; Takara, K.; Dang, K. An integrated WebGIS system for shallow landslide hazard early warning. (Eds) Understanding and Reducing Landslide Disaster Risk. WLF 2020. ICL Contribution to Landslide Disaster Risk Reduction. Springer, Cham. 2020, pp. 195–202. https://doi.org/10.1007/978-3-030-60311-3_22
9. Vung, D.V.; Tran, T.V.; Duc, H.N.; Huy. D.N. Advancements, challenges, and future directions in rainfall-induced landslide prediction: A comprehensive review. *J. Eng. Technol. Sci.* **2023**, *55(4)*, 466–478. https://doi.org/10.5614/j.eng.technol.sci.2023.55.4.9.
10. Gao, Y.; Zhang, Y.; Ma, C.; Zheng, X.; Li, T.; Zeng, P.; Jin, J. Failure process and stability analysis of landslides in Southwest China while considering rainfall and

supporting conditions. *Front. Environ. Sci*. **2023**, *10*, 1084151. https://doi.org/10.3389/fenvs.2022.1084151.

11. Zhang, J.; Qian, J.; Lu, Y.; Li, X.; Song, Z. Study on landslide susceptibility based on multi-model coupling: A case study of Sichuan Province, China. *Sustainability* **2024**, *16*, 6803. https://doi.org/10.3390/ su16166803.
12. Chen, J.H.; Lee, C.F. Landslide mobility analysis using MADflow. *Int. Forum Landslide Disaster Manage. Hong Kong, China* **2007**, *2*, 857–874.
13. Pirulli, M.; Mangeney, A. Results of back-analysis of the propagation of rock avalanches as a function of the assumed rheology. *Rock Mech. Rock Eng*. **2008**, *41(1)*, 59–84. https://doi.org/10.1007/s00603-007-0143-x.
14. Roth, W. Dreidimensionale numerische Simulation von Felsmassenstürzen mittels der Methode der Distinkten Elemente (PFC). PhD Dissertation, Institute for Engineering Geology, Vienna University of Technology. 2003.
15. Hungr, O.; McDougall, S. Two numerical models for landslide dynamic analysis. *Comput. Geosci*. **2009**, *35(5)*, 978–992. https://doi.org/10.1016/j.cageo.2007.12.003.
16. Sassa, K. Geotechnical model for the motion of landslides. Proceeding of 5th international symposium on landslides. "Landslides", Balkema, Rotterdam, 1988, 1, 37–56.
17. Ha, N.D.; Sayama, T.; Sassa, K.; Takara, K.; Uzuoka, R.; Dang, K.; Pham, T.V. A coupled hydrological-geotechnical framework for forecasting shallow landslide hazard—a case study in Halong City, Vietnam. *Landslides* **2020**, *17*, 1619–1634. https://doi.org/10.1007/s10346-020-01385-8.
18. Sassa, K.; Dang, K.; He, B.; et al. A new high-stress undrained ring-shear apparatus and its application to the 1792 Unzen–Mayuyama megaslide in Japan. *Landslides* **2014**, *11*, 827–842. https://doi.org/10.1007/s10346-014-0501-1.
19. Setiawan, H.; Sassa, K.; Takara, K.; Ostric, M.; Miyagi, T.; Fukuoka, H. TXT-tool 4.081-1.2: Mechanism of the Aratozawa large-scale landslide induced by the 2008 Iwate-Miyagi earthquake. In (eds) Landslide Dynamics: ISDR-ICL Landslide Interactive Teaching Tools. Springer, Cham. 2018, pp. 819–831.
20. Jovančević, S.D.; Nagai, O.; Sassa, K.; Arbanas, Ž. TXT-tool 3.385-1.2: Deterministic Landslide Susceptibility Analyses Using LS-Rapid Software. In: (eds) Landslide Dynamics: ISDR-ICL Landslide Interactive Teaching Tools. Springer, Cham. 2018, pp. 169–179.
21. Gradiški, K.; Sassa, K.; He, B.; Arbanas, Ž.; Arbanas, S.M.; Krkač, M.; Kvasnička, P.; Oštrić, M. TXT-tool 3.385-1.1: Application of integrated landslide simulation model LS-rapid to the Kostanjek Landslide, Zagreb, Croatia. In: Sassa K, Tiwari B, Liu KF, McSaveney M, Strom A, Setiawan H (eds) Landslide Dynamics: ISDR-ICL Landslide Interactive Teaching Tools. Springer, Cham. 2018, pp. 101–109.
22. Dang, K.; Sassa, K.; Konagai, K.; Karunawarden, A.; Bandara, R.M.S.; Hirota, K.; Tan, Q.; Ha, N.D. Recent rainfall-induced rapid and long-traveling landslide on 17 May 2016 in Aranayaka, Kegalle District, Sri Lanka. *Landslides* **2019**, *16(1)*, 155–164. https://doi.org/10.1007/s10346-018-1089-7.
23. Dang, K.; Loi, D.H.; Sassa, K.; Duc, D.M.; Ha, N.D. Hazard assessment of a rainfall-induced deep-seated landslide in Hakha City, Myanmar. (Eds) Understanding and Reducing Landslide Disaster Risk. WLF 2020. ICL Contribution to Landslide Disaster Risk Reduction. Springer. Cham. 2020, pp. 249–257. https://doi.org/10.1007/978-3-030-60706-7_23.
24. Loi, D.H.; Lam, H.Q.; Sassa, K.; Takara, K.; Dang, K.; Thanh, N.K.; Tien, P.V. The 28 July 2015 rapid landslide at Ha Long city, Quang Ninh, Vietnam. *Landslides* **2017**, *14(3)*, 1207–1215. https://doi.org/10.1007/s10346-017-0814-y.
25. Quang, L.H.; Loi, D.H.; Sassa, K.; Takara, K.; Ochiai, H.; Dang, K.; Abe, S.; Asano, S.; Ha, D.N. Susceptibility assessment of the precursor stage of a landslide threatening Haivan Railway Station, Vietnam. *Landslides* **2018**, *15*, 309–325. https://doi.org/10.1007/s10346-017-0870-3.

Table of content